Chaperone BiP:

Master regulator of the Unfolded Protein Response (UPR) and its role in regulation of angiogenesis

Dissertation

zur Erlangung des Grades

Doktor der Naturwissenschaften

Im Fachbereich Biologie

an der Johannes Gutenberg-Universität

in Mainz

Laura Anna Anspach

geb. am 02.06.1986

in Grünstadt

Mainz, Januar 2015

Dekan:

1. Berichterstatter:

2. Berichterstatter:

Tag der mündlichen Prüfung:

Abbreviations

°C	Degree Celsius
µg	Microgram
µl	Microliter
µM	Micromolar
ms	Milliseconds
↓	Down-regulated
~	Circa
A	
ADAM	A disintegrin and metalloproteinase
AGPC	Acid guanidinium thiocyanate-phenol-chloroform extraction
AMD	Age-related macular degeneration
ANG1	Angiopoietin-1
APS	Ammonium persulphate
ATF4/6	Activating transcription factor 4/6
ATP	Adenosine triphosphate
B	
bFGF	Basic fibroblast growth factor
BiP	Binding immunoglobulin protein
BSA	Bovine serum albumin
bZIP	Basic leucine zipper
C	
Ca	Calcium
Calcein-AM	Calcein acetomethoxyl ester
CD	Cluster of differentiation

Abbreviations

cDNA	Complementary DNA
CMP	Cell matrix buffer
CS	Cytoskeleton
Ct	Cycle threshold
COPII	Coat protein complex II
D	
DGCR8	DiGeorge syndrome critical region gene 8
Dll4 (1)	Delta-like ligand 4 (1)
DMSO	Dimethylsulfoxide
DNA	Deoxyribonucleic acid
ds	Double stranded
E	
ECGS	Endothelial cell growth supplement
ECM	Extracellular matrix
EDTA	Ethylenediaminetetraacetic acid
EGF	Epidermal growth factor
EIA	Enzyme immunoassay
eIF2α	Eukaryote translation initiation factor 2α
EDRF	Endothelium derived relaxing factor
ER	Endoplasmatic reticulum
ERAD	ER-associated degradation
ERK	Extracellular signal-regulated kinase
ET-1	Endothelin-1
EtOH	Ethanol
F	
F-actin	Filamentous actin

FACS	Fluorescent-activated cell sorting
f c	Final concentration
FCS	Fetal calf serum
Flt-1/4	Fms-related tyrosin kinase ¼
fwd	Forward
G	
GI	GlutaMAX-I
H	
h	Hour
HCV	Hepatitis C virus
HEPES	4-(2-hydroxyethyl)-1-piperazineethanesulfonic acid
HGF	Hepatocyte growth factor
HIF1α	Hypoxia-inducible factor 1α
HRP	Horseradish peroxidase
Hsp	Heat shock protein
HSV	Herpes simplex virus
HSPA5	Heat shock 70 kDA protein
I	
ICAM-1	Intercellular adhesion molecule 1
IHC	Immunohistochemistry
IHC-P	Immunohistochemistry Paraffin
IF	Immunofluorescence
IFNγ	Interferon γ
IL1β	Interleukin 1β
IL-8	Interleukin 8
IMDM	Iscove´s Modified Dulbecco´s Medium

IRE1α	Inositol-requiring protein 1α
IRS	Immunoreactive Remmele Score
J	
K	
KDR	Kinase insert domain receptor
L	
LPS	Lipopolysaccharide
M	
MAPK	Mitogen-activated protein kinase
MCP-1	Monocyte chemotactic protein 1
MEFs	Mouse embryonic fibroblasts
min	Minute
mi-RISC	microRNA-induced silencing complex
miRNA	microRNA
mln	million
MMP	Matrix metalloproteinases
mRNA	Messenger RNA
MTS	(3-(4,5-dimethylthiazol-2-yl)-5-(3-carboxymethoxyphenyl)-2-(4-sulfphenyl)-2H-tetrazolium)
N	
Na-Hep	Sodium heparin
NFκB	Nuclear factor 'kappa-light-chain-enhancer' of activated B cells
NO	Nitric oxide
nt	nucleotides

O

oPD	o-Phenylenediamine Dihydrochloride

P

P/S	Penicillin/Streptomycin mix
PAA	Polyacrylamide
PBS	Phosphate-buffered saline
PC medium	PromoCell Endothelial Cell Basal Medium
PCR	Polymerase chain reaction
PDGF	Platelet-derived growth factor
PDI	Protein disulfide isomerase
PECAM-1	Platelet/endothelial cell adhesion molecule 1
PERK	Protein kinase RNA-like ER kinase
PFA	Paraformaldehyde
PHA-L	Phytohemagglutinin-L
PI	Propidium Iodide
PlGF	Placental growth factor
PP	Percentage of positive stained cells
pre-miRNA	Precursor miRNA
pri-miRNA	Primary miRNA
PS	Phosphatidylserine
PTGS	Post-transcriptional gene silencing

Q

qRT PCR	Quantitative real-time PCR

R

RA	Rheumatoid arthritis
rev	Reverse

RHO	RAS homologue
RIDD	Regulated IRE1-dependent decay
RIN	RNA integrity number
RNAs	Ribonucleic acid molecules
rpm	Rounds per minute
RPMI	Roswell Park Memorial Institute
RT	Room temperature
RQ	Relative Quantification
S	
s	Second
ss	Single stranded
S1P/S2P	Site ½ protease
SDs	Standard deviations
SDS	Sodium dodecyl sulfate
SDS-PAGE	SDS-polyacrylamide gel electrophoresis
sFlt-1	Soluble Flt-1
sHsp	Small heat shock proteins
SI	Optical stain intensity
T	
TBE buffer	Tris-Borat-EDTA buffer
TEMED	Tetramethylethylenediamine
TGFβ	Transforming growth factor β
TIE2	Tyrosine kinase with immunoglobulin-like and EGF-like domains 2
TIMP3	Tissue inhibitor of metalloproteinase 3
TNFα	Tumor necrosis factor α

Tun	Tunicamycin
TRBP	Transactivation-responsive RNA-binding protein
U	
U	Units
UPR	Unfolded protein response
UTR	Untranslated region
V	
V	Volts
VCAM-1	Vascular cell adhesion molecule 1
VE-cadherin	Vascular endothelial cadherin
VEGF	Vascular endothelial growth factor
VEGF-R	Vascular endothelial growth factor receptor
vWF	Von Willebrand factor
VVO	Vesiculo vacuolar organelles
W	
W	Western Blot
X	
Xbp1	X box-binding protein 1
XRNs	Cellular exoribonucleases
Y	
Z	

Contents

1 Introduction

1.1 The endothelium

The endothelium is built of endothelial cells, which line the vascular system. Approximately 1 kg of total weight of an adult is occupied by the endothelium (Sumpio *et al.,* 2002). A monolayer of the cells forms the interior of the vessels, which is aligned to the basal membrane, on which mural cells (smooth muscle cells and pericytes) are embedded. The endothelium adopts numerous functions in the cardiovascular system, for example the exchange of oxygen and carbon dioxide or the supply of nutrients with the surrounding tissue (Limaye and Vadas, 2007). With regard to barrier function of the endothelium, three main types of the endothelium can be distinguished: (1) the continuous endothelium is characterized by formation of tight junctions between the individual endothelial cells. These tight junctions are responsible for the low permeability of the continuous endothelium, which is, for example, a part of the vascular system in muscles or of the blood-brain-barrier. Only ions or small molecules like oxygen and water are able to pass the barrier. (2) The fenestrated endothelium is found in the pancreas, the glomeruli of the kidney or in endocrine glands. Larger molecules are capable of crossing the barrier via pores in the endothelial cells with a diameter of 60 – 80 nm. Despite containing the pores, the fenestrated endothelium exhibits a continuous basal lamina. (3) The sinusoidal or discontinuous endothelium possesses larger openings between the endothelial cells, in which cells are not in contact with each other, and exhibits a high permeability. In this type of endothelium the surrounding basal lamina is perforated. It is primarily located in the liver, bone marrow or the spleen (Risau, 1995).

In addition to acting as a barrier in order to transfer substances, the endothelium has further important tasks (Fig. 1). Thus, it plays a crucial role in the regulation of blood pressure. For maintenance of an efficient vascular homeostasis, a well-equalized balance between vasoconstriction and vasodilation is necessary (Deanfield *et al.,* 2007). A number of signaling molecules ensure this balance, most of them being secreted by the endothelium itself. Endothelial cells, inter alia, produce the vasoconstricting peptide endothelin-1 (ET-1) (Agapitov and Haynes, 2002). Additionally, endothelial cells release nitric oxide (NO), a vasoactive molecule that is classified as endothelium-derived relaxing factor (EDRF) and leads to smooth muscle relaxation. Production of NO in endothelial cells is stimulated by signal transferred through ET-1 among others (Chowdhary and Townend, 2001). Endothelial dysfunction

is of great pathophysiological relevance and is associated with arteriosclerosis, hypertension, diabetic angiopathies and heart failure. Deficiency of NO production, in particular, is associated with the aforementioned diseases (Stehouwer *et al.,* 1997; Eren *et al.,* 2013; Sumpio *et al.,* 2002).

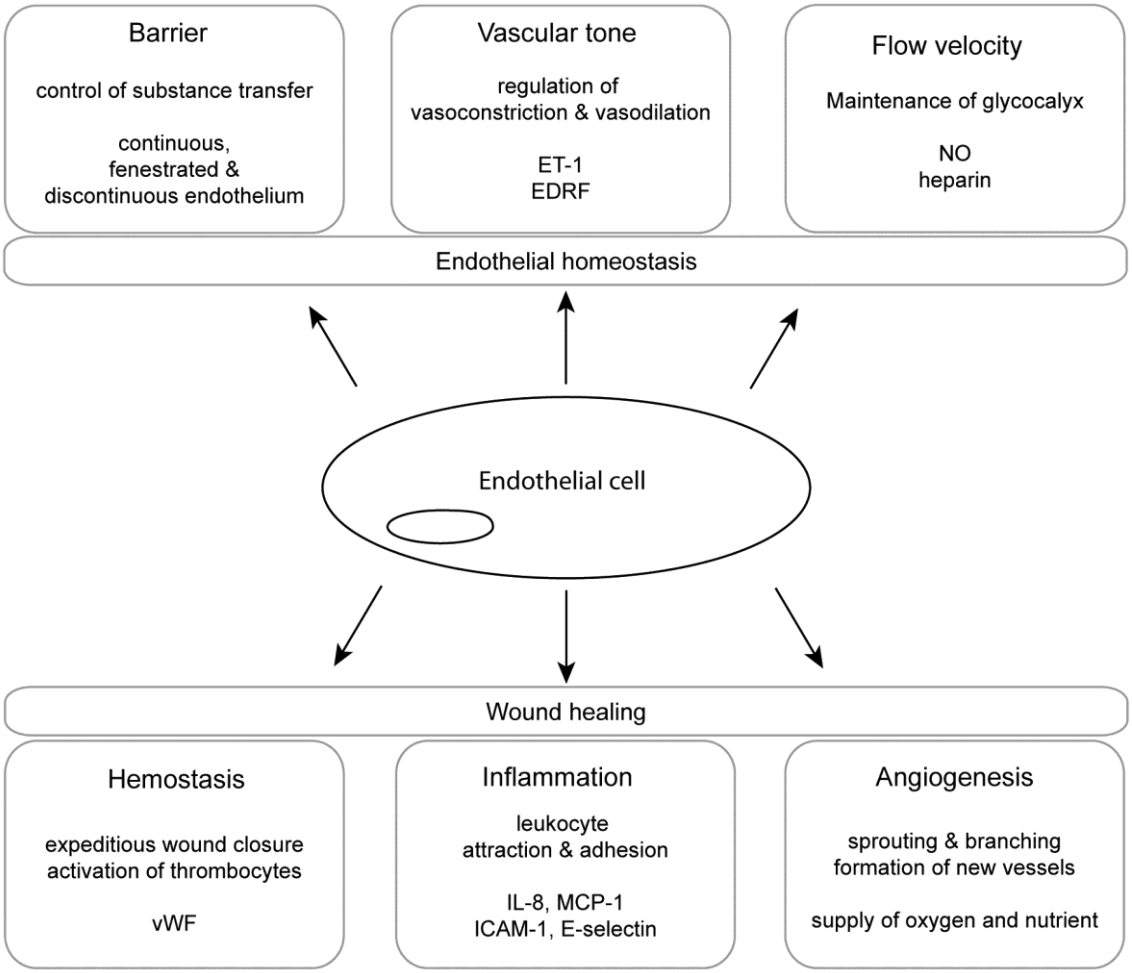

Fig. 1: Functions of endothelial cells in the vascular system.
Important role of endothelial cells involved in endothelial homeostasis and in wound healing processes.

First, endothelium is covered with a glycocalyx. On account of this layer, thrombocytes are not able to stick to the endothelium and an unimpaired blood flow is guaranteed (Reitsma *et al.,* 2007). In addition, endothelial cells secrete signal molecules like heparin or NO with an anti-coagulatory effect (Agapitov and Haynes, 2002). A disruption of a blood vessel activates hemostasis, which leads to an expeditious wound closure and cessation of bleeding. Within primary or cellular hemostasis, adhesion and aggregation of thrombocytes occur. Because of the vessel damage and consequently destruction of the glycocalyx, platelets come in contact with the endothelium and the extracellular matrix (ECM), especially collagen. Mediated by the von Willebrand Factor (vWF), which represents an important endothelial cell marker, platelets adhere to the

vessel wall (Schafer, 1995). This contact leads to an activation of the thrombocytes, and proceeds in three steps. First, α-granules are released to attract and activate further thrombocytes (Blair and Flaumenhaft, 2009). The second phase of platelet activation results in modulation of the cytoskeleton and formation of pseudopodia. Platelets become sticky and a better cross-linking of platelet to platelet or platelet to the endothelial cells is ensured. In the third step of thrombocyte activation, aggregation of the platelets takes place. Hence, primary hemostasis is completed with formation of the first thrombus (Clemetson, 2012). The following step is referred to as blood coagulation, or secondary hemostasis. The first wound closure will be stabilized. Activated thrombocytes express receptors, which bind to fibrinogen derived from blood plasma or other sticky compounds like fibronectin or thrombospondin produced by activated platelets themselves (Ruf and Ruggeri, 2010). Many pro-coagulants and clotting factors are involved in the coagulation cascade, e.g. prothrombin, which is synthesized in the liver. As a result of activation, the protein develops enzymatic protease activity and triggers polymerization of fibrinogen to fibrin. Covalent bonds are formed and a fibrin network engulfing further thrombocytes and erythrocytes is formed to build a thrombus (Furie and Furie, 2008). Within the so-called retraction phase, the volume of the thrombus is minimized and strengthened due to retraction of thrombocytes. Coagulation represents the preliminary step for the wound healing process (Osdoit and Rosa, 2001).

1.2 Wound healing

Wound healing is defined as a process to restore structure and function of injured or diseased tissue – *restitutio ad integrum*. The process starts with inflammatory and exudation phase. Wound secretion, generated from blood plasma enters the wound site to clear the lesion of pathogenic microorganisms and foreign matter. It also contains cells of the immune system, which start to clean the wound (Martin, 1997). Neutrophils release proteases to breakdown damaged tissue and initiate the respiratory burst to combat pathogens. T-helper cells produce cytokines to maintain an inflammatory response and to activate macrophages, which are responsible for regeneration. This process involves elimination of cell debris, bacteria and dead cells by phagocytosis, as well as the secretion of various signal molecules to induce angiogenesis, granulation tissue formation, reepithelialization and the production of new ECM (Velnar *et al.,* 2009). Immune cells are stimulated, among other factors, by low concentration of oxygen in their environment. Endothelial cells play a major role during the inflammatory phase by attracting immune cells (see below). Inflammation in the wound healing process undertakes the tasks to fight against infection, to clear

debris and induce proliferation of cells during the proliferation phase. A subsequent decrease of pro-inflammatory factors in the wound site initiates the proliferation phase (Werner and Grose, 2003). Following release of chemotactic stimuli, endothelial cells are attracted into the lesion and vascularization to achieve an increased supply of oxygen, nutrients and immune cells takes place. Migration of endothelial cells and angiogenesis are induced mostly by vascular endothelial growth factor (VEGF) but also by hypoxic conditions and the existence of lactic acid inside the wound area (Wong and Crawford, 2013). Simultaneously, collagenases start to degrade the clot. In this process, termed fibrinolysis, the fibrin network, formed during coagulation, is degraded by plasmin, an enzyme that breaks down the polymer (Cesarman-Maus and Hajjar, 2005). Matrix-metalloproteases (MMPs) remove the basement membrane to ensure migration of the cells. Additionally, fibroblasts enter the wound and proliferate due to stimulation by growth factors, such as platelet-derived growth factor (PDGF) and transforming growth factor (TGF-β), but also by fibronectin and hypoxia (Clark, 1990). Within fibroplasia ECM is deposited, collagen is produced and further growth factors are released to attract epithelial cells into the wound site (Montesano and Orci, 1988). Because of generation of so-called granulation tissue, this phase of wound healing process is also called the granulation phase. Granulation tissue fills up the tissue defect and consists of new blood vessels, fibroblasts, inflammatory cells, myofibroblasts, which are differentiated from fibroblasts, and components of the provisionally formed ECM (Midwood *et al.,* 2004). Subsequently, epithelial cells can enter the wound to build up a new barrier between the injured tissue and the environment. Keratinocytes, also known as callus-forming cells, are involved in this process. At the same time, the scab is degraded by plasmin and MMPs to establish a required viable surface for migrating cells (Clark, 1990). The last phase in wound healing is maturation. In this process, tensile strength in the wound area is increased as a result of replacement of collagen III, a component of the provisional ECM, by collagen I, rearrangement of the collagen fibers, their cross-linking and alignment along tension lines. Furthermore, the lesion is dehydrated, and no longer required blood vessels are eliminated in the scar tissue (Greenhalgh, 1998). In general, this phase lasts approximately one to two years. A weakened immune system can lead to incomplete removal of cell debris or bacteria and other pathogens from the wound site. In this situation, a decay in the inflammatory phase does not take place and a proliferation phase is not initiated. This leads to the development of chronic wounds, for example *venous ulcer* (Midwood *et al.,* 2004). Defects in subsequent phases of wound healing can also cause negative effects. Thus pathological scarring like the keloid scar is one of the outcomes (Desmouliere *et al.,* 2005).

1.3 Inflammation

During hemostasis, coagulation and wound healing, endothelial cells make a significant contribution. With regard to inflammation, activation of endothelial cells by TNFα, synthesized by macrophages and monocytes, and IL-1β, leads to release of inflammatory chemokines, including interleukin-8 (IL-8) and monocyte chemoattractant protein 1 (MCP-1) (Peters *et al.,* 2003). IL-8 acts on neutrophil chemotaxis, whereas MCP-1 attracts monocytes to the site of inflammation (Dinarello, 2000). In this respect, attraction and interaction of leukocytes with endothelial cells plays an important role (see Fig. 2). In the original model, the adhesion cascade consists of three steps: selectin-mediated rolling, chemokine-triggered activation and integrin-dependent arrest (Ley, 1996). Recent studies on the leukocyte adhesion cascade have shown that the original version needs to be expanded. The three step cascade is thus extended with the steps: slow rolling, adhesion strengthening, intraluminal crawling, paracellular and transcellular migration as well as migration through the basement membrane (Ley *et al.,* 2007). The attachment of leukocytes is mediated by P- and E-selectin, expression of which in endothelial cells is known to be highly up-regulated under pro-inflammatory conditions (Patel *et al.,* 2002). In the case of high density of selectins, tethering leukocytes are stopped immediately, whereas leukocytes are only slowed down if the density of selectins is low (slow rolling) (Alon and Feigelson, 2002). Signals of selectin binding are triggered in endothelial cells and also in ligand-presenting leukocytes. Activation of leukocytes, rolling arrest and a firm adhesion to endothelial cells is promoted by the intercellular adhesion molecule (ICAM-1) and vascular cell adhesion molecule (VCAM-1) (Peters *et al.,* 2003). Adhesion is additionally strengthened by activation of integrin-generating signals. Leukocytes crawl over endothelial cells to find preferred sites of transmigration. Interaction of a leukocyte and an endothelial cell, mediated by ICAM1, leads to an increased intracellular Ca^{2+} level, which activates p38 MAPK (mitogen activated protein kinase) and RHO (RAS homologue) GTPase signaling pathways. This event effects endothelial cell contractility (Huang *et al.,* 1993). Paracellular migration of leukocytes is supported by rearrangement of the cytoskeleton in endothelial cells. Due to inflammation, stress fibers are formed, which influence cell shape and reduction of intercellular contacts (Weber *et al.,* 1998). The expression of vascular endothelial cadherin (VE-cadherin), platelet/endothelial cell adhesion molecule 1 (PECAM-1) and CD99 (cluster of differentiation 99) facilitate transendothelial migration (Ley *et al.,* 2007). Furthermore, transcellular migration of leukocytes through the body of endothelial cells has been observed (Cinamon *et al.,* 2004; Carman and Springer, 2004, Carman and Springer, 2004). Vesiculo-vacuolar organelles (VVOs) are used by leukocytes as a gateway to pass through the

endothelial cells (Dvorak and Feng, 2001). However, the paracellular route represents the preferred way for leukocytes to pass the endothelium. Approximately 5-20% of transmigrating cells move across endothelial cells paracellularly *in vitro* (Carman and Springer, 2004). After transmigration, the leukocytes pass the endothelial basement membrane and the pericyte sheath. Leukocytes search for the sites containing low content of basement membrane components, e.g. laminin-10 or collagen IV, to pass the endothelial basement membrane. Pursuing this strategy, leukocytes find gaps between pericytes, which are co-localized with low-expression sites of basement membrane components (Wang *et al.,* 2006).

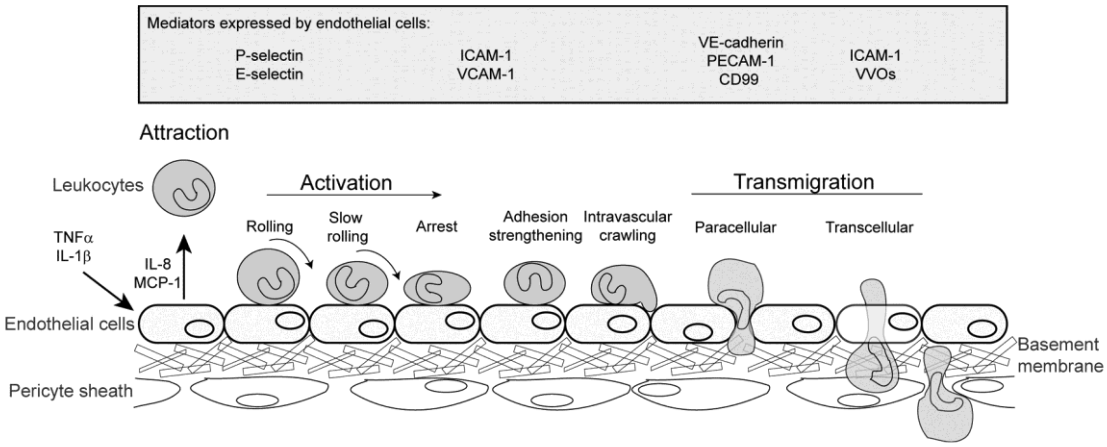

Fig. 2: Leukocyte adhesion cascade - interaction of leukocytes and endothelial cells in the inflammatory response.

Leukocyte adhesion cascade consists of selectin-mediated rolling, slow rolling, arrest, adhesion strengthening, intraluminal crawling, paracellular or transcellular migration and migration through the basement membrane (modified according to Peters *et al.,* 2003; Ley *et al.,* 2007).

1.4 Angiogenesis

The term angiogenesis, already mentioned in the context of wound healing, describes the formation of new blood vessels from the already existing microcirculation. Endothelial cells play an important role in this process as well. Angiogenesis is often described as a separate event from vasculogenesis, which mostly involves the formation of new vessels from progenitor cells during embryonic development (Nissen *et al.,* 1998; Risau, 1997). However, Asahara et al. found progenitor endothelial cells in the peripheral blood of adults and demonstrated the formation and sprouting of blood vessels in adults as a coupled complex vasculogenic and angiogenic process (Asahara *et al.,* 1997). These progenitor endothelial cells can be found in bone marrow, adipose tissue and peripheral blood. They are recruited by tissue ischemia or deficiency of oxygen to the place of demand, guided by angiogenic factors like VEGF or angiopoeitin. At the site of need, they differentiate to mature endothelial cells and

contribute to formation of new blood vessels. Thus, a high regenerative potential is attributed to progenitor endothelial cells (Doyle *et al.,* 2006; Khakoo and Finkel, 2005).

Formation of new blood vessels, for simplicity referred to as angiogenesis, is a complex process, which involves a number of morphogenic events, e.g. sprouting and branching, formation of a lumen, anastomosis and remodeling (Eilken and Adams, 2010). The principle of the formation of new capillaries is separated into two steps, the activation and resolution phase. In the activation phase, endothelial cells are activated by the pro-angiogenic factor VEGF (Sumpio *et al.,* 2002). The subsequent release of NO causes vasodilatation. This event and the additional release of proteases induce degradation of basal lamina and ECM. Endothelial cells start to migrate towards an angiogenic stimulus, proliferate and build up new vessels (Lamalice *et al.,* 2007; Ausprunk and Folkman, 1977, Ausprunk and Folkman, 1977). Connections between individual vessels and sprouts are formed in the process of anastomosis (Eilken and Adams, 2010). Within the subsequent resolution phase, covering of the vessels with mural cells stabilizes newly formed vessels. Thus, pericytes and smooth muscle cells for maturation are attracted by angiogenic and arteriogenic factors (Senger and Davis, 2011).

All these processes are highly regulated by pro- and anti-angiogenic factors (Risau, 1997). A mechanical induction of angiogenic processes is discussed in the literature, although it is not well characterized. Mechanical effects of shear stress or increased muscle contraction are debated to affect extension of the vessel network (Prior *et al.,* 2004). However, angiogenesis is mostly induced by chemical stimulation, in which growth factors and cytokines are relevant. Pro-angiogenic factors include, for example, VEGF, the main factor in angiogenesis, basic fibroblast growth factor (bFGF), hepatocyte growth factor (HGF), tumor necrosis factor α (TNFα), epidermal growth factor (EGF) and angiopoeitins. In contrast, thrombospondin-1, prolactin and angiostatin are ranked among the anti-angiogenic factors (Risau, 1997). In particular VEGFA represents a pro-angiogenic factor, which triggers many events at molecular level (Zachary, 2003; Senger and Davis, 2011; Nissen *et al.,* 1998; Geudens and Gerhardt, 2011; Gerhardt *et al.,* 2003). The VEGF family consists of several members (VEGFA, VEGFB, VEGFC, VEGFD and placental growth factor (PlGF)), whereby VEGFA is considered to be the most important growth factor for angiogenesis. There are five different isoforms of the growth factor identified, generated by alternative splicing in the course of transcription. Among the isoforms $VEGF_{(121,\ 145,\ 165,\ 189,\ 206)}$, $VEGF_{165}$ constitutes the main form. It is expressed by macrophages, T-lymphocytes, fibroblasts, keratinocytes, smooth muscle cells and endothelial cells as well (Tischer *et al.,* 1991; Kroll and Waltenberger, 2000). It is secreted into the ECM, but also remains

bound to the cell surface (Veikkola and Alitalo, 1999; Kroll and Waltenberger, 2000). Binding to its receptors, VEGFA triggers migration and proliferation of endothelial cells acting e.g. as a chemotactic agent, differentiation of progenitor endothelial cells, vascularization and remodeling of vascular structures. Furthermore, proteolytic activity of endothelial cells is stimulated, which results in a contribution to degradation of the ECM. Additionally, VEGFA regulates vascular permeability by stimulating NO release and improves cell survival in new blood vessels (Alon *et al.,* 1995). The growth factor is expressed by various cell types, but in low amounts in the adult organism. Expression of VEGFA is regulated at molecular level mainly by hypoxia via the hypoxia-inducible factor 1α (HIF1α) pathway (Levy *et al.,* 1996). The pro-angiogenic stimulus of VEGFA is transmitted by receptors via tyrosine kinase activity. There are three different VEGF-receptors (VEGF-R) present, which exhibit different binding specificities and affinities for members of the VEGF family (Veikkola and Alitalo, 1999). VEGF-R1 (fms-related tyrosin kinase 1; Flt-1) and VEGF-R2 are specific for vascular endothelial cells, whereas VEGF-R3 (fms-related tyrosin kinase 4; Flt-4) expression appears in endothelial cells of the lymphatic system (Geudens and Gerhardt, 2011). VEGFA binds primarily to VEGF-R2, also referred to as the kinase insert domain receptor (KDR).

Indeed, Flt-1 shows an affinity for VEGF-A, but elicits low response due to weak tyrosine kinase activity. It is presumed that Flt-1 acts as a decoy receptor. It seizes VEGF and thus reduces signaling through KDR (Fischer *et al.,* 2008). This model is supported by studies which reported an embryonic lethality due to Flt-1 deficiency and an overproliferation of endothelial cells, as well as dysmorphology of vasculature as a result of Flt-1 knockout in embryonic stem-cell-derived vessels (Kearney *et al.,* 2004; Fong *et al.,* 1995). On the other hand, VEGFA-KDR signaling triggers differentiation and proliferation of endothelial cells (Shalaby *et al.,* 1995). The receptor has a higher affinity to bind VEGF-A and it is known that angiogenesis, and also vasculogenesis, is especially activated through VEGF-A-KDR signaling (Waltenberger *et al.,* 1994). KDR knockout mice were defective in formation of the vascular system (Shalaby *et al.,* 1995). Triggering VEGF-A signal through KDR is mostly transferred via the Ras/MAPK signaling pathway (Kroll and Waltenberger, 2000).

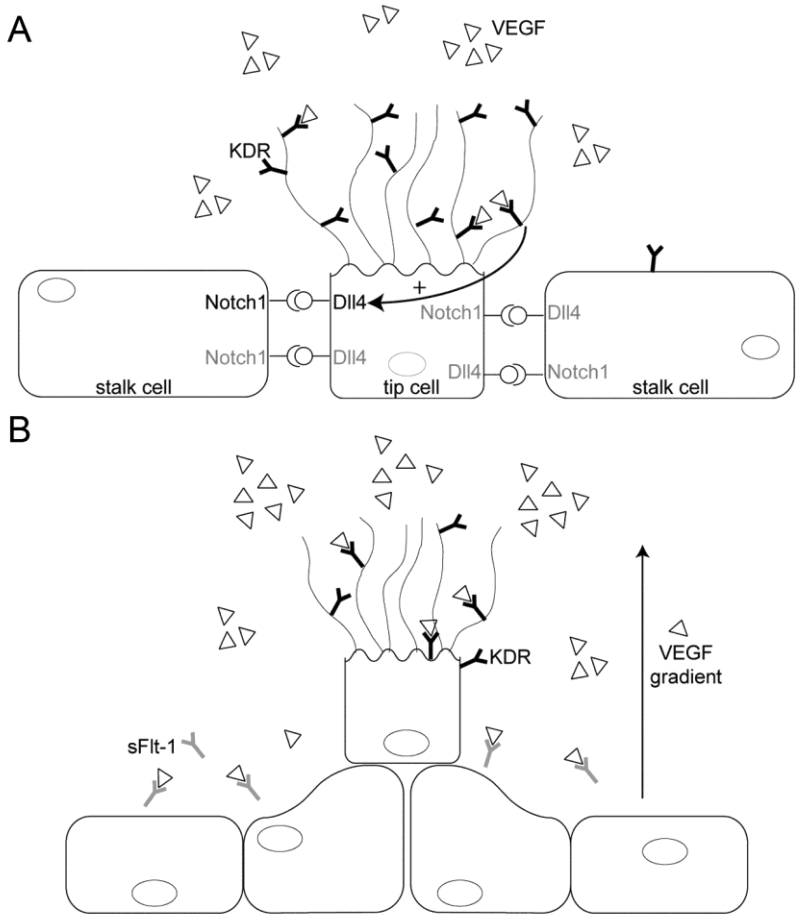

Fig. 3: Initial steps of angiogenesis.

Notch-Dll4 signaling control differentiation into tip and stalk cell phenotype (A). Sprouting occurs along a VEGF gradient (modified according to Geudens and Gerhardt, 2011).

Following the concept of tip-stalk cell sprouting, two phenotypes of endothelial cells, the tip cell and the stalk cell, occur during formation of a new blood vessel. They differ in gene expression profile and functional specifications. Tip cells show a high migratory behavior, they are polarized and exhibit filopodia, whereat stalk cells are highly proliferative. It is the task of the stalk cells to form the lumen of the newly formed vessels (Ruhrberg *et al.,* 2002; Gerhardt *et al.,* 2003). In contrast to stalk cells, tip cells show a high expression level of KDR, PDGFB, delta-like ligand 4 (Dll4) or MMP14 (Gerhardt *et al.,* 2003; Hellström *et al.,* 2007). In quiescent endothelium, endothelial cells are not distinguishable and present common 'cobblestone' morphology (Bussmann *et al.,* 2011). Becoming tip or stalk cell is determined by Notch-signaling pathway, a cell-cell contact-dependent communication mechanism, described in Fig. 3 A (Geudens and Gerhardt, 2011). This pathway plays an important role in embryonic development and in differentiation of several cell types (Thurston and Kitajewski, 2008). In endothelial cells Notch receptors 1 and 4 are present, which act as receptor molecules outside the cell and intracellularly as transcription factors. Endothelial cells

also express Notch ligands Dll-1, Dll-4 and Jagged1. Via ligand and receptor interaction, cells come into contact with each other and the pathway is activated. Notch intracellular domain is cleaved by receptor-associated metalloproteinase ADAM (a disintegrin and metalloproteinase) transferred to the nucleus, where it acts as a transcription factor, regulating expression of target genes (Mumm and Kopan, 2000). Notch activation results in inhibition of tip cell formation and promotes differentiation into a stalk cell, characterized as well through inhibition of KDR (Lobov *et al.,* 2007; Leslie *et al.,* 2007; Hellström *et al.,* 2007). Upon endothelial cell activation with VEGF, the cells compete for tip cell position. Cells are highly sensitive for imbalances between VEGF and Notch signaling. Even slight differences in local VEGF concentration, which occur randomly, and differences in gene expression pattern are recognized and affect endothelial cell fate (Jakobsson *et al.,* 2010). Low activation of Notch leads to increased expression of e.g. Dll4 and decreased expression in Notch1, characterizing an endothelial tip cell and *vice versa*. Activation of Notch inhibits KDR and Dll4 expression, which leads to differentiation of a limited number of tip cells. In turn, VEGF-KDR-signaling induces Dll-4-Notch-signaling. In this way, the tip cell inhibits the stalk cell to differentiate into another tip cell (Williams *et al.,* 2005; Leslie *et al.,* 2007). Differentiated tip cells sprout along a VEGF gradient (Fig. 3 B), whereas stalk cells proliferate and produce components of the basement membrane simultaneously. Additionally, they associate with pericytes to achieve stabilization of the newly formed vessel. In addition, the guiding VEGF gradient is reinforced by the sprouting vessel itself. Stalk cells produce soluble Flt-1 (sFlt-1), which intercepts VEGF. In this process, a negative regulatory effect of Flt-1 is reflected again. Hence, the VEGF concentration is perceived to be higher in the area of the tip cell (Chappell *et al.,* 2009). Many regulatory events take place during angiogenic sprouting.

The lumen of blood vessels is formed according to three different mechanistic theories: (1) intracellular vacuole coalescence, in which vacuoles form a lumen within one stalk cell; (2) intercellular vacuole exocytosis, which describes formation and release of exocytotic vacuoles in the intercellular space of stalk cells; and (3) lumenal repulsion, a process in which the apical membrane of stalk cells is repelled (Blum *et al.,* 2008; Kamei *et al.,* 2006; Strilić *et al.,* 2009). To build up a vessel network, sprouting vessels form connections with each other. In particular, VE-cadherin represents an important connective molecule. In general, it is known to be expressed in the area of cell-cell contacts. Strikingly, expression was also observed in tip cells (Almagro *et al.,* 2010). With the help of these cell-cell contact molecules filopodia of individual tip cells associate with each other to form anastomoses (Fig. 4). A supporting role of macrophages by production of soluble factors or tyrosine kinase with immunoglobulin-

like and EGF-like domains 2 (TIE2) and Notch signaling is discussed (Schmidt and Carmeliet, 2010).

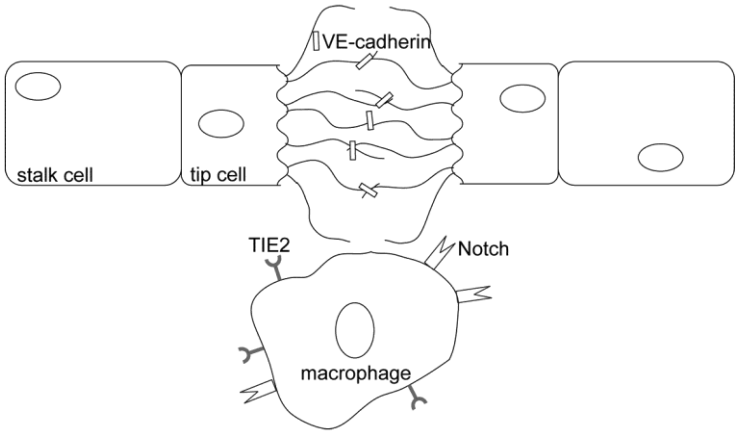

Fig. 4: Anastomosis of endothelial tip cells within the process of sprouting angiogenesis. (Modified according to Geudens and Gerhardt, 2011)

In adults recurrent regeneration of blood vessels takes place in line with wound healing or the female reproductive cycle. With regard to pathological vascularization, angiogenesis occurs in tumor progression, inflammation and tissue ischemia. For example, due to an insufficient supply of oxygen in the case of tumor development, malignant tissues produce signal molecules, which induce angiogenesis to guarantee a supply of oxygen and nutrients (Folkman, 1995). An up-regulation of VEGFA is detectable, for example, in the serum of patients after myocardial infarction (Kranz *et al.,* 2000). Dysfunctions in the angiogenic process, especially with regard to initiation of the event, are known to be associated with an ER (endoplasmatic reticulum) stress situation (Dong *et al.,* 2011; Salminen and Kauppinen, 2010).

1.5 Unfolded Protein Response

During protein synthesis, chains of amino acids are established, which are subsequently released into the lumen of the endoplasmatic reticulum (ER). Here, the proteins are folded to generate secondary structure. Without having their native and specific conformation, proteins are not functional. Rarely, the folding process appears spontaneously. Enzymes, called chaperones, catalyze most of the oxygen-dependent reactions of protein folding (Buchner, 2002). Due to the fact that chaperones show an increased synthesis rate under high temperature, they are also designated as heat shock proteins (Hsps). Several members of different Hsp families are known: Hsp100-, Hsp90-, Hsp70-, Hsp60-family and a group of small heat shock proteins (sHsps). They are distinguished by their molecular mass and prevailing sequence homologies (Ellis and van der Vies, 1991). Binding immunoglobulin protein (BiP), also known as Grp78

(78 kDA glucose regulating protein) or HSPA5 (heat shock 70 kDA protein 5) (Haas and Wabl, 1983; Pouysségur *et al.,* 1977) represents an important member in cell homeostasis. Working as a chaperone, the process of protein folding is ATP (adenosine triphosphate) dependent. As a result of ATP hydrolysis, the chaperone interacts with the unfolded protein through its substrate-binding domain. The protein is folded in cooperation with protein disulfide isomerase (PDI) (Mayer *et al.,* 2000). BiP is also involved in translocation machinery across the ER membrane and the transfer backwards of aberrant proteins, which are designated for degradation by proteasomes (Gething, 1999). Besides a principal function in the protein folding process, the chaperone acts as a stress sensor protein in ER stress signaling, called the Unfolded Protein Response (UPR). As a result of several stress factors, unfolded or misfolded proteins accumulate in the lumen of the ER and lead to an activation of the signaling pathway, resulting in a response to counteract the stress situation. The prime aim is the re-establishment of homeostasis (Ron and Walter, 2007) by up-regulation of chaperone expression, expansion of the ER network, activation of ERAD (ER-associated degradation) and repression of global translation (Schröder and Kaufman, 2005). On the other hand, a prolonged ER stress situation and ongoing activation of the UPR initiate apoptosis (Tabas and Ron, 2011). Thus, UPR assumes a central role in many diseases (Walter and Ron, 2011), such as e.g. type II diabetes. In this case, β-cells of the pancreas are affected by a high synthesis rate of insulin (Fonseca *et al.,* 2011). Additionally, many types of cancer are associated with persistent UPR activation, especially tumors that occur in secretory tissues (Walter and Ron, 2011; Lin *et al.,* 2008; Li *et al.,* 2011). Otherwise, UPR is involved in several metabolic processes like lipid and cholesterol metabolism and energy homeostasis. Furthermore, the signaling pathway is important for inflammation, cell differentiation and innate immunity (Hetz, 2012).

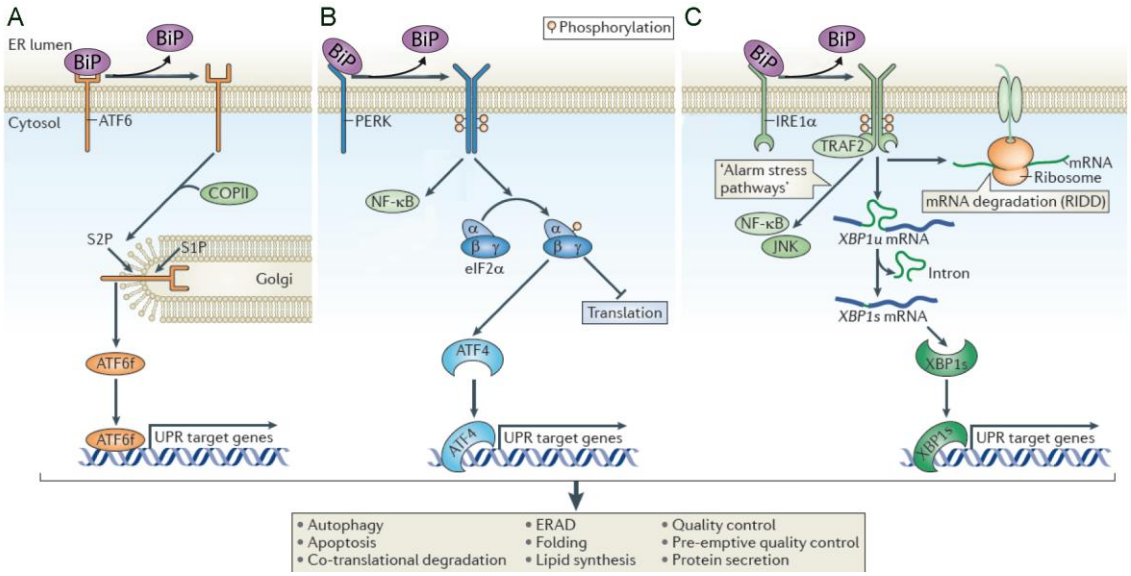

Fig. 5: Individual pathways of the Unfolded Protein Response (UPR).
ATF6 (A), PERK (B) and IRE1α (C) mediated signaling (modified according to Hetz, 2012).

The UPR signaling pathway consists of three coupled, but individual pathways, described in Fig. 5. The UPR stress sensors ATF6 (activating transcription factor 6), PERK (protein kinase RNA-like ER kinase) and IRE1α (inositol-requiring protein 1α) are located in the membrane of rough ER, the place of protein synthesis, translocation and folding (Schröder and Kaufman, 2005). Within these UPR pathways, three different mechanisms of signal transfer are available: unconventional messenger ribonucleic acid molecule (mRNA) splicing, phosphorylation/ dephosphorylation and proteolysis (Ron and Walter, 2007). Under homeostatic conditions, chaperone BiP exhibits affinity for these receptors and the binding inhibits UPR signaling. Upon accumulation of unfolded proteins in the lumen of the ER BiP dissociates from the receptors because of a higher affinity to bind unfolded proteins. Because of BiP release, suppressing effects on spontaneous dimerization of IRE1α and PERK are revoked and the signaling is activated (Bertolotti *et al.,* 2000). Removal of BiP also results in a de-masking effect of the Golgi-localization signal of ATF6 (Fig. 5 A, (Shen *et al.,* 2002) leading to an interaction of the receptor protein with coat protein complex II (COPII). These protein complexes generate vesicles in which ATF6 is transferred to the Golgi apparatus (Schindler and Schekman, 2009). On arrived there, the protein is integrated in the membrane of the Golgi and processed by site 1 protease (S1P) and site 2 protease (S2P). Accordingly, the cytosolic domain fragment of ATF6, which contains a basic leucin zipper (bZIP) domain, is released and acts in the nucleus as a transcription factor (Hetz, 2012).

The transfer of stress signal via the PERK pathway starts with the dimerization and autophosphorylation of the receptor (Fig. 5 B). Subsequently, the initiation factor for translation eIF2α (eukaryotic translation factor 2α) is phosphorylated by the receptor, leading to a common attenuation of translation (Dey *et al.,* 2010). On the other hand, mRNAs containing special features in the 5'-untranslated region (UTR), for example ATF4 are preferred for translation under these conditions (Wek *et al.,* 2006). ATF4 acts as a transcription factor regulating gene expression of UPR target genes, which are involved in autophagy, apoptosis or antioxidant response (Ron, 2002). $Perk^{-/-}$ knockout cells demonstrate the relevance of this pathway for translation, as the regulation of translation in these cells was not ensured (Harding *et al.,* 2000). Besides inhibition of translation, activation of PERK leads to the initiation of 'alarm stress pathways'. Thus, NFκB signaling is activated, resulting in regulation of genes involved in redox metabolism and the inflammatory response (Schröder and Kaufman, 2005).

Upon activation of the IRE1α pathway (Fig. 5 C), RNase activity of the receptor is stimulated by dimerization and autophosphorylation, which processes mRNA encoding X box-binding protein (XBP1) by unconventional mRNA splicing. An intron of 26 nucleotides is removed from unspliced mRNA (Xbp1u) to obtain a spliced variant (Xbp1s). The active form of the transcription factor Xbp1 is synthesized, which then regulates the expression of proteins of the protein folding machinery and ERAD (Lee *et al.,* 2002). A further consequence of IRE1α activation by high stress conditions, which leads to clustering of receptor molecules, is the degradation of mRNA molecules localized in the lumen of the ER. This process is called regulated IRE1-dependent decay (RIDD). Because of RNase domain activity of the receptor IRE1α, residual ER located mRNA molecules are processed at a consensus site, similar toXbp1u. Afterwards, substrates of cellular exoribunucleases (XRNs) are added to the 5'- and 3'-ends of the RNAs and that leads to a fast degradation (Maurel *et al.,* 2014; Hollien and Weissman, 2006). In addition, adaptor protein TNFR-associated receptor (TRAF2) is recruited by the receptor, resulting in activation of apoptotic signaling (Urano *et al.,* 2000). Activation of alarm signaling via p38, extracellular signal kinase (ERK) and NFκB are also documented (Hetz and Glimcher, 2009).

In summary, as a result of upcoming ER stress, the master regulator of the UPR, BiP, detaches from the receptors ATF6, PERK and IRE1α. Thus, the UPR is activated and the signal is transmitted via three different signaling pathways. The transferred stress signal results in regulation of protein expression involved in autophagy, apoptosis, co-translational degradation, ERAD, folding, lipid synthesis, quality control, pre-emptive quality control and protein secretion (Hetz, 2012).

1.6 microRNAs – a way to regulate gene expression

The described processes are highly regulated by various signaling pathways. Several mechanisms are involved and even more proteins. At least, gene expression of target proteins is affected. A special mode of regulating gene expression is the effect of microRNA molecules (miRNAs). miRNAs are small RNA molecules with a length of 20-22 nucleotides (nt) and they are part of posttranscriptional regulation mechanism in the cell. Most genes are known to be regulated by miRNAs (Friedman *et al.,* 2008) and the latter are closely involved in many biological processes. Additionally, miRNA families have emerged as multiple hallmarks of cancer (Chen *et al.,* 2014). miRNAs are encoded in introns of protein-coding or non-coding genes. Some miRNA sequences are clustered in polycistronic transcripts, indicating a coordinated expression within specific processes (He and Hannon, 2004). Transcription of miRNAs is regulated by autoregulatory feedback loops (Krol *et al.,* 2010). The biogenesis and mode of action of microRNA molecules are illustrated in Fig. 6.

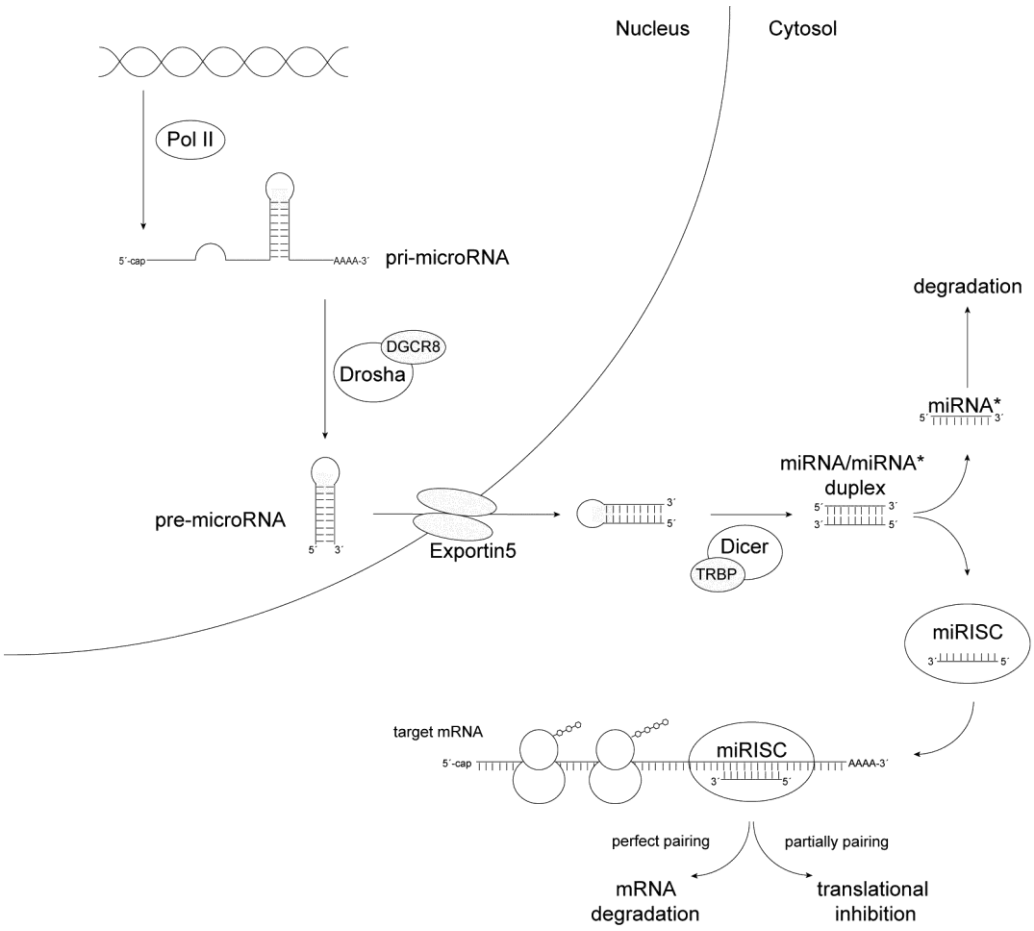

Fig. 6: Biogenesis and mode of action of microRNA molecules in mammalian cells.

Processed by RNA polymerase II, primary miRNA (pri-miRNA; ~100 nt) contains 5'cap and 3'polyadenylation (Sonkoly and Pivarcsi, 2009). RNA molecule with hairpin structure is processed by an enzyme named Drosha, a dsRNA specific ribonuclease, which cooperates with the dsRNA binding protein DGCR8 (DiGeorge syndrome critical region gene 8). Cap and poly-A-tail are eliminated and the hairpin miRNA precursor molecule (pre-miRNA; ~70 nt) is transferred to the cytosol via a transport protein, Exportin5. An RNase III, called Dicer forms miRNA/miRNA*-duplexes (~20 nt) from pre-miRNA with the help of coactivator transactivation-responsive RNA-binding protein (TRBP) (Krol *et al.,* 2010). The miRNA guide strand is incorporated into the microRNA-induced silencing complex (miRISC), whereby passenger strand (miRNA*) is degraded. The miRNA-RISC complex binds to the 3'UTR of target mRNA and due to complementarity of the miRNA and its target sequence protein synthesis is inhibited, either by repression of translation or degradation of the mRNA via deadenylation. In this regard, complementarity of the seed sequence is crucial for the mode of inhibition. A nearly perfect match of sequence between the nucleotides 2 and 8 (seed sequence) presumably leads to decay of the mRNA whereas imperfect binding guides repression of translation (Krol *et al.,* 2010; He and Hannon, 2004; Bartel, 2009).

1.7 Aim of the study

Endothelial cells represent an important part of the vasculature. Hence, they play an essential role in the maintenance of the homeostasis of the body (Fig. 1). A deficiency in endothelial cell functions or an uncontrolled stimulation leads to pathological events like atherosclerosis, hypertension, sepsis or tumor vascularization. Despite intensive research in the field, the regulation of angiogenesis is not yet fully understood. Employment of VEGF to treat poorly vascularized ischemic tissue or anti-VEGF therapies in cancer presents several limitations. Nevertheless, new signaling pathways involved in the regulation of angiogenesis are constantly emerging and thus new targets provide the opportunity to improve existing pro- or anti-angiogenesis therapies.

Highly regulated processes like vascularization are accompanied by increased metabolic effort, as well as by a high protein synthesis rate. Hence, a link to the ER stress signaling pathway UPR, which regulates protein homeostasis, could be established. For a better understanding of the role of UPR in angiogenesis this study focused on BiP due to its major role as stress sensor protein of the UPR signaling pathway and its additional function as a protein folding chaperone. For this, BiP was down-regulated in primary endothelial cells and endothelial-specific processes were subsequently examined. The effect of BiP down-regulation on inflammatory responses of endothelial cells was analyzed by measuring expression of the adhesion molecules, ICAM-1 and E-selectin, or the release of the inflammatory cytokines, IL-8 and MCP-1. Furthermore, essential mechanisms in angiogenesis, particularly migration and the ability to form capillary like structures, were investigated using BiP down-regulated cells. To understand more deeply the effects of BiP on angiogenesis, metabolic activity, proliferation, apoptosis, the expression of VEGR receptors and miRNAs were studied in endothelial cells with down-regulated BiP. Finally, in order to elucidate the relevance of BiP and UPR *in vivo* in physiology and pathology, histological examination was performed with regard to the expression of UPR components BiP, PERK, IRE1α and ATF4 in endothelial cells as well as stromal cells of embryonic and adult skin, granulation tissue and benign and malignant tumors. These latter *in situ* observations were intended to study proof of principle of the the *in vitro* signals generated in the experimental set-up and thus test their relevance for human medicine.

2 Materials and methods

2.1 Materials

2.1.1 Chemicals

Name	Company
Acrylamide/Bisacrylamid solution 19:1, 40%	Bio-Rad, Hercules
Agarose Low EEO	AppliChem, Darmstadt
Albumin solution, 35% in DPBS	Sigma-Aldrich, St. Louis
Alexa Fluor® 594 Phalloidin	Life technologies, Carlsbad
APS	Bio-Rad, Hercules
Arvin	Baxter Deutschland, Unterschleißheim
Blocking reagent	Roche, Freiburg
Bromophenol blue	Bio-Rad, Hercules
BSA	Sigma-Aldrich, St. Louis
Calcein-AM	Invitrogen, Carlsbad
CASYton	Roche, Freiburg
Ciprofloxacin Kabi infusion solution	Fresenius Kabi, Graz
Collagen type I	MP Biomedicals Inc., Solon, Ohio
Collagenase type I	Worthington, Lakewood
Dako Antibody Diluent	Dako, Hamburg
Dako EnVision™ FLEX Wash Buffer (20x)	Dako, Hamburg
Dako Hematoxylin Code CS700	Dako, Hamburg
Dako Target Retrieval Solution (10x), pH6-9	Dako, Hamburg

Name	Company
DMSO	Sigma-Aldrich, St. Louis
DNA ladder 1kb	New England BioLabs, Frankfurt
DNA ladder 100bp	New England BioLabs, Frankfurt
Dulbecco´s phosphate buffered saline	Sigma-Aldrich, St. Louis
Endothelial cell growth supplement	BD Biosciences, Bedford
Entellan	Merck, Darmstadt
Ethanol, p.a.	AppliChem, Darmstadt
Ethidium bromide solution 0,025%	Roth, Karlsruhe
FACS Clean Solution	BD Biosciences, Franklin Lakes
FACS Flow Seth Solution	BD Biosciences, Franklin Lakes
FACS Rinse Solution	BD Biosciences, Franklin Lakes
Fetal calf serum	Sigma-Aldrich, St. Louis
Fibrinogen	Fluka Analytical, Basel
Fibronectin	Roche, Freiburg
Fungizone	Gibco, Carlsbad
Gel/Mount	BiØmeda, Co., Forster City
Gelatin	Sigma-Aldrich, St. Louis
GlutaMAX-I	Gibco, Carlsbad
H_2O_2	Merck, Darmstadt
HCl, 37%	Merck, Darmstadt
HEPES	Sigma-Aldrich, St. Louis
Hoechst Stain 33342	Sigma-Aldrich, St. Louis

Name	Company
IFNγ	Sigma-Aldrich, St. Louis
IL-1β	Strathmann Biotech AG, Hamburg
IMDM	Gibco, Carlsbad
Lectin PHA-L, AlexaFluor 488 conjugated	Invitrogen, Eugene
LPS	Sigma-Aldrich, St. Louis
M199 medium	Sigma-Aldrich, St. Louis
M199 medium, 10x	Sigma-Aldrich, St. Louis
Methanol, p.a.	AppliChem, Darmstadt
MTS	Promega, Madison
Nucleic Acid Sample Loading buffer 5x	Bio-Rad, Hercules
oPD tablets, 20 mg	Sigma-Aldrich, St. Louis
PBS	AppliChem, Darmstadt
Penicillin/Streptomycin mix	PromoCell, Heidelberg
PFA	Merck, Darmstadt
PI/RNase Staining Solution Buffer	BD Pharmingen, Heidelberg
Ponceau S solution	Sigma-Aldrich, St. Louis
Power SYBR® Green PCR Master Mix	Applied Biosystems, Foster City
PromoCell Endothelial Basal Medium MV	PromoCell, Heidelberg
Random Primer $d(N)_6$	Microsynth, Balgach
Rotiphorese® 10x SDS-PAGE	Roth, Karlsruhe
Rotiphorese® 10x TBE buffer	Roth, Karlsruhe
RotiLoad-1 loading buffer	Roth, Karlsruhe

Name	Company
RPMI Medium 1640 (1x)+GLUTAMAX™-I	Gibco, Carlsbad
SDS	Serva, Heidelberg
Streptavidin-biotinylated HRP complex	Amersham Pharmacia Biotech, Freiburg
SuperSignal West Dura chemiluminescent substrate	Thermo Scientific, Bonn
Sodium heparin (Na-Hep)	Sigma-Aldrich, St. Louis
TEMED	Bio-Rad, Hercules
TNFα	Sigma-Aldrich, St. Louis
Tris-HCl 1M	Sigma-Aldrich, St. Louis
Tris Pufferan®	Roth, Karlsruhe
Triton X-100	Sigma-Aldrich, St. Louis
TRIzol® Reagent	Life technologies, Carlsbad
Trypsin-EDTA	Gibco, Carlsbad
Tween 20	Serva, Heidelberg
Xylol	Merck, Darmstadt

2.1.2 Buffers

Stacking gel	
H_2O	3.3 ml
1M Tris-HCl pH 6.8	0.57 ml
20% SDS	22.5 µl
Acrylamide/Bisacrylamide	0.57 ml
TEMED	4.5 µl
10% APS	45 µl

SDS-Resolving gel		7.5%	10%	12.5%	15%
	H_2O	6.5 ml	5.7 ml	5.1 ml	4.3 ml
	1,5M Tris-HCl pH 8.8		3 ml		
	20% SDS		60 µl		
	Acrylamide/Bisacrylamide	2.3 ml	3.0 ml	3.6 ml	4.5 ml
	TEMED		6 µl		
	10% APS		60 µl		

Laemmli Stock for PAGE	
Tris	30 g
Glycine	144 g
H_2O_{dest}	ad 1 l

PAGE running buffer		
	Rotiphorese 10x SDS-PAGE	100 ml
	H_2O_{dest}	ad 1 l

PAGE transfer buffer		
	Laemmli Stock	100 ml
	MeOH	200 ml
	H_2O_{dest}	ad 1 l

2.1.3 Instruments

Instrument	Model	Supplier
Analytical Balance	AI205	Sartorius, Göttingen
Autostainer	Plus	Dako, Hamburg
Balance	LC420	Sartorius, Göttingen
Bioanalyzer	2100	AgilentTechnologies, Santa Clara
Blotting system – wet	Mini TransBlot® module	Bio-Rad, Hercules
Blotting system – wet	Mini-PROTEAN® transfer chamber	Bio-Rad, Hercules
Blotting system – semidry	Trans-Blot® Turbo Blotting System	Bio-Rad, Hercules
Cell counter	CASY – TTC	Roche, Freiburg
Centrifuge	Megafuge 1.0	Heraeus, Hanau
CHEMI-SMART	5100	Peqlab, Erlangen

Instrument	Model	Supplier
Digital Sonifier®	SLPe	Branson, Danbury
Electrophoresis apparatus	Mini-PROTEAN® Tetra Cell	Bio-Rad, Hercules
Flow Cytometer	FACSCalibur	BD Biosciences, Franklin Lakes
Fluorescent Microscope	BZ-9000	Keyence, Neu-Isenburg
Fluorescent Microscope	Ix71 with Delta Vision	Applied Precision, USA
Fluorescent microplate reader	GENios Plus	Tecan, Crailsheim
Horizontal electrophoresis	SubCell GT	Bio-Rad, Hercules
Liquid nitrogen tank	MVE Cryosystem 3000	German-Cryo, Jüchen
Microscope, phase contrast	CTR6000	Leica, Wetzlar
NanoDrop	ND-100	ThermoScientific, Waltham
Transfection System	Neon®	LifeTechnologies, Carlsbad
Power supply	Power Pac 3000	Bio-Rad, Hercules
Real-Time PCR System	7300	Applied Biosystems, Foster City
Rolling mixer	RM5	Karl Hecht GmbH, Sondheim
Shaker	REAX3	Heidolph, Schwalbach
Shaker	UNIMAX1010	Heidolph, Schwalbach
Sliding microtome		Leica, Wetzlar
UV radiator		Bachhofer, Reutlingen

2.1.4 Consumables

Consumable	Supplier
1.5 ml, 2 ml tubes	Eppendorf, Hamburg
6, 24, 96-well cell culture plates	TPP, Trasadingen
12.5 cm^2, 25 cm^2, 75 cm^2 cell culture flasks	Greiner bio-one, Frickenhausen
15 ml, 50 ml tubes	Greiner bio-one, Frickenhausen
5 ml Polystyrene Round-Bottom Tube	Greiner bio-one, Frickenhausen
µ-Slide 8-well, ibiTreat	Ibidi, Martinsried
Cannulas	Braun, Melsungen
CASYton dilution liquid	Innovatis, Reutlingen
Cell scraper	BD Falcon, San Jose
Culture-Insert, µ-Dish 35mm, low, ibiTreat	Ibidi, Martinsried
Cell Strainer, 40 µm Nylon	BD Biosciences, Franklin Lakes
Cover slips, 24x50mm	Menzel, Braunschweig
Cryo 1°C Freezing Container	Nalgene, Rochester
Cryovials	Nalgene, Rochester
F96 Maxisorp NUNC-Immuno Plate	Thermo Scientific, Bonn
FIA-Plate, black, 96-well, flat bottom	Greiner bio-one, Frickenhausen
Lab-Tek II CC2 Glas Chamber Slide	Nunc, Rosklide, Denmark
Mircoplate, 96-well, PS, F-Bottom, crystal-clear	Greiner bio-one, Frickenhausen
Optical adhesive film	Applied Biosystems, Foster City
Protran BA85 Nitrocellulose Transfer Membrane	GEHealthcare, Chalfont StGiles
Real-time PCR optical 96-well reaction plate	Applied Biosystems, Foster City
Scalpels	Braun, Tuttlingen

Consumable	Supplier
Syringe filters	Nalgene, Rochester
Super Frost Slides	Menzel, Braunschweig
Whatman 3mm CHR	VWR, Darmstadt
Whatman GB003 Blotting Paper	VWR, Darmstadt

2.1.5 Kits & Arrays

Kit	Supplier
Agilent RNA 6000 Pico Kit	Agilent Technologies, Santa Clara
Anaerobic indicator	OXOID Ltd., Hants
AnaeroGen™Compact	In vitro diagnosticum, Hampshire
Annexin V-FITC Apoptosis Detection Kit II	BD Biosciences, Franklin Lakes
Dako EnVision+System-HRP; K4011	Dako, Hamburg
DuoSet human CCL2/MCP-1 ELISA kit	R&D Systems, Wiesbaden
DuoSet human CXCL8/IL-8 ELISA kit	R&D Systems, Wiesbaden
EndoFree® Plasmid Maxi Kit	Qiagen, Hilden
Human MicroRNA Array III	Signosis Inc., Sunnyville
miRNeasy Mini Kit	Qiagen, Hilden
RNeasy Micro Kit	Qiagen, Hilden
Neon® Transfection System 10µl Kit	Life Technologies, Carlsbad
Omniscript RT Kit	Qiagen, Hilden
Taq PCR Core Kit	Qiagen, Hilden

2.1.6 Antibodies

Antibody	Source	Application	Supplier
Anti-ATF4	rabbit	IHC-P	Proteintech, Manchester
Anti-BiP	rabbit	W, IHC-P	Cell Signaling, Danvers
Anti-Caspase3	Rabbit	W	Cell Signaling, Danvers
Anti-CD31	mouse	IF	Millipore, Darmstadt
Anti-ERK2	rabbit	W	SantaCruzBiotechnology, Heidelberg
Anti-E-Selectin	mouse	EIA	Bender MedSystems, Vienna
Anti-Grp94	rabbit	W	Cell Signaling, Danvers
Anti-FLT 1	rabbit	W	Cell Signaling, Danvers
Anti-ICAM-1	mouse	EIA	Bender MedSystems, Vienna
Anti-IRE1α	rabbit	W, IHC-P	SantaCruzBiotechnology, Heidelberg
Anti-KDR	rabbit	W	Cell Signaling, Danvers
Anti-Ki67	mouse	EIA	Dako, Glostrup
Anti-PERK	rabbit	W, IHC-P	Cell Signaling, Danvers
Anti-phospho-Tyrosin	rabbit	W	Cell Signaling, Danvers
Anti-rabbit secondary antibody, HRP-linked	Goat	W	Jackson-Immunoresearch, West Grove

2.1.7 Oligonucleotides

2.1.7.1 Primers

Primer	Sequence
ATF4 fwd	5’-CTGCCCGTCCCAAACCTTAC-3’
ATF4 rev	5’-CTGCTCCGCCCTCTTCTTCT-3’
ATF6 fwd	5'-CAGAACCCCAGCCACTTTCT-3’
ATF6 rev	5’-GGCTCCGGTGAAGAGAGACT-3’
BiP fwd	5’-ACTATGAAGCCCGTCCAGAAAGT-3’
BiP rev	5’-TCGAGCCACCAACAAGAACA-3’
FLT1 fwd	5’-AAGCCACCAACCAGAAGGGCT-3’
FLT1 rev	5’-GACTTGTCCGAGGTTCCTTGAACAG-3’
IRE1α fwd	5’-CTGGAGCCTAGAGAAGCAGC-3’
IRE1α rev	5’-TTCTCATGGCTCGGAGGAGA-3’
KDR fwd	5’-TAGGCACGGCGGTGATTGCC-3’
KDR rev	5’-GTTCCCCTCCATTGGCCCGC-3’
PERK fwd	5’-CCTTGGTGTCATCCAGCCTT-3’
PERK rev	5’-ATGCTTTCACGGTCTCGGTC-3’
RPL13A fwd	5’-CCTGGAGGAGGAGAGGAAAGAGA-3’
RPL13A rev	5’-TCCGTAGCCTCATGAGCTGTT-3’
VEGF fwd	5’-CGAGGGCCTGGAGTGTGT-3’
VEGF rev	5’-CCGCATAATCTGCATGGTGAT-3’

Primer	Sequence
Xbp1 u/s fwd	5’-CTGGAACAGCAAGTGGTAGA-3’ (Shang, 2005)
Xbp1 u/s rev	5’-CTGGGTCCTTCTGGGTAGAC-3’ (Shang, 2005)
Xbp1 unspliced fwd	5’-CAGACTACGTGCACCTCTGC-3’
Xbp1 spliced fwd	5‘-TCTGCTGAGTCCGCAGCAGG-3‘ (Szegezdi *et al.,* 2008)
Xbp1 unspliced/spliced rev	5’-CTTCTGGGTAGACCTCTGGG-3’ (Szegezdi *et al.,* 2008)
Xbp1 unspilced fwd	5’-ACAGCGCTTGGGGATCATGGATG-3’
Xbp1 unspilced rev	5’-CTGGGCCTGCACGTAGTCTGAGT-3’

Not cited primers were generated using BLAST on NCBI homepage (http://blast.ncbi.nlm.nih.gov/Blast.cgi?PAGE_TYPE=BlastSearch&BLAST_SPEC=OGP__9606__9558).

All primer pairs were synthesized by Microsynth, Balgach.

2.1.7.2 siRNAs

siRNA (target protein)	Sequence (antisense)	Supplier
Silencer® Negative Control #1		Ambion, Austin
s6980 (BiP)	UCUAGUAUCAAUGCGCUCCtt	Ambion, Austin
s6981 (BiP)	UACGCUACAGCUUCAUCUGgg	Ambion, Austin
S18102 (PERK)	UCUUGUUCCAUUUCGUCACta	Ambion, Austin
S200432 (IRE1α)	UAACAUACCAGAUGUCCUGct	Ambion, Austin

2.1.8 Plasmids

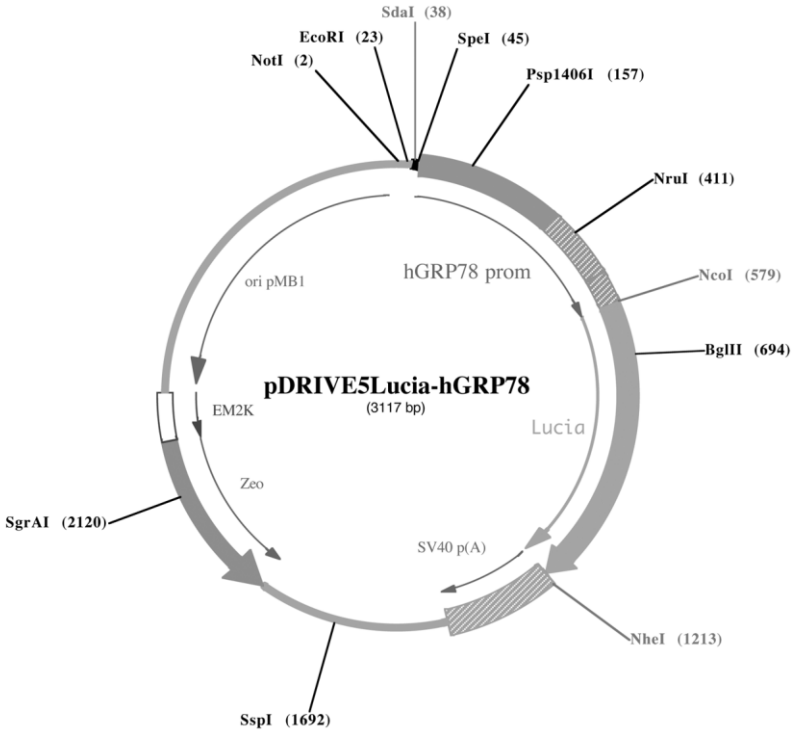

Fig. 7: Reporter vector map pDRIVE5Lucia-hGRP78.

Reporter vector with a size of 3117 bp contains several features. Thus, the reporter gene encodes for Lucia®, a secreted coelenterazine-utilzing luciferase. The gene is located downstream of the promoter for human GRP78 (synonymic for BiP). Additionally, the plasmid contains SV40 polyadenylation signal, the origin of replication for *E.coli* pMB1 Ori, EM2K as a bacterial promoter for constitutive expression of antibiotic resistance gene in *E.coli* and Zeo gene encodes Zeocin™ resistance for selection of transformed *E.coli*.

2.1.9 Software

Software	Developer
2100 expert software	Agilent
GraphPad Prism 5	GraphPad software
ImageJ	National Institute of Health
SDS Software	Applied Biosystems

2.2 Methods

2.2.1 Cell culture

2.2.1.1 Isolation of human umbilical vein endothelial cells (HUVEC)

Endothelial cells used for *in vitro* experiments were isolated from the vein of umbilical cord (Peters *et al.,* 2002; Jaffe *et al.,* 1973). After birth, umbilical cords were preserved in transport buffer, consisting of HEPES buffer, 1% Penicillin/Streptomycin mix (Pen/Strep), 1 % Ciprofloxacin Kabi and 1 % Fungizone. Isolation of the endothelial cells was completed within 4 days after birth.

For isolation transport buffer was discarded and remains of blood were removed from the umbilical cord. Cannulas were inserted into the vein of the umbilical cord, the vessel was washed using HEPES buffer, while permeability and tightness of the vein were inspected. Afterwards the vein was filled with collagenase type I (f.c. 0.05 % in HEPES) and the umbilical cord was incubated at 37°C for 15 min. After digestion, the enzyme solution containing detached cells was collected in a 50 ml tube. The vein was rinsed again with 20 ml of cell culture medium to collect remaining cells. The solutions were combined and the cell suspension was centrifuged at 390 x g for 5 min. The cell pellet was resuspended in common cell culture medium M199 containing 20% fetal calf serum (FCS), 1 % Pen/Strep, 0.34 % GlutaMAX-I (GI), 25 µg/ml endothelial cell growth supplement (ECGS) and 25 µg/ml sodium heparin, seeded onto a 25 cm^2 flask pre-coated with 0.2 % gelatin and incubated in a humidified atmosphere at 37°C (5 % CO_2). First seeding was considered passage 0. Medium was changed every two to three days.

2.2.1.2 Cell lines

In addition, several cell lines were used for transfection of the cells with reporter gene assay. Two cell lines used were of endothelial origin. The ISO-HAS-1 cell line represents a clone of the ISO-HAS cell line (Masuzawa *et al.,* 1999), in which a feeder layer of mouse cells was removed (Unger *et al.,* 2002). Originally, the endothelial cell line originates from a human haemangiosarcoma. The cell line, HPMEC-ST1, was generated from immortalized human pulmonary microvascular endothelial cells co-transfected with pSV30neo and pC1.neo.hTERT as already published (Krump-Konvalinkova *et al.,* 2001). HeLa cells, gained from a cervix adenocarcinoma, were used as control cells without endothelial origin. The cell line was purchased from ATCC (LGC Standards GmbH, Wesel).

2.2.1.3 Passaging of the cells

In general, cells were cultured in 25 cm^2 or 75 cm^2 flasks depending on the required amount of cells for particular experiments. When the cells reached confluence, the cell monolayer was detached with 0.25% trypsin-EDTA. The enzymatic reaction was stopped with medium containing FCS, in most cases with the cell-specific culture medium (for an overview see Tab. 1). According to a cell type-dependent splitting ratio, cells were seeded in a new cell culture flask or applied in an experiment-dependent format. One trypsinization step was seen as a change in passage. All experiments using HUVEC were performed in passage 3. Cell lines were used in higher passages. Commonly, the cell lines were cultured over a time period of three months.

Tab. 1: Overview of cell culture medium for the cell types used.

Cell type	Cell culture medium	Coating	Splitting ratio
HUVEC	M199 (20% FCS, , 1 % P/S, 0.34 % GI, 25 µg/ml ECGS, 25 µg/ml Na-Hep)	0.2% gelatin	1:3
ISO-HAS-1	PromoCell Endothelial Basal Medium MV (15% FCS, 1 % P/S, 10 µg/ml Na-Hep, 2,5 µg/ml bFGF)	0.2% gelatin	1:3
HPMEC-ST1	PromoCell Endothelial Basal Medium MV (15% FCS, 1 % P/S, 10 µg/ml Na-Hep, 2,5 µg/ml bFGF)	0.2% gelatin	1:3
HeLa	RPMI (10 % FCS, 1 % P/S)	No coating	1:5

2.2.1.4 Cell freezing

For storage of e.g. isolated primary endothelial cells, the cells were frozen. For this the monolayer was detached with 0.25% trypsin-EDTA, the reaction was stopped with common cell culture medium and the cell suspension centrifuged at 390 x g for 5 min. The cell pellet was resuspended in cell culture medium containing 10% DMSO and filled in cryovials. For slow freezing process the vials were placed at -80°C in the Cyro 1°C Freezing Container overnight. Afterwards, the vials were transferred to liquid nitrogen. For culturing frozen cells again, the vials were thawed briefly at 37°C and, the cell suspension was centrifuged (390 x g, 5 min) to remove DMSO and the cells were seeded in the conventional cell culture medium (Tab. 1).

2.2.1.5 Cell seeding densities

Cells were seeded on pre-coated equipment at specific densities, depending on the experiments planned (Tab. 2). To count the cells, the monolayer was detached with trypsin, the reaction was stopped with FCS-containing medium and 100 µl of cell suspension were diluted in 10 ml CASYton. The suspension was measured in a CASY cell counter using a cell-specific protocol.

Tab. 2: Cell seeding densities.

Format	Density [cells/well]
6-well	200 000 – 300 000
24-well	50 000 – 100 000
96-well	15 000
8-well glass chamber slide	100 000
Culture-Insert, µ-Dish	70 000 per side

2.2.1.6 Treatment of endothelial cells with different stimuli

To investigate the expression of RNA and proteins in endothelial cells in response to different stimuli cells were seeded in an experiment-dependent format. The day after seeding cell culture medium was changed. On day three the cells were treated with different compounds added to fresh cell culture medium. The concentrations used are presented in the Tab. 3.

Tab. 3: Used concentrations of specific treatment

Stimuli	Concentration
Tunicamycin	2 µg/ml
TNFα	75 U/ml; 300 U/ml
VEFG	50 ng/ml
bFGF	5 µg/ml
IL1β	10 U/ml
IFNγ	500 U/ml
LPS	1µg/ml
SubAB	100 ng/ml
$SubA_{A272}B$	100 ng/ml
Camptothecin	6 µM

In the case of anoxic treatment an anaerobic pouch system (AnareroGen™Compact) was used. At the selected time point the cells were pre-seeded on a cell culture plate, and put into a plastic pouch. Additionally, a paper gas-generating sachet, containing ascorbic acid and activated carbon, was added and the pouch was closed tightly. In contact with air, a chemical reaction is activated in the sachet, in which oxygen is absorbed and carbon dioxide is produced. Due to this process an anoxic atmosphere is created. An anaerobic indicator was added to the system to monitor experimental conditions.

2.2.2 Transfection of cells

Cells were transfected with siRNA molecules or plasmid DNA via electroporation using the Neon® Transfection System and Neon® Transfection System 10µl Kit. Cells were detached and centrifuged (390 x g, 5 min) to remove cell culture medium and prevent the influence of FCS on transfection. The cell pellet was resuspended in R-Solution, 12 µl per 200.000 cells, which constitutes one electroporation setup. Subsequently, 50 nM siRNA or 0.3 µg plasmid DNA were added per transfection. The electroporation needles were loaded with cell suspension containing siRNA/plasmid DNA and put into the electroporation station. An electrical impulse was set which perforated the cell membrane and siRNAs/plasmid entered the cell. Intensity, length and amount of electrical impulse are specific for cell types and have to be considered for successful transfection (for cell specific adjustments see Tab. 4). After setting the electrical impulse the cells were transferred into a new reaction tube and centrifuged (2500 rpm; 5 min). The supernatant was removed to eliminate transfection buffer and the cells were resuspended in cell culture medium without FCS and seeded in the format selected for a particular experiment (for densitiy and coating see Tab. 2). 6 to 8 h after transfection FCS was added. The day after transfection the medium was changed. Success of transfection with siRNAs was checked via real time qPCR or Western Blot analysis for every experiment. The experiments with down-regulation of a minimum of 50 % were selected for further analysis.

Tab. 4: Technical adjustment for electroporation of different cell types

Cell type	Pulse voltage	Pulse width	Number of pulses
HUVEC	1300	20	2
ISO-HAS-1	1300	20	2
HPMEC-ST1	1200	20	2
HeLa	1400	20	2

2.2.3 Cell viability

2.2.3.1 MTS conversion assay

For indirect measurement of cytotoxicity, metabolic activity of cells was estimated using the MTS conversion assay. Conversion of MTS (3-(4.5-dimethylthiazol-2-yl)-5-(3-carboxymethoxyphenyl)-2-(4-sulfphenyl)-2H-tetrazolium) to formazan was detected photometrically. MTS was diluted in medium (1:5) and added to the cells. After

incubation of the cells at 37°C and 5%CO_2 for 1.5h supernatants were transferred to a new microplate. Optical density was measured at 492 nm. For the blank sample medium with MTS incubated in a well without cells was used.

2.2.3.2 Crystal violet staining

At the end of an experiment cell culture medium was aspirated and cells were washed with PBS. After the washing step the cells were fixed with 2-propanol for 15 min. To remove the alcohol, the cells were washed again with PBS-0.05 Tween 20 for three times. Afterwards the cells were stained with 0.1 % crystal violet solution for 20 min with agitation. Samples were washed with water to remove surplus staining solution and air dried. Subsequently, crystal violet was extracted by the incubation with 33 % CH_3COOH for 20 min under gentle shaking. The supernatant was transferred to a new microplate. Optical density was measured at 600 nm. Pure 33 % CH_3COOH acted as blank. Due to the fact that crystal violet stains cell nuclei, the values were used to determine relative cell number (Gillies *et al.,* 1986).

2.2.4 Molecular biology – gene expression analysis

2.2.4.1 RNA isolation

2.2.4.1.1 RNA isolation using RNeasy Micro Kit

RNA was isolated using the RNeasy Micro Kit (Qiagen), which combines RNA binding properties of a silica membrane with the speed of microspin technology. To lyse the cells medium was aspirated and the cell layer washed with PBS. After the washing step RLT buffer containing 10 µl/ml ß-mercaptoethanol was added directly to the cells to stabilize the lysate. If RNA was not isolated immediately, samples were stored at -80°C. Subsequently, RNA in the cell lysates was precipitated with 1 volume of 70% EtOH, the mixture was added to a RNeasy spin column and centrifuged for 15 s at 10000 rpm at RT. Subsequent to this, 350 µl RW1 buffer were added per column, followed by centrifugation with previous adjustments. In the next step incubation with DNase I for 15 min led to digestion of DNA. The column was then rinsed again with 350 µl RW1 buffer and subsequently washed with 500 µl RPE buffer (centrifugation step: 10000 rpm, 15 sec, RT), followed by washing with 500 µl of 80% EtOH (centrifuged for 2 min). To dry the membrane the column was then centrifuged with opened lid for 5 min. Finally, 14 µl of RNase free water was added to the membrane and columns were centrifuged for 1 min at maximum speed again to elute isolated RNA.

2.2.4.1.2 RNA isolation using phase separation in combination with column-based isolation kit

For isolating RNA from the cells embedded in collagen/fibrin gel, phase separation, a step of acid guanidinium thiocyanate-phenol-chloroform extraction (AGPC) (Chomczynski and Sacchi, 1987) and further purification using column-based isolation methodology were combined.

The medium was removed and samples were lysed with 350 µl TRIzol® Reagent. 70 µl of chloroform were added and the mixture was vortexed vigorously. After incubation on ice for 5 min, the samples were centrifuged for 10 min at maximum speed. Three phases were formed, whereby the lower organic phase contained proteins, the interphase contained DNA and in the upper aqueous phase RNA molecules were enclosed. This aqueous layer was harvested very carefully and transferred to a new RNase-free tube. Afterwards, equal volume of 70 % EtOH was added to start precipitation. From this point RNA isolation was carried out with the kit system. Thus, the aqueous phase/EtOH mixture was added to the RNeasy spin column from the RNeasy Micro Kit and RNA isolation was continued as described above.

2.2.4.2 RNA quantification and quality control

The concentration of isolated RNA was measured using a NanoDrop spectrophotometer. To comply with purity standard of isolated RNA and to guarantee successful cDNA synthesis, absorbance ratios were maintained in a range of A_{260}/A_{280} = 1.8 - 2.1 and A_{260}/A_{230} = 1.0 - 2.1. A low A_{260}/A_{280} value indicates contamination with proteins and a low A_{260}/A_{230} value is a sign of high salt or phenol concentration.

Quality of RNA was monitored using Agilent RNA Pico Array and Bioanalyzer according to the manufacturer's user manual. As recommended, RNA amounts in a range of 50-5000pg were used. RNA was denatured to minimize secondary structure by incubating samples at 72°C for 2 min. A gel dye mix was loaded onto a chip. Set in the chip priming station, the gel dye mix was pressed into capillaries of the chip. Loaded with samples and ladder, the chip was put into Bioanalyzer and RNA was separated by capillary electrophoresis. Finally, the results were shown as an electropherogram or a gel. On the base of the entire electrophoretic trace of an RNA sample, the software determines RNA integrity number (RIN). RNA with RIN of 8-10 was used for further experiments to ensure RNA integrity with regard to RNA quality, comparison of samples and reproducibility of experiments.

2.2.4.3 Reverse Transcription

To synthesize complementary DNA (cDNA), RNA was reverse transcribed using Omniscript RT Kit (Qiagen). Amounts of 10 to 1000 ng RNA were used. The same quantities from different samples of an experimental series were taken. The reaction volume was adjusted to 10 µl with RNase free H_2O. 10 µl of the mastermix (containing 2.5 µl H_2O, 2 µl 10x Buffer RT, 2 µl dNTP Mix (5mM each dNTP), 2 µl Random Primer (100 µM), 0.5 µl Inhibitor (20 U), 1 µl Omniscript Reverse Transcriptase) were then added and the samples were incubated at 37°C for 60 min. cDNA samples were stored at -20°C.

2.2.4.4 Polymerase Chain Reaction (PCR)

To amplify cDNA products, the Polymerase Chain Reaction (PCR) was used. During the denaturation step, the reaction was heated to 94°C for 30 s, which resulted in melting of DNA template and primers due to disruption of hydrogen bonds between complementary bases of the DNA strands. As a result the templates are available as single stands of DNA. In the ensuing annealing step reaction the temperature was reduced to 50-65°C for 30 s, allowing annealing of the primers to the single-stranded DNA template. Annealing temperature was adjusted according to specific primers. Primer-template hybrids served as a matrix for the DNA polymerase, which bound and synthesized complementary strand of DNA. This process occurred in the elongation step where temperature according to polymerase temperature optimum was applied, but commonly 72°C was adjusted.

For semi-quantitative PCR, the Taq PCR Core kit was used. Each primer, forward and reverse, was applied in a concentration of 0.8 µM. cDNA obtained from 10 ng RNA was used for each reaction in a total volume of 25 µl. The reaction was performed in a thermocycler with the following program:

The reaction started with incubation at 95°C for 10min to activate the polymerase. Denaturation step: 94°C 30sec, annealing step: 56-65°C (depending on the primer composition) 30sec and elongation step: 72°C 30sec was repeated 35 times in total. At the end, samples were incubated at 72°C for 10min to guarantee complete reaction. PCR products were stored at 4°C until gel electrophoresis.

2.2.4.5 Agarose gel electrophoresis

Amplified PCR products were separated via gel electrophoresis using agarose gels. The gels contained the intercalating agent ethidium bromide in a concentration of 0.16 µg/ml to stain the amplification products. Depending on the product size 1 – 3 % agarose gels were used. Samples were mixed with loading buffer and loaded into the wells of the gel. Due to voltage application (80-100 V) negatively charged DNA molecules move towards the positively charged anode. Because of different sizes and accompanied weight, PCR products were separated. Electrophoresis was performed in 1 x Tris-Borat-EDTA buffer (TBE buffer). With help of adequate markers (1 kb DNA ladder or 100 bp ladder), sizes of the products were checked upon ethidium bromide visualization in ultraviolet light.

2.2.4.6 Quantitative real time PCR

Using quantitative real-time PCR (qRT PCR) gene expression at RNA level was investigated. qRT PCR was performed with a SYBR Green DNA binding fluorescent dye. cDNA obtained from 3,75 ng RNA was taken for each reaction. For specific amplification 12.5 pmol of each primer, forward and reverse, were added to 12.5 µl Power SYBR® Green PCR Master Mix and cDNA. Reactions were adjusted to a total volume of 25 µl with H_2O. qRT PCR was performed in an Applied Biosystems 7300 Real-Time PCR System. The reaction was started at 95°C for 10 min followed by 40 cycles of amplification at 15 s at 95°C and 1 min at 60°C. DNA dissociation at the end of reaction was performed by slowly raising the temperature from 60°C to 95°C to confirm the product specificity.

The data were analyzed using SDS Software to obtain Ct (cycle threshold) values. To determine relative gene expression with the Ct method, RPL13A mRNA was used as endogenous control. Ct values of endogenous control were subtracted from Ct values of the gene of interest and this resulted in the so-called ΔCt value to secure the equal amount of template in each reaction. Subsequently, ΔCt of the control sample was subtracted from ΔCt of the experimental sample to obtain ΔΔCt. Relative expression of the gene of interest was calculated with the formula RQ (relative quantification) = $2^{-\Delta\Delta Ct}$.

For statistical evaluation log10 of RQ values were compared. Due to the fact that control was always set as 1, it was assumed that the data were not normally distributed. Therefore, for real time PCR statistics Wilcoxon test was applied.

2.2.4.7 microRNA biology

2.2.4.7.1 microRNA isolation and quantification

For investigation of microRNA expression profile, total RNA, including small RNA molecules (RNAs), was isolated using the miRNeasy Mini Kit according to the user manual. For this, cells were lysed with 700 µl QIAzol® Lysis Reagent per 6-well at the end of an experiment. Transferred to 1.5 ml reaction tube, the samples were vortexed for 1 min to perform homogenization. After 5 min of incubation at RT, 140 µl of chloroform were added and the samples were mixed again vigorously. Different phases were separated by centrifugation (1200 x g, 15 min, 4°C). The upper aqueous phase, which contains RNA molecules, was transferred to a new reaction tube and 1.5 volumes of 100% EtOH were added to ensure binding properties of RNA molecules with a minimum of 18 nucleotides. Samples were mixed by pipetting up and down and transferred to an RNeasy Mini spin column. RNA molecules bind to the silica-based membrane and deposits of phenols and other contaminants were washed away in three subsequent washing steps. The membrane was dried with an additional centrifugation step at 1200 x g for 1 min at RT. Total RNA including small RNAs was eluted with 30 µl of RNase free water. The amount of isolated RNA as well as RNA quality were measured as described in 2.2.4.2.

2.2.4.7.2 microRNA array

With the help of the Human MicroRNA Array III the expression of 132 miRNAs and their isoforms was assessed. The array analysis was performed according to the manufacturer´s instructions. The principle of the array is shown in Fig. 8.

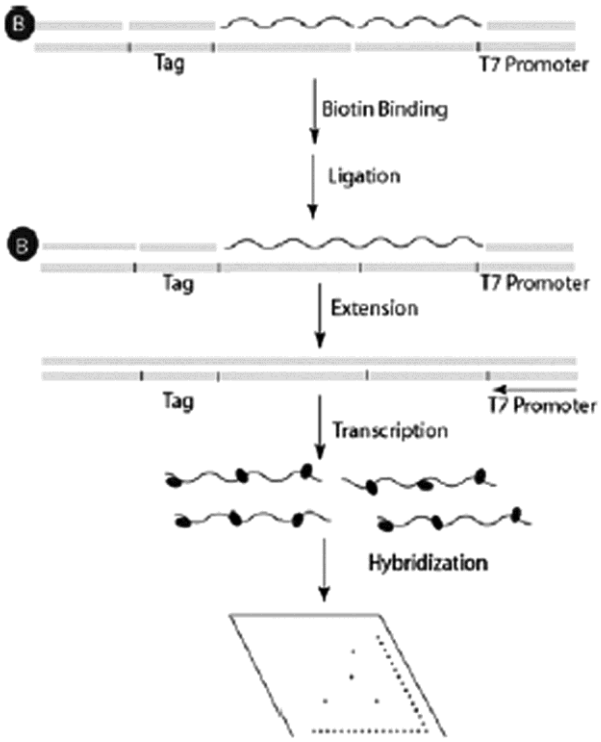

Fig. 8: Principle of the Human MicroRNA Array III.

Isolated total RNA containing small RNAs was mixed with the provided oligo mix, array detection oligo and annealing buffer. The molecule was targeted by two oligos which hybridize half of the miRNA each. The samples were incubated for 5 min at 72°C and for 90 min at 53°C and in the case of perfect matching miRNA/oligo hybrids were formed. Subsequently, beads and bead-binding buffer were added to the samples and incubated at 37°C for 30 min. The beads bound to the RNA/DNA duplex afforded the opportunity for selective magnetic bead separation. Simultaneously, free oligos and RNAs molecules were washed away. Combined with ligation buffer and ligase, samples were incubated for 90 min at 37°C. In this step miRNA-directed oligos were ligated. Biotin binds to the hybrids and DNA ligase ligate the strands. Following addition of extension buffer and incubation at 94°C for 2 min, 54°C for 1 min, 72°C for 1.5 min and 94°C for 30 s led to separation of ligated molecules from the beads. Due to extension, stability of the complementary oligos was increased. After exposure of the samples to a magnetic field, the solution was kept for further steps, whereby beads were discarded. Labeling mix and T7 RNA polymerase were added. During the incubation phase of 1 h at 37°C ligated DNA molecules were amplified. Array membranes were pre-hybridized with warm hybridization buffer at 42°C for 60 min. Subsequently, samples were added to the membranes. They were incubated overnight at 42°C under shaking and the membranes then washed with hybridization buffer. In the following detection step, membranes were washed with detection buffer, blocked

with blocking buffer for 30 min at RT under shaking and Streptavidin-HRP conjugate was added. After incubation for 45 min at RT membranes were washed three times with detection buffer. Upon adding Substrate A and B (mixed in equal amounts), chemiluminescence was recorded with a CHEMI-SMART 5100. The array was evaluated using the schematic diagram of the array normalized to positive and internal controls.

2.2.4.8 Molecular cloning

2.2.4.8.1 Purification of reporter plasmid in miniscreen

Reporter vector was bought ready-to-use from InvivoGen. GT116 *E.coli* bacteria (phenotype: *F-, mrcA, Δ(mrr-hsdRMS-mcrBC), Ø80lacZΔM15, ΔlacX74, recA1, endA1 Δdcm ΔsbcC-sbcD*) were already transformed by the plasmid. Lyophilized bacteria were resuspended in 1 ml LB medium and streaked on Zeocin™ LB agar plates cast of *E.coli* Fast-Media® Zeo agar (provided with bacteria). Plates were incubated over night at 37°C. Single colonies were picked, transferred to a master plate for preservation and raised in 5 ml Fast-Media® Zeo agar liquid (also provided) at 37°C.

To check if the cells really contained pDRIVE5Lucia-hGRP78 vector, the plasmid DNA was isolated and analyzed later via restriction digestion. For this, 1.5 ml of the liquid culture were centrifuged for 1 min at maximum speed and the supernatant was removed. Cells were resuspended in 300 µl TENS solution (containing: 10 mM Tris pH 7.5, 1 mM EDTA, 0.1 N NaOH, 0.5 % SDS) and vortexed for 5 s. 150 µl of sodium acetate (3 M, pH 5.2) were then added and the suspension vortexed again for 5 s and the samples centrifuged for 2 min. The supernatant was transferred to a new reaction tube and the pellet, which contained bacterial debris, was discarded. 900 µl of pre-chilled (-20°C) 100 % EtOH were added to the supernatant to precipitate DNA. After spinning the samples for 5 min, the DNA pellet was washed with 1 ml of 70 % EtOH. Supernatant was removed and the pellet was air-dried, subsequently resuspended in 30 µl TE buffer (10 mM Tris pH 7.5, 1 mM EDTA) and the DNA concentration measured using a NanoDrop spectrophotometer.

2.2.4.8.2 Restriction digestion of the reporter plasmid

For analyzing the accuracy of the plasmid, isolated plasmid was subjected to restriction digestion. One digestion reaction contained 2 µg plasmid DNA, 2 µl of Tango buffer, 1 µl restriction enzyme A, 1 µl restriction enzyme B (or 2µl of enzyme in single restriction) and filled up with H_2O up to a final volume of 20 µl. For linearization of the plasmid, samples were digested with the restriction enzyme NheI. Enzymes NheI and

Psp1406I were used for double digestion. Restriction was executed for 1 h at 37°C. DNA fragments were separated via electrophoresis using 1 % agarose gel. With the help of the restriction map the outcome of restriction was assessed. Appearance of one fragment with a size of 3117 bp in linearized sample and two fragments with sizes of 1056 bp and 2061 bp indicated that the isolated plasmid was the pDRIVE5Lucia-hGRP78 vector.

2.2.4.8.3 Endotoxin-free plasmid purification

For purification of the plasmid in high concentration for the experiments, the EndoFree® Plasmid Maxi Kit was used following the manufacturer's user manual. After positive restriction digestion, 5 ml of LB medium containing Zeocin were inoculated with positive bacteria colonies from the master plate. The bacterial suspension was incubated overnight at 37°C and 200 rpm. The next day, 250 ml of LB medium containing Zeocin were inoculated with the preparatory culture in a shaking flask with baffles and incubated overnight at 37°C and 160 rpm. Afterwards, the LB culture was harvested by spinning at 600 x g for 15 min at 4°C in a 50 ml tube. Supernatant was discarded and the previous step was repeated until the whole culture was harvested. The bacterial pellet was resuspended in 10 ml buffer P1, 10 ml of buffer P2 being added and mixed by inversion to lyse bacteria. The lysate was incubated for 5 min at RT. Subsequently, 10 ml of chilled buffer P3 were added, the lysate was mixed again by inverting and transferred to a barrel of a kit containing cartridge. After 10 min of incubation, the cell lysate was pressed through the cartridge. 2.5 ml buffer ER were added to the filtered lysate, mixed by inverting and incubated for 30 min on ice. Meanwhile, the QIAGEN-tip was equilibrated with 10 ml QBT buffer. After incubation time, the filtered lysate was applied to the tip which was then washed twice with 30 ml QC buffer. Isolated and purified DNA was eluted using 15 ml buffer QN into an endotoxin-free tube. DNA was further precipitated by adding 0.7 volumes of isopropanol. Samples were centrifuged at 10000 x g for 45 min at 4°C and the supernatant carefully removed. The glassy pellet was washed with 5 ml endotoxin-free 70% EtOH and centrifuged again under the same conditions for 15 min to remove precipitated salts and replace the isopropanol for better solubility. The supernatant was removed and the pellet air-dried for 5-10 min. Finally, the pellet was redissolved in 100-150 µl endotoxin-free TBE buffer. The concentration of purified plasmid DNA was measured using a NanoDrop spectrophotometer. Restriction digestion was performed to check the plasmid, as described in 2.2.4.8.2.

The master plate with *E.coli* colonies positive for pDRIVE5Lucia-hGRP78 was stored at 4°C. Additionally, glycerol culture was prepared for long-time storage at -80°C. Thus,

600 µl cells grown in LB medium and 600 µl sterile 100 % glycerol were mixed and transferred to a cryo vial.

2.2.4.9 Reporter gene assay

Purified reporter plasmid was transfected into the different cell lines via electroporation 2.2.2. 48h after transfection, cells were stimulated with different stimuli. All substances were applied in Endothelial Basal Medium MV containing 0.5 % FCS, 1 % P/S, 10 µg/ml Na-Hep, 2.5 µg/ml bFGF. After 15 min, 30 min, 1 h, 2 h, 4 h, 8 h and 24 h 10 µl of the medium were transferred into a black 96-well plate. Per well, 50 µl of coelenterazine-based luminescence assay reagent QUANTI-Luc™ were added and bioluminescence was measured directly in a microplate reader GENios Plus. Produced light signal was registered as relative light units and normalized to the signal of transfected, but untreated cells. Non-transfected cells represented the blank sample.

2.2.5 Protein biochemistry – protein expression analysis

2.2.5.1 ELISA

For detection of IL-8 and MCP-1 release by HUVEC into the cell culture medium DuoSet IL-8 and MCP-1 ELISA kits were used. First, Maxisorp NUNC-Immuno Plates were pre-coated with 100 µl/well capture antibody diluted in PBS (f c 4 µg/ml) and incubated overnight at RT. Afterwards, wells were washed with PBS-0.05% Tween 20 (300 µl/well). By adding 300 µl/well Block Buffer or Reagent Diluent (depending on Kit) unspecific binding sites were saturated. After 1 h of incubation, plates were washed again. Then, 100 µl of samples (supernatant of experiments, stored at -80°C) or standards diluted in Reagent Diluent were added and incubated for 2 h at RT. After a further washing step, the wells were incubated with 100 µl of biotinylated Detection Antibody (100 ng/ml) for 2 h at RT. Plates were washed again and 100 µl of the working dilution of Strepatvidin-HRP were applied for 20 min (incubated in the dark). After another washing step, 100 µl of Substrate Solution (mixture of H_2O_2 and tetramethylbenzidine) were added to each well for 20 min. The reaction was stopped by 50 µl of 2 N H_2SO_4 and the optical density was measured at 450 nm with the wavelength correction at 540 nm in a plate reader. The amount of the protein of interest was determined from the standard curve.

2.2.5.2 Detection of protein expression in fixed cells by enzyme immunoassay (EIA)

The expression of ICAM, E-selectin or Ki-67 was investigated in fixed cells by enzyme immunoassay (EIA). HUVEC were washed with PBS and fixed with a 2:1 methanol/ethanol mixture for 15 min at RT. Afterwards, the cells were washed 3 times again to remove the alcohol completely. For saturation of unspecific binding sites, fixed cells were incubated with blocking reagent and 1 % H_2O_2 for 30 min at 37°C. Treatment with H_2O_2 depleted the activity of endogenous peroxidase and represented an important step for the detection. Subsequently, the samples were incubated with a primary antibody diluted in blocking reagent for 45 min at 37°C with shaking (50 rpm). Following washing with PBS + 0,025 % Tween 20 for 3 times, the cells were incubated with biotinylated secondary antibody for 45 min at 37°C with 50 rpm shaking. After additional 3 washing steps the samples were incubated with biotinylated Streptavidin-HRP complex for 60 min at 37°C with shaking and washed again 6 times with PBS + 0,025 % Tween 20. Due to addition of substrate solution containing 5 ml 10 x citrate buffer, 45 ml H_2O, 1 o-phenylenediamine dihydrochloride (oPD) tablet (20 mg) and 20 µl 30% H_2O_2, a colorimetric reaction was initiated. The reaction was stopped by applying 3 M HCl and the solution transferred to a new microplate. Optical density was measured at 492 nm against a blank sample, which consisted of a mixture of substrate and stop solution that was not in contact with cells.

Due to the fact that Ki-67 is located in the nucleus, an additional permeabilization step with 0.1 % Triton X-100 in PBS for 5 min at RT had to be performed and was carried out after cell fixation. Moreover, the secondary antibody used for Ki-67 assay was HRP-linked.

2.2.5.3 Whole cell protein extraction

To extract whole cell protein, cells were lysed using 1 x RotiLoad-1 loading buffer. First, medium was aspirated and cell layer washed with PBS. Then, 80 µl of lysis buffer were added. Finally, samples were transferred to a reaction tube using a cell scraper. Sonication was employed to break up DNA.

Alternatively, for experiments investigating, for example, apoptosis, detached and dead cells were also lysed. For this, cell culture medium was aspirated and cells were washed with PBS. Both medium and PBS were collected. Afterwards, cells in monolayer were detached by incubation with trypsin. The reaction was stopped by adding medium containing FCS. The cell suspension was collected and combined with the cells in the supernatant. Subsequently, the cell suspension was centrifuged for

5 min at 390 x g, the supernatant aspirated and the cell pellet lysed with RotiLoad-1. Samples were stored at -20°C.

2.2.5.4 SDS – polyacrylamide gel electrophoresis (SDS-PAGE)

Protein extracts were separated according to molecular weight using denaturing polyacrylamide gels according to (Laemmli, 1970). Resolving gels consisted of various percentages of polyacrylamide (PAA), which depended on the size of the protein of interest. For large proteins, low PAA percentage gels were used, while small proteins where separated using high percentages of PAA: Initially, the resolving gel solution (7.5 – 15 % PAA, 375 mM Tris-HCl, pH 8.8, 0.1% SDS, 0.05% APS, 0.005% TEMED) was poured between two glass plates. n-butanol was placed on top to form a plane border. After the gel was polymerized, n-butanol was removed and stacking gel solution (5 % PAA, 125 mM Tris-HCl, pH 6.8, 0.1 % SDS, 0.05 % APS, 0.005 % TEMED) was added on top of the resolving gel. While still in a liquid condition, a comb was put between the glass plates to produce the wells after polymerization. The gels were stored for few days at 4°C in a humid environment until use.

Before loading, whole cell protein extracts were sonicated (10 impulses, 1 sec/impulse, amplitude 40%) to break down DNA molecules and denatured at 95°C for 5 min to disrupt secondary structure. In order to observe the electrophoretic front, samples were stained with 0.5 µl of 1% bromophenol blue solution. 12 to 15 µl sample per well were loaded onto the gel. Electrophoresis was carried out at 200 V in PAGE running buffer in a 4-gel vertical electrophoresis system (Mini-PROTEAN® Tetra Cell). Up to 4 gels were run in parallel.

2.2.5.5 Western Blot analysis

In Western Blot analysis, separated proteins from SDS-PAGE were transferred to a membrane. Two methodologies, wet and semi-dry western blotting, were applied. In wet western blotting, gels and nitrocellulose membrane were equilibrated in PAGE transfer buffer. Afterwards, gel from SDS PAGE was put on top of a nitrocellulose membrane and covered with 3 sheets of filter paper from both sides. Additionally covered with wet sponges, the set-up was placed vertically in the holder of a Mini Trans-Blot® module. The membrane has to be orientated to the anode side to guarantee an accurate transfer of the proteins from the gel to the membrane. Finally, the Mini Trans-Blot® module was put into a Mini-PROTEAN® transfer chamber and filled up with PAGE transfer buffer. An ice container was placed into the chamber to avoid heating. The transfer was carried out at 350 mA for 1 h.

For semi-dry western blotting the membranes were prepared by incubating for 30 s in PAGE transfer buffer, 2-3 min in distilled water and 10 min in PAGE transfer buffer under agitation according to the user's manual. Gels were equilibrated for 10 min in PAGE transfer buffer. The blot was arranged in the intended cassettes as follows: 3 humidified filter paper sheets, the membrane, the gel and further 3 humidified filter paper sheets. Per cassette two blot processes were performed. For the transfer process a preprogrammed Standard SD transfer protocol (25 V, 1.0 A, 30 min) arranged from Trans-Blot® Turbo Blotting System was used.

To control protein transfer, membranes were stained with ponceau S by short incubation of the membranes in the staining solution. Afterwards, membranes were washed three times for 5 min each in wash buffer (PBS-0.2% Tween 20). For saturation of unspecific binding sites, membranes were blocked in blocking solution (5% milk powder in PBS containing 0.2% Tween 20) for a minimum of 2 h at RT. Subsequently, membranes were incubated overnight at 4°C on a roll mixer with a specific primary antibody diluted in blocking solution (for dilutions of specific primary antibodies see Tab. 5). After membranes were washed again (3 times for 5 min in wash buffer), they were incubated with a corresponding species-specific HRP-linked secondary antibody. For the detection of antibody-labeled target proteins, membranes were covered with the Super Signal West Dura Extended Detection Substrate for 5 min, dispensable substrate was removed and chemifluorescence was recorded with a CHEMI-SMART 5100 instrument. For correction of possible unequal protein loading, ERK2 was detected on every membrane and used as reference protein in the analysis.

Tab. 5: Applied dilution and species of antibodies used for Western Blot.

Antibody	Dilution	species
Anti-BiP	1:1000	rabbit
Anti-ERK2	1:3000	rabbit
Anti-FLT1	1:1000	rabbit
Anti-Grp94	1:1000	rabbit
Anti-KDR	1:1000	rabbit
Anti-rabbit secondary antibody, HRP-linked	1:3000	goat

2.2.6 Fluorescent-activated cell sorting (FACS) analysis

In flow cytometry the cells suspended in a stream of fluid pass a laser and fluorescent intensity can be measured. It is a flexible method to investigate a range of concepts. Within this study, an apoptosis assay was performed by detection of a phospholipid, stage of cell cycle being analyzed via determination of DNA content and glycolsylation status via specific labelling of glycoresidues on the cell surface with fluorescent conjugated lectin.

2.2.6.1 Annexin V-FITC Apoptosis Assay

In the context of this study, the presence of the phospholipid phosphatidylserine (PS) was analyzed to investigate apoptosis. PS is translocated from the inner to the outer side of cell membrane if cells are in early stage of apoptosis (Vermes *et al.,* 1995). Double staining with propidium iodide (PI) was performed to distinguish between apoptosis and necrosis. Apoptotic cells showed an intense staining for Annexin V and a low staining for PI, whereas high fluorescent signal for Annexin V and PI signalized necrotic cells. In the latter case, the membrane was perforated and it was possible to stain DNA in the cells. For this staining, the Annexin V-FITC Apoptosis Detection Kit II was used. At the end of an experiment medium as well as PBS with which cells were washed were collected to include detached cells for the staining process. The cell layer was trypsinized and the cells were combined with the cells in the medium. The cell suspension was centrifuged (390 x g, 5 min, RT) and the pellet washed twice with ice-cold PBS and subsequently resuspended in 100 µl of 1 x Binding Buffer. The suspension was transferred to FACS tubes and 5 µl of each, the recombinant Annexin-FITC labeled protein and PI were added. Incubation was performed in the dark for 15 min. Afterwards, 400 µl of 1 x Binding Buffer were added and 10000 cells from every sample were measured in an FACSCalibur Flow Cytometer. For instrument settings, apoptotic cells were stained with Annexin V-FITC or PI alone.

2.2.6.2 Cell cycle determination

Within the cell cycle, a cell passes different phases to prepare for cell division. In G0/1 phase cells have one copy of DNA, whereas two copies are presented in G2 and M phase. If the cells are in S phase, they are in process of replicating DNA and contain between one and two copies. The fact that cells contain different copies of DNA within different cell cycle phases is utilized to determine cell cycle distribution by staining DNA with propidium iodide (PI). If the fluorescence intensity increased 2-fold, the cells are in G2/M phase, whereas 1-fold intensity signalize G0/1 phase. Cells presenting a lower

fluorescent signal are in a so called sub G1 fraction, which contains apoptotic cells (Kalejta RF, Shenk T, Beavis AJ, 1997; Douglas *et al.,* 1995).

At the end of an experiment medium was collected, cells were washed with PBS and trypsinized. The combined cell suspension was centrifuged (390 x g, 5 min, 4°C) and the pellet resuspended in 200 µl of ice-cold PBS. Cells were subsequently fixed by adding ice-cold 70% EtOH under vortexing and the samples were incubated at -20°C for a minimum of 2h or until staining could be performed.

For the staining process, samples were centrifuged at 1000 x g for 5 min at 4°C and washed two times with 1 ml PBS. The pellet was resuspended in PBS containing 1% BSA and afterwards 500 µl of PI/RNase Staining Solution Buffer (BD Pharmingen, Heidelberg) were added. RNase is added to ensure that only DNA is stained by PI. Every step was performed on ice. The samples were transferred to a FACS tube through a 40 µm Nylon cell strainer and incubated for 30 min at RT. Samples were stored at 4°C until fluorescence measurement with FACSCalibur. Per sample 10000 cells were analyzed. For data analysis, counted cells were gated to exclude doublets and triplets.

2.2.6.3 Analysis of glycosylation process

During a glycosylation process glycoresidues are added to newly synthesized and processed proteins (Blom *et al.,* 2004). These moieties could be detected with the help of lectins. Lectins are glycoproteins containing saccharide-binding sites. With the help of these, they specifically bind to particular sugar residues on the cell surface. Because of this behavior they are used to investigate the status of glycosylation.

At the end of an experiment cell culture medium, PBS of a washing step and trypsinized cells were collected by centrifugation (390 x g, 5 min, RT). The cell pellet was washed with PBS and resuspended in 100 µl PBS containing 1% BSA. 5 µl of lectin PHA-L (AlexaFluor 488 conjugated) were added and incubated on ice for 30 minutes. Subsequently, samples were centrifuged again. Cell pellets were resuspended in 300 µl PBS and transferred to FACS tubes. Fluorescence was measured using FACSCalibur Flow Cytometer (10000 counts/sample). Unstained cells were used as negative fraction for analysis. For the control of inhibition of glycosylation cells were treated with 2 µg/ml tunicamycin.

2.2.7 Staining methods

2.2.7.1 Immunofluorescence staining

For investigation of endothelial cell morphology, cells were seeded in an 8-well glass chamber slide. At the end of experiment, the cells were washed briefly with 3.7% paraformaldehyde (PFA) in cytoskeleton (CS) buffer and fixed afterwards with 3.7% PFA for 15 min at RT. Subsequently, samples were washed 3 times with PBS. Until further usage, samples were stored at 4°C covered with PBS. For immunofluorescent staining, cells were permeabilized with 0.1% Triton X-100 in PBS for 5 min. Afterwards, cells were washed again with PBS and incubated with FITC-conjugated antibody against CD31 (CBL468F Ms X Hu CD31 FITC, Millipore, Darmstadt) or Alexa Fluor® 549 conjugated Phalloidin for actin staining (both 1:40 diluted in PBS/1% BSA) for 1 h and washed again 4 times with PBS. For amplifying the signal CD31-stained samples were additionally incubated with secondary antibody (Alexa Fluor® 488 goat anti-mouse IgG, Life technologies, Carlsbad, diluted 1:1000 in PBS/1% BSA) for 45 min. After 4 washing steps with PBS, cell nuclei were stained using 1 µg/ml Hoechst Stain 33342 for 5 min. Every incubation step was performed in a dark environment. Samples were washed twice with PBS and once with distilled water. After removing the chamber construction, the glass slide was covered with mounting medium and glass cover slides. Finally, slides were stored at 4°C until the mounting medium became solid. Microscopical examination was performed with the fluorescent microscope Ix71 with Delta vision (Applied Precision, USA).

2.2.7.2 Immunohistochemical staining

To investigate protein expression in human tissue, biopsies of different types of tissues from various patients were stained for proteins of interest. Biopsies were obtained from patients at the University Medical Center Mainz. The investigation of these tissues was in accordance with the rules of the responsible ethical committee of the state of Rhineland-Palatinate.

Biopsies were formalin-fixed and embedded in paraffin. They were then sectioned using a microtome and the sections were transferred to microscope slides. The slides were incubated over night at 60°C to soften the paraffin. After cooling for 10 min, sections were deparaffinised in xylol and rehydrated in ethanol. Then, slides were incubated in xylol three times for 5 min each. Xylol was drained off and slides were incubated for 2-3 min in descending ethanol baths with 100 %, 100 %, 96 %, 70 % and 50 % EtOH. To complete rehydration, samples were submerged in pure water. Afterwards slides were prepared for staining by incubating in Dako Target Retrieval

Solution (pH 6 or 9, see Tab. 6) for 30 min at 95°C. Staining of the sections was performed in a Dako Autostainer Plus using Dako EnVision™ + System-HRP (DAB) K4011. The protocol for staining was as follows: washing of the slides with Dako EnVision™ FLEX WASH BUFFER (1x), endogenous enzyme blockage using 3 % H_2O_2 diluted in PBS for 5 min to block peroxidase in the tissue and to avoid unspecific staining. Afterwards, slides were washed again and incubated with primary antibody diluted in Dako Antibody Diluent for 1h (dilution factor is listed in Tab. 6). A further washing step was followed by incubation with Dako Labelled Polymer-HRP for 30 min and two washing steps. Subsequently, slides were incubated with chromogen DAB-5007 for 5 min, washed and exposed again to chromogen DAB-5007 for 5 min. To stop the reaction of DAB-5007, slides were washed with H_2O. For staining of the nuclei, sections were stained with Dako Hematoxylin CS700 for 3 min and washed again. After the program of the autostainer, slides were additionally washed with tap water to complete hemalaun staining. Afterwards, samples were washed with distilled water and dehydrated by incubating in ascending ethanol baths of 50-95 % EtOH for 2-3 min, each followed by two incubations in fresh 100 % EtOH baths for 5 min. Finally, sections were incubated in xylol three times for 5 min each. Stained sections were covered with Entellan and a cover slide.

Tab. 6: Overview of primary antibodies used for immunohistochemical staining

Antibody	Dilution	pH
anti-BiP	1:200	6
anti-PERK	1:200	6
anti-IRE1α	1:50	9
anti-ATF4	1:100	6

The intensity and distribution of the specific immunohistochemical staining reaction was evaluated using a semi-quantitative method as described by Remmele and Stegner (1987). The Immunoreactive Remmele Score (IRS) score was calculated as follows: IRS=SI x PP, where SI is the optical stain intensity (graded as 0 = no, 1 = weak, 2 = moderate, and 3 = strong staining) and PP - the percentage of positive stained cells. The PP was defined as 0 = no staining, 1 = <10%, 2 = 11–50%, 3 = 51–80%, and 4 = >81%. Stained endothelial cells were counted per 50 vessels. Stained stromal cells were counted per 50 cells. IRS was defined as: 0-2 negative, 3-5 weakly positive, 6-8 moderately positive, 9-12 strongly positive.

2.2.8 Wound healing and migration assay

For wound healing and migration assays, µ-Dishes from ibidi (35mm, low, ibiTreat) were used. The cells were seeded in fibronectin-coated culture inserts, which each contained two chambers. Growth areas were defined by a removable silicon insert. At the seeding density of 70 000 cells per chamber, the cell layer reached confluency 48h after transfection, the time point of maximum down-regulation. Cell culture medium was changed one day after seeding. To start the migration assay the cells were washed 2 times with cell culture medium, and the insert was removed carefully using sterile forceps. 400 µl of cell culture medium was added cautiously to the µ-Dish and the migration of the cells was observed over time. At selected time points (0h, 8h, 24h and 32h) three pictures of every sample were taken at different positions of the gap using a phase contrast microscope (Leica). Images were analyzed with the help of the online-based WIMASIS WimScratch application.

2.2.9 Angiogenesis Assays

2.2.9.1 2D Angiogenesis Assay – Collagen gel

Cells were seeded on 24 well plates and grown until the monolayer reached confluence. Gel mix (containing 500 µl collagen I (3 mg/ml), 300 µl distilled H_2O, 100 µl 10x M199 and 100 µl cell matrix buffer (CMP) per ml gel mix) were prepared on ice. 300 µl gel mix were added on top of the cells. Polymerization took place at 37°C for 30 min. Finally, 500 µl pre-warmed PromoCell Endothelial Cell Basal Medium (PC medium; supplemented with 15 % FCS, 1 % P/S, 10 µg/ml sodium heparin and 2.5 ng/ml bFGF) were put on top of the gel. 24 and 48 h later, cells were stained with calcein-AM (10 mM). The images were taken using a fluorescence microscope (Keyence). Total tube length, total tubes and total branching points were quantified with help of the WimTube application of Wimasis.

2.2.9.2 3D Angiogenesis Assay – Collagen-fibrin gel

To investigate angiogenic behavior of HUVEC in 3D, the cells were embedded in a collagen-fibrin gel and the formation of capillary-like structures was observed. First, cells were trypsinized and resuspended in PC medium. 1.5 million (mln) cells per ml gel were used. 1 ml of gel consisted of 255 µl collagen type I (3 mg/ml), 100 µl fibrinogen (200 U/ml), 300 µl PC medium without FCS, 255 µl 2xIMDM, 80 µl cell suspension and 10 µl Arvin. The gel was prepared on ice to delay premature polymerization. By adding Arvin, polymerization of the gel was initiated. Expeditiously, 350 µl of the collagen-fibrin gel containing endothelial cells were added per well (24 well format). After incubation at

37°C in a CO_2 incubator for 20 min, gels were covered with PC medium containing 5 % FCS (not heat-inactivated), 1 % P/S, 5 ng/ml bFGF and 50 ng/ml VEGF to stimulate angiogenesis. Medium was changed every second day. At the time point of interest, live staining with 10 mM calcein-AM was performed. Images were taken using a fluorescence microscope (Keyence) and quantitative analysis performed by Wimasis. Parameters, such as total tube length, total tubes and total branching points were determined.

2.2.10 Statistical analysis

Experimental results are represented as means ± standard deviations (SDs). Primary cells from different donors were used as replicates, the number of which is designated as “n”. In case of cell lines, performing independent experiments at different time points and passages were used as replicates. Additionally, technical replicates within one experiment were performed to decrease pipetting errors, but not used for statistical analysis. Due to the small number of n in biological experiments, normal distribution of the data was assumed. The t-test was used for statistical evaluation. Because of the use of the same donor within one experiment the paired t-test was selected. If more than two independent factors were to be investigated within one experiment, two-way ANOVA was applied for evaluation. If parametric distribution of the data could not be assumed, the non-parametric Wilcoxon signed rank test was performed. Evaluations were carried out using Microsoft Excel and GraphPad Prism 5.

3 Results

3.1 Down-regulation of BiP in primary endothelial cells

3.1.1 BiP down-regulation using siRNA

HUVEC were transfected with BiP-specific siRNAs via electroporation. These siRNA molecules encode specific sequences targeting different areas of 3'UTR of BiP mRNA resulting in BiP down-regulation. A down-regulation up to 70% was achieved at mRNA level and up to 95% at protein level, when cells were transfected with siRNA molecule s6980 (Fig. 9). Transfection using s6981 was less efficient compared to transfection with s6980. Less pronounced down-regulation of BiP was reached at both mRNA and protein level with s6981, whereby the mean value for down-regulation was higher than 50%. For the following experiments, transfection controls were performed to test the efficiency of BiP down-regulation. Only the experiments with down-regulation of at least 50% were used for statistical evaluation. The down-regulation reached its maximum 48h after transfection, and 96h after transfection the down-regulation was still stable. These time points were selected for further experiments.

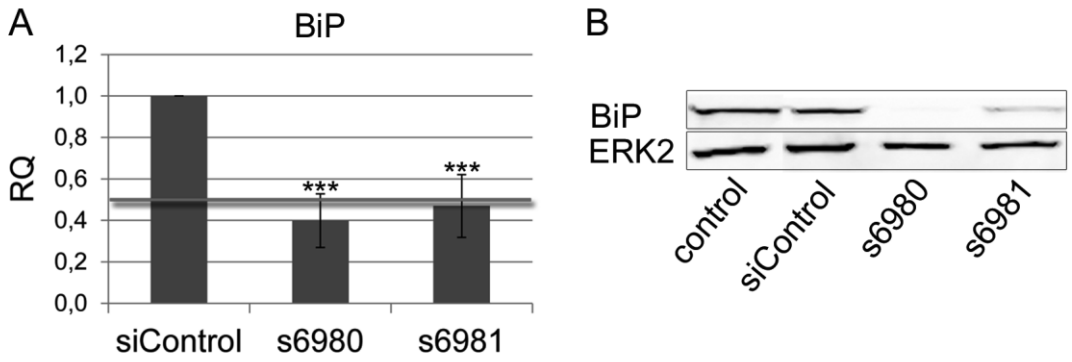

Fig. 9: BiP down-regulation after transfecting HUVEC with siRNA molecules.

HUVEC were electroporated with siRNA molecules s6980 and s6981 that specifically target BiP mRNA. Expression of BiP was investigated at RNA level using real time PCR (A, means ± SDs; n=13) and at protein level via SDS-PAGE and Western Blot analysis (B) 48h after transfection, respectively. The line marks 50% threshold of down-regulation. For controls untransfected cells (control) or cells transfected with unspecific siRNA molecule with no homologies for human mRNAs (siControl) were used. For Western Blot analysis ERK2 was detected as a reference protein and normalization of applied protein amount (statistics: Wilcoxon test, compared to control; p***≤0.001).

3.1.2 BiP depletion with SubAB toxin

In an alternative approach, BiP was down-regulated by treating the cells with subtilase AB (SubAB). This holotoxin specifically cuts BiP protein into two fragments and inactivates the chaperone. To specify the effect of SubAB, a mutated form of the toxin, $SubA_{A272}B$, was used as an additional control (Paton *et al.,* 2006). Furthermore, cells were treated with tunicamycin (Tun), a nucleotide sugar analogue, which causes inhibition of N-glycosylation (Price and Tsvetanova, 2007) and, additionally, accumulation of unfolded proteins in the ER. This compound is widely used as a positive control for UPR activation in literature (Mao and Crowder, 2010; Diehl *et al.,* 2011). UPR activation led to an increase of BiP expression at protein level (Fig. 10 A), with a decrease of BiP being detectable in cells treated with SubAB. $SubA_{A272}B$ treatment did not change expression of BiP. HUVEC were also treated with SubAB for different time periods. Already after 3h of treatment, BiP cleavage by SubAB was detected at protein level. A decrease of BiP content and a simultaneous increase of BiP fragments were observed with increasing time of treatment compared to BiP level in untreated cells, used as control (Fig. 10 B).

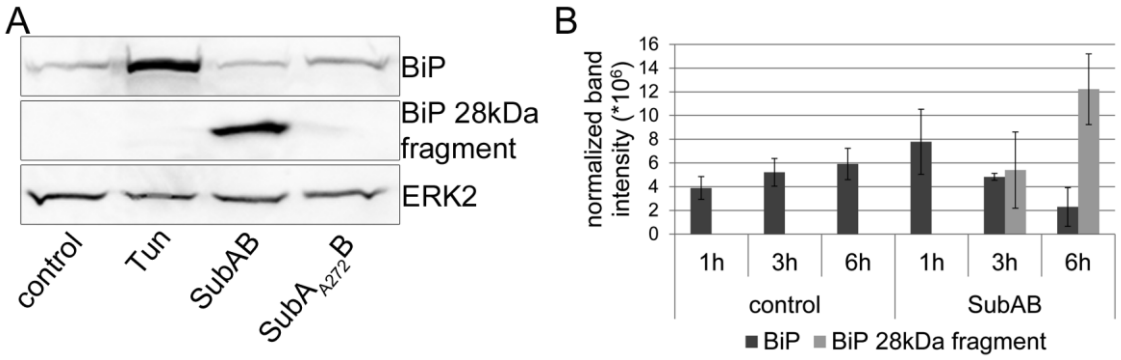

Fig. 10: BiP deprivation due to SubAB activity.

HUVEC were treated with 100 ng/ml SubAB or $SubA_{A272}B$. As positive control of BiP up-regulation, cells were stimulated with 2 mg/ml tunicamycin. In addition, untreated cells were used as control. SDS-PAGE and Western Blot permitted detection of BiP and non-functional BiP fragment, a result of SubAB treatment. ERK2 was detected as reference protein (A). Quantification of Western Blot analysis of two different donors showed increase of BiP fragment level and simultaneous decrease of BiP protein already after 3h of treatment. Data are shown as normalized band intensity (B); (means ± SDs; n=2).

Additionally, BiP expression was investigated at mRNA level in primary endothelial cells in response to treatment with SubAB, which acts primarily at protein level. As a positive control, cells were treated with tunicamycin to induce BiP expression by UPR activation. As early as 2h after SubAB treatment, expression of BiP at mRNA level started to increase in comparison to untreated cells. After 8h of incubation, induction of BiP mRNA expression reached a maximum. After 18h of treatment with the toxin, BiP expression settled at a high level which was present up to 48h of incubation (Fig. 11).

This shows that while 3h after addition of SubAB cleavage of BiP protein takes place, the toxin simultaneously induces BiP expression at mRNA level. In contrast, up-regulation of BiP at mRNA level was not observed in cells in which BiP was down-regulated with the help of siRNA molecules (Fig. 9).

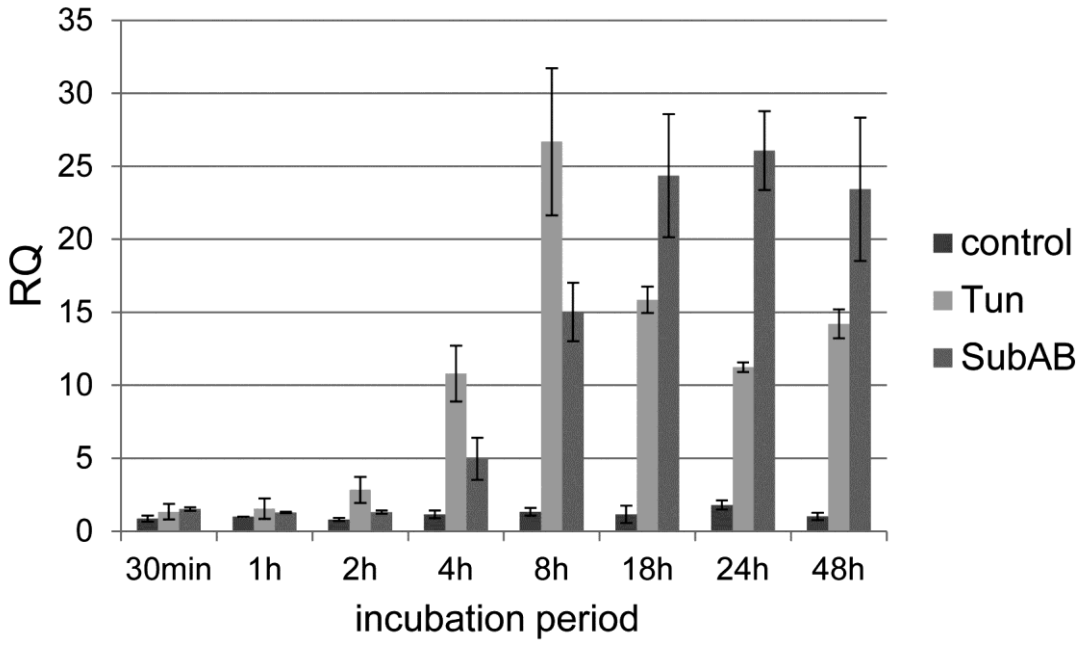

Fig. 11: BiP up-regulation at mRNA level as a result of SubAB treatment.
HUVEC were treated with 2 µg/ml tunicamycin or 100 ng/ml SubAB toxin for various time periods. Using real time PCR expression of BiP was investigated at RNA level. Data are depicted as relative quantification (RQ, means ± SDs; n=2).

3.1.3 Stability of BiP down-regulation

Additionally, transfection of the endothelial cells was analyzed for stability of BiP down-regulation in the presence of the UPR-activating agent tunicamycin. Thus, siRNA-transfected HUVEC, as well as SubAB-treated cells were exposed to tunicamycin, and the expression level of BiP was evaluated at protein level (Fig. 12). In control experiments without tunicamycin treatment, down-regulation of s6980 and s6981 transfected cells was apparent. As expected, tunicamycin induced BiP expression. However, increasing the tunicamycin concentration did not lead to an additional induction of protein expression. SubAB treatment led to BiP cleavage, as shown before. A parallel treatment of SubAB and tunicamycin did not seem to increase the amount of uncut BiP protein. Similar to untransfected cells, up-regulation of BiP was observed in cells transfected with control siRNA stimulated with tunicamycin. In contrast, tunicamycin treatment showed no effect on siRNA s6980- and s6981-transfected cells.

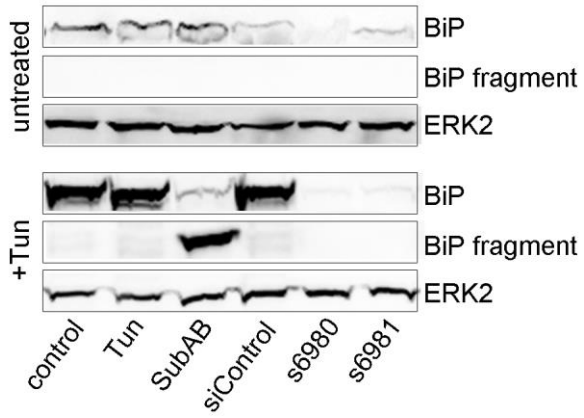

Fig. 12: Stability of BiP down-regulation in the presence of UPR activating agent tunicamycin.

BiP expression was analyzed at protein level using Western Blot in tunicamycin- and SubAB-treated cells, as well as s6980- and s6981- transfected cells. For controls, untreated cells and cells transfected with control siRNA were used. In addition, samples were treated with 2 µg/ml tunicamycin 48h after transfection for 18h to induce ER stress and accompanied BiP expression to verify stability of BiP down-regulation. For reference protein ERK2 was detected.

3.2 Characterization of BiP down-regulated cells

In this study BiP down-regulated cells were characterized for viability, proliferation or apoptosis. In addition, the cellular process of glycosylation or the expression of endothelial specific markers was analyzed. To support the results the data generated with HUVEC, in which BiP was down-regulated using siRNA molecules, were compared to results gained in the cells treated with SubAB. Moreover, cells were treated with tunicamycin to induce an ER stress situation.

3.2.1 Morphology of BiP down-regulated cells

To compare HUVEC morphology of BiP down-regulated cells with control cells, fluorescent staining for filamentous actin (F-actin) and CD31 was performed. As a structure protein, actin represents an important component of the cytoskeleton. Via polymerization it forms microfilaments, named F-actin. Cells were analyzed for the presence of stress fibers, which are described as higher cytoskeletal structures of cross-linked F-actin filaments. Especially in endothelial cells they play an important role in cell migration (Lamalice *et al.,* 2007). HUVEC transfected with BiP siRNA showed so-called “cobblestone” morphology characteristic of endothelial cells, similar to untransfected or siControl-transfected cells (data not shown). F-actin staining (Fig. 13, red) showed no observable differences between untransfected cells and cells transfected with control siRNA, although a few stress fibers were detectable in s6980- and s6981-transfected cells. However, this effect was not consistent when studied by the staining of HUVEC from four different donors.

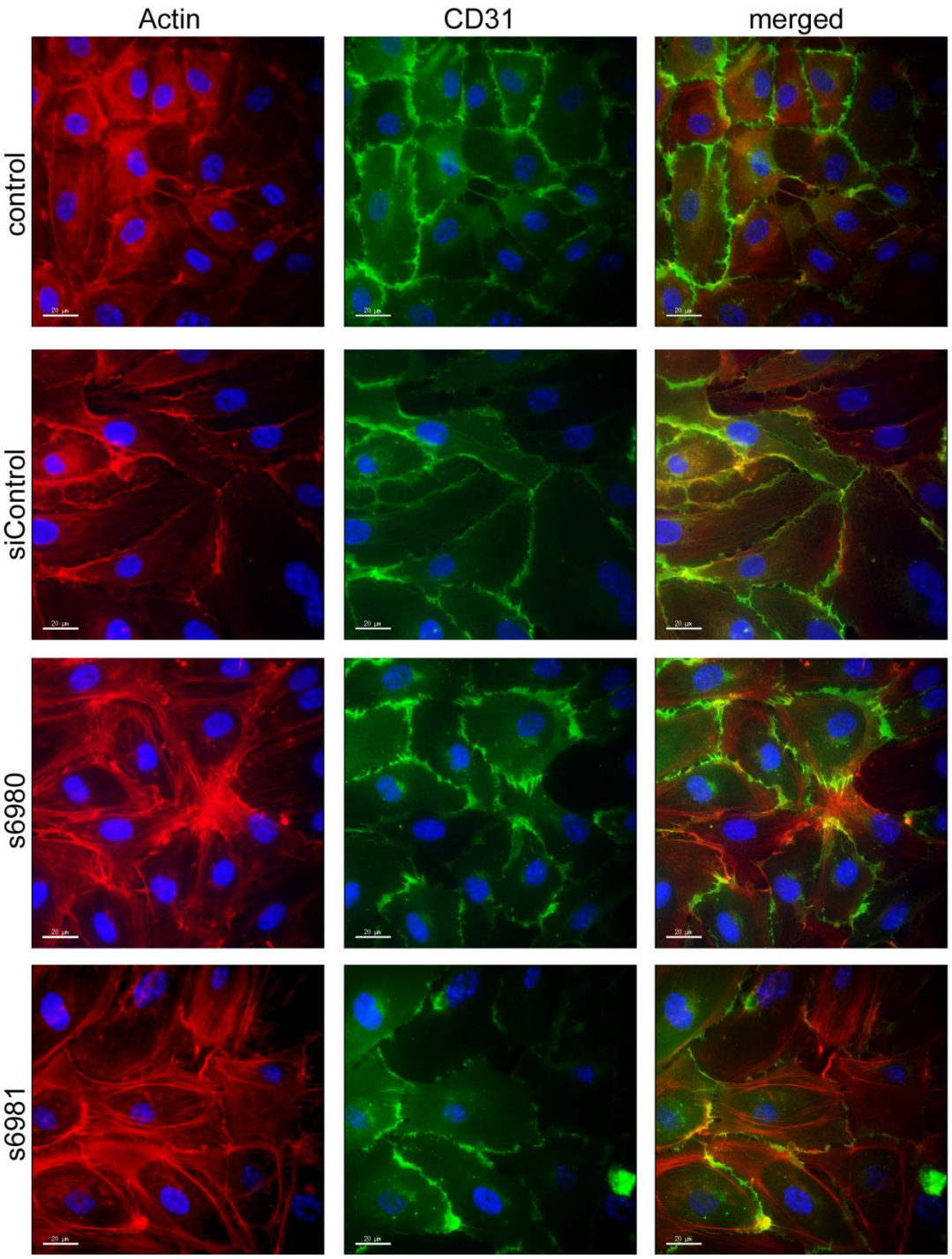

Fig. 13: Fluorescent staining of actin and CD31 in transfected HUVEC.
Non-transfected cells, cells transfected with control siRNA and BiP-down-regulated cells (s6980 and s6981) were stained for actin (red) and CD31 (green), scale bar: 20µm.

CD31 is an intercellular contact protein in endothelial cells and its continuous distribution is used to characterize the integrity and functionality of endothelial cell layers (Fig. 13, green). As with F-actin, expression of the marker did not differ between different samples. The distribution of stained CD31 appeared similar in untransfected,

siControl and s6980-transfected HUVEC. However, s6981-transfected cells showed a moderate decrease of CD31 expression.

3.2.2 Metabolic activity of BiP down-regulated cells

To exclude possible toxic effects of transfection or the subsequent BiP down-regulation, the viability of cells was analyzed using the MTS assay. BiP down-regulated cells showed no differences in metabolic activity compared to control cells. Whereas a decrease in metabolic activity was observed in the cells cultured for 96h compared to 48h and 72h, no differences were observed between transfected and control cells at each time point. Tunicamycin treatment compromised viability of HUVEC cultured for 72h, whereas untreated and tunicamycin-treated cells showed similar metabolic activity 96h after transfection. Furthermore, tunicamycin did not affect cell viability of BiP down-regulated cells compared to control cells. The viability of siControl cells, s6980- and s6981- transfected cells was nearly similar at individual time points. Moreover, comparison of viability within individual samples over time and following treatment was similar as well (72h and 72h + tunicamycin; 96h and 96h + tunicamycin treatment) (Fig. 14).

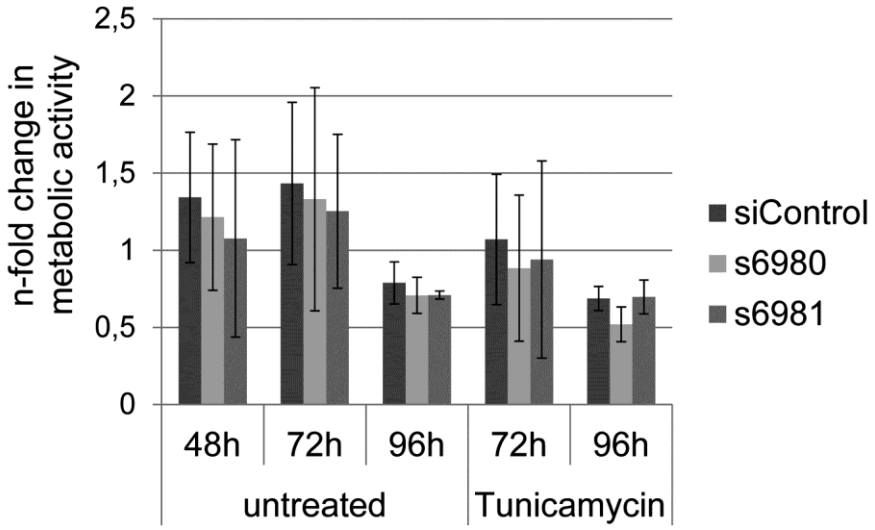

Fig. 14: Metabolic activity of BiP down-regulated cells.

HUVEC were transfected with siRNA molecules s6980 and s6981. Control cells were transfected with control siRNA. 48h after transfection, the time point of maximum down-regulation, cells were treated with 2 µg/ml tunicamycin for 24h (72h sample) or 48h (96h sample). Results are shown as n-fold change in metabolic activity. Metabolic activity of untransfected cells after 48h was set as 1. For evaluation, the cell number of each sample was analysed by the crystal violet assay (means ± SDs; statistics: paired t-test; n=3).

3.2.3 Proliferation of BiP down-regulated cells

Proliferation of the siRNA-transfected cells was analyzed by determining the expression of Ki-67, a well-known proliferation marker. Fig.15 shows a time-dependent increase in Ki67 expression starting 4h after transfection, the time point at which the cells were mostly adherent, and continuing up to 72h. At the same time, no significant differences in Ki-67 expression were observed between samples at 4, 24 and 48h. 72h after transfection, cells transfected with siRNA s6980 showed a significant decrease in Ki67 expression compared to control cells. Expression of Ki-67 in s6981-transfected cells was not changed compared to control. The level of Ki-67 96h after transfection dropped and was comparable to the expression level in the cells 48h after transfection. Differences between BiP down-regulated and control cells could not be detected at this time point. In response to tunicamycin treatment, the expression of the proliferation marker was strongly decreased 72h after transfection compared to untreated cells at the same time point. Reduced Ki-67 expression after tunicamycin treatment was also detected 96h after transfection. Cells treated with tunicamycin showed similar Ki-67 expression compared to s6980-transfected cells 72h after transfection. Additional induction of ER stress in s6980-transfected cells by tunicamycin treatment did not induce further changes in Ki-67 expression.

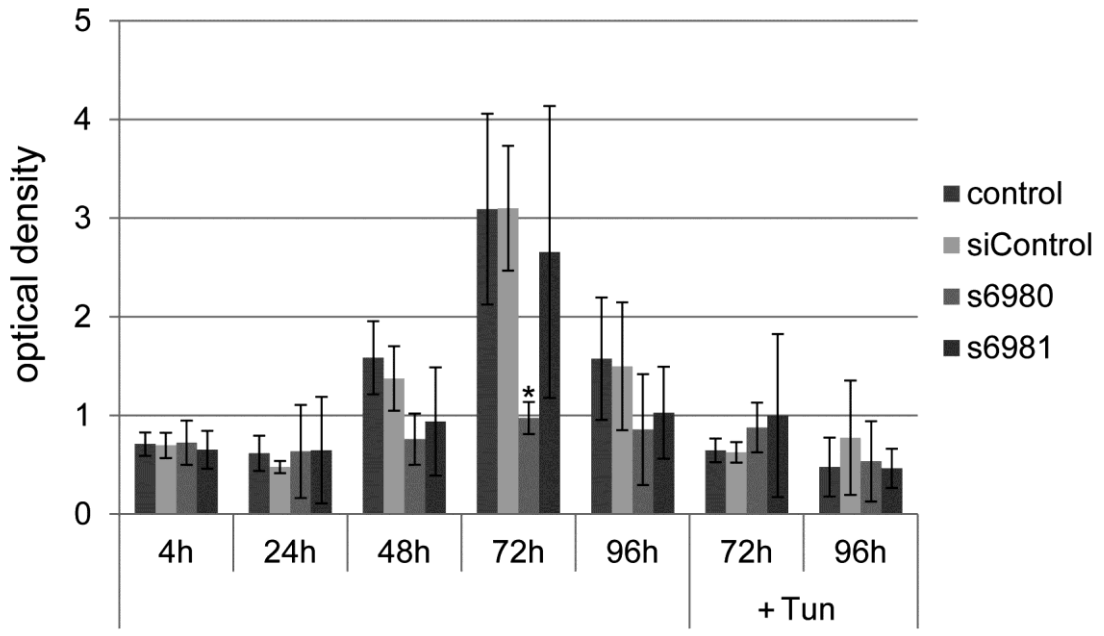

Fig. 15: Expression of the proliferation marker Ki-67.

HUVEC were transfected with control siRNA (siControl) and siRNA molecules s6980 and s6981. Controls contain untransfected cells. 4h, 24h, 48h, 72h and 96h after transfection cells were fixed and the proliferation marker Ki-67 was detected via EIA. Additionally, samples were treated with 2 µg/ml tunicamycin for 24h (72h sample) or 48h (96h sample). Results are presented as optical density, absolute values being related to cell number (means ± SDs, statistics: paired t-test, data compared to corresponding control, significant difference: *p≤0.05; n=3).

3.2.4 Apoptosis

ER stress due to accumulation of unfolded proteins in the lumen of the ER is known to induce apoptosis. To investigate whether BiP down-regulation can induce cell death in endothelial cells, different apoptotic events were analyzed in HUVEC transfected with BiP-specific siRNA and compared to UPR activation by tunicamycin.

Cysteine proteases, enzymes which are involved in the transduction of the cell death signal, are called caspases (cysteine-aspartic acid proteases). Caspase3 is one of the downstream effector caspases and its activation is a widely used marker for cell death. During the signal transducing process the inactive form of the protein, called pro-caspase3, is cleaved and thereby activated. Using SDS-Page and Western Blot analysis pro-caspase3 and the activated form of the enzyme were detected (Fig. 16).

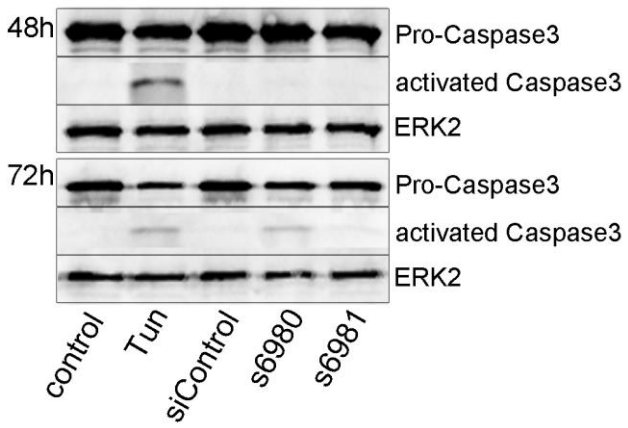

Fig. 16: Caspase3 activity in BiP down-regulated cells and under ER stress.

HUVEC were transfected with siRNA molecules s6980 and s6981 to down-regulate BiP. Additionally, cells were treated with tunicamycin to induce ER stress and activation of the UPR. Samples were lysed 48h and 72h after transfection. Using SDS-Page and Western Blot, proteins were separated and pro-caspase3 and its activated form were detected. ERK2 was detected as reference protein.

Due to accumulation of unfolded proteins in the lumen of the ER, generated by tunicamycin treatment, apoptosis was activated at all time points. Thus, the cleaved form of caspase 3 was detectable in the tunicamycin-treated samples, whereas in untransfected cells, negative siRNA-transfected cells, s6980- and s6981-transfected cells the activated form of the enzyme was not found 48h after transfection, when BiP down-regulation is at a maximum. 72h after transfection, activated Caspase3 was also detectable in s6980-transfected cells. A weak band could be also seen in s6981-transfected cells, while in control cells no cleaved form of the enzyme was found.

To further investigate apoptotic activity in BiP down-regulated cells FACS analysis was performed where the cells were stained for Annexin V and PI (Vermes *et al.,* 1995). Depending on the intensity of the fluorescent signal elicited by PI and/or Annexin V staining, cells were separated into categories of necrotic cells (1) with high fluorescent intensity of PI and Annexin V, living cells (2) with low intensity measured for both, or apoptotic cells (3) which showed a high fluorescent signal for Annexin V but low signal for PI (see Fig. 17). As positive control of dying cells, cells were treated with 6 µM camptothecin, a compound which inhibits nucleic acid synthesis by repression of activity of mammalian DNA topoisomerase I (Hsiang *et al.,* 1985). As Fig. 17 A shows, most of the cells treated with campthothecin appeared in quadrants 1 and 3, indicating that most of the cells were in a necrotic or apoptotic stage, whereas the majority of cells in the control sample were counted in quadrant 2, which contains living cells. Activation of ER stress by tunicamycin also led to an increase of apoptotic and necrotic cells. Slight increase of apoptotic and necrotic cells was also detectable in SubAB treated cells. Comparing control samples and control siRNA-transfected cells, no differences could be detected. Importantly, in HUVEC-transfected with the BiP-specific siRNA molecules s6980 and s6981 most of the cells appeared in the quadrant of living cells 96h after transfection.

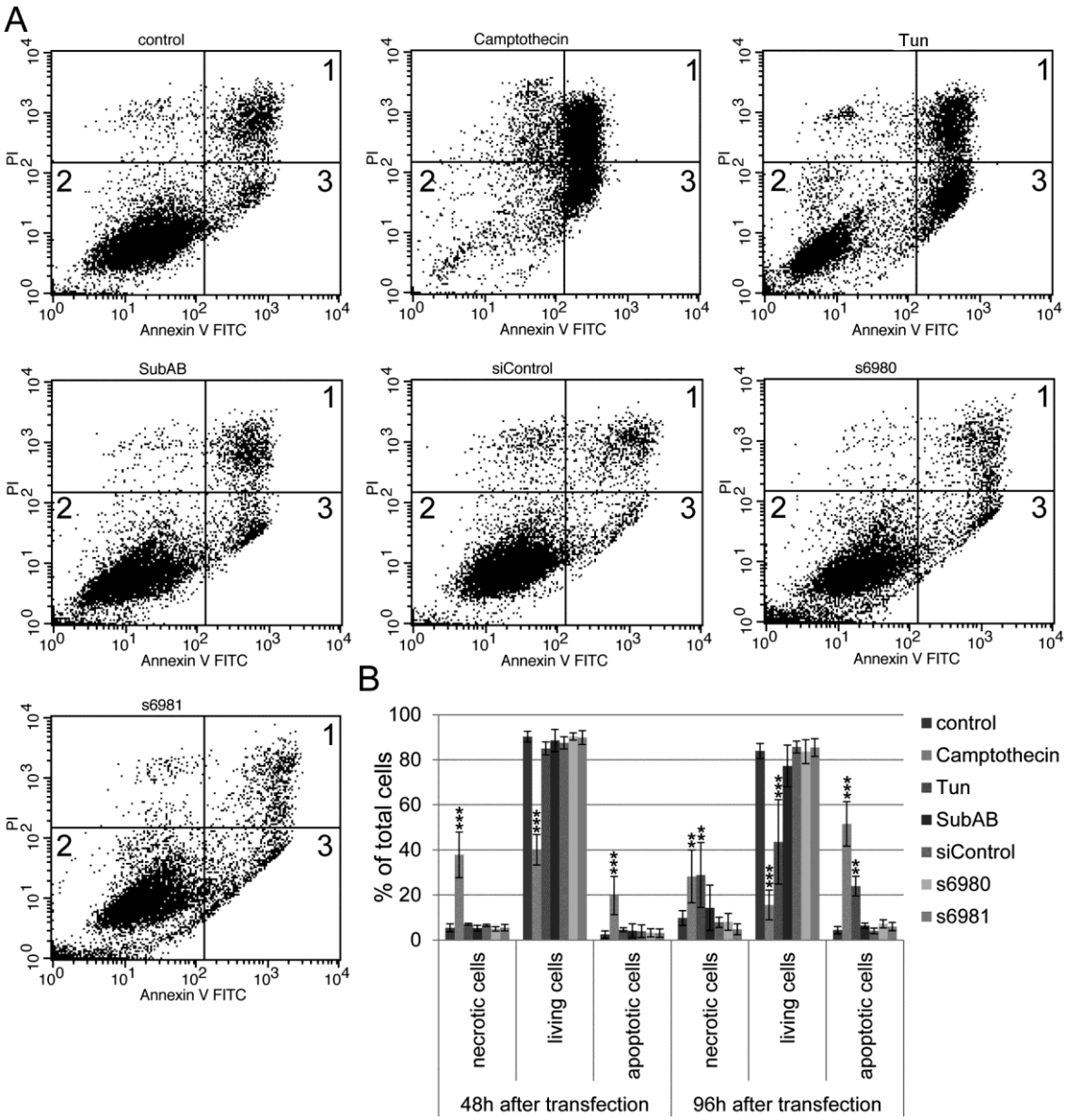

Fig. 17: Distribution of apoptotic, living and necrotic cells in population of BiP down-regulated cells.

HUVEC stained for Annexin V and PI 48h and 96h after transfection with siRNA molecules. For positive control, cells were treated with 6 µM camptothecin for 24h (48h sample) and 48h (96h sample) to induce apoptosis. To activate ER stress, cells were treated with 2 µg/ml tunicamycin for 24h (48h sample) and 48h (96h sample). To cross-check BiP down-regulation, cells were treated with 100 ng/ml SubAB toxin for 24h (48h sample) and 48h (96h sample). Cells were stained for annexin V and PI and the fluorescent signals were measured by flow cytometry. Results are plotted as fluorescent signal of PI staining against annexin V FITC (A, 96h after transfection). Plots are gated to distinguish necrotic cells (1), living cells (2) and apoptotic cells (3). Summarized data of quadrants stats are presented in % of total cells 48h and 96h after transfection (B, means ± SDs; statistics: two-way ANOVA **p≤0.01, ***p≤0.001, data compared to the corresponding control; n=4).

Distribution of necrotic, living and apoptotic cells in various samples of four different donors were analyzed by quadrant statistics and illustrated in relation to the total cell population of 100% 48h and 96h after transfection (Fig. 17 B). 48h after transfection increased numbers of necrotic and apoptotic cells were detectable in camptothecin-

treated samples. This was also reflected in the proportion of living cells in camptothecin-treated samples, which was significantly decreased. At this time point no increase in the number of apoptotic or necrotic cells could be detected in experimental samples. 96h after transfection, the numbers of necrotic and apoptotic cells were also increased significantly in tunicamycin-treated samples. Here, the proportion of necrotic cells was greater than the apoptotic fraction. Similarly, SubAB treatment increased the quantity of necrotic cells, but remarkably not of apoptotic cells 96h after transfection. A moderate but not significantly reduced quantity of living cells was detected in tunicamycin-treated cells 96h after transfection. SubAB treatment led to a slight decrease of living cells, with simultaneous increase of necrotic population. Comparing percentages of necrotic, living and apoptotic cells in untransfected control and siControl sample, the distribution was similar 48h and 96h after transfection. In s6980-transfected cell population, the major part of the cells was alive 48h as well as 96h after transfection. The number of apoptotic cells slightly increased, but the difference of apoptotic cells in siControl and s6980-transfected cells was statistically not significant. S6981-transfected cells showed similar pattern of necrotic, living and apoptotic section in total cells 48h after transfection, as well as 96h after transfection compared to s6980-transfected cells. In addition, down-regulation of the protein did not show the same effect compared to tunicamycin-treated cells 96h after treatment. Depletion of BiP as a result of SubAB treatment was comparable to the distribution of necrotic, living and apoptotic proportion in siRNA-transfected cells.

An additional method to investigate apoptotic activity of BiP down-regulated cells is based on cell cycle determination. PI staining of the fixed cells allows FACS detection of the cells at different stages of the cell cycle, while at the same time apoptotic cells in the so-called “SubG1 phase” can be detected (Douglas *et al.,* 1995). After camptothecin treatment, which is known to induce apoptosis, most of the cells were in SubG1 phase, which reflects DNA degradation due to apoptotic activity. Just a few cells were detectable in G0/1, S and G2/M phase. In contrast, experimental samples showed a distribution more similar to untreated cells, although with varying numbers of cells in different phases of the cell cycle and apoptotic cells.

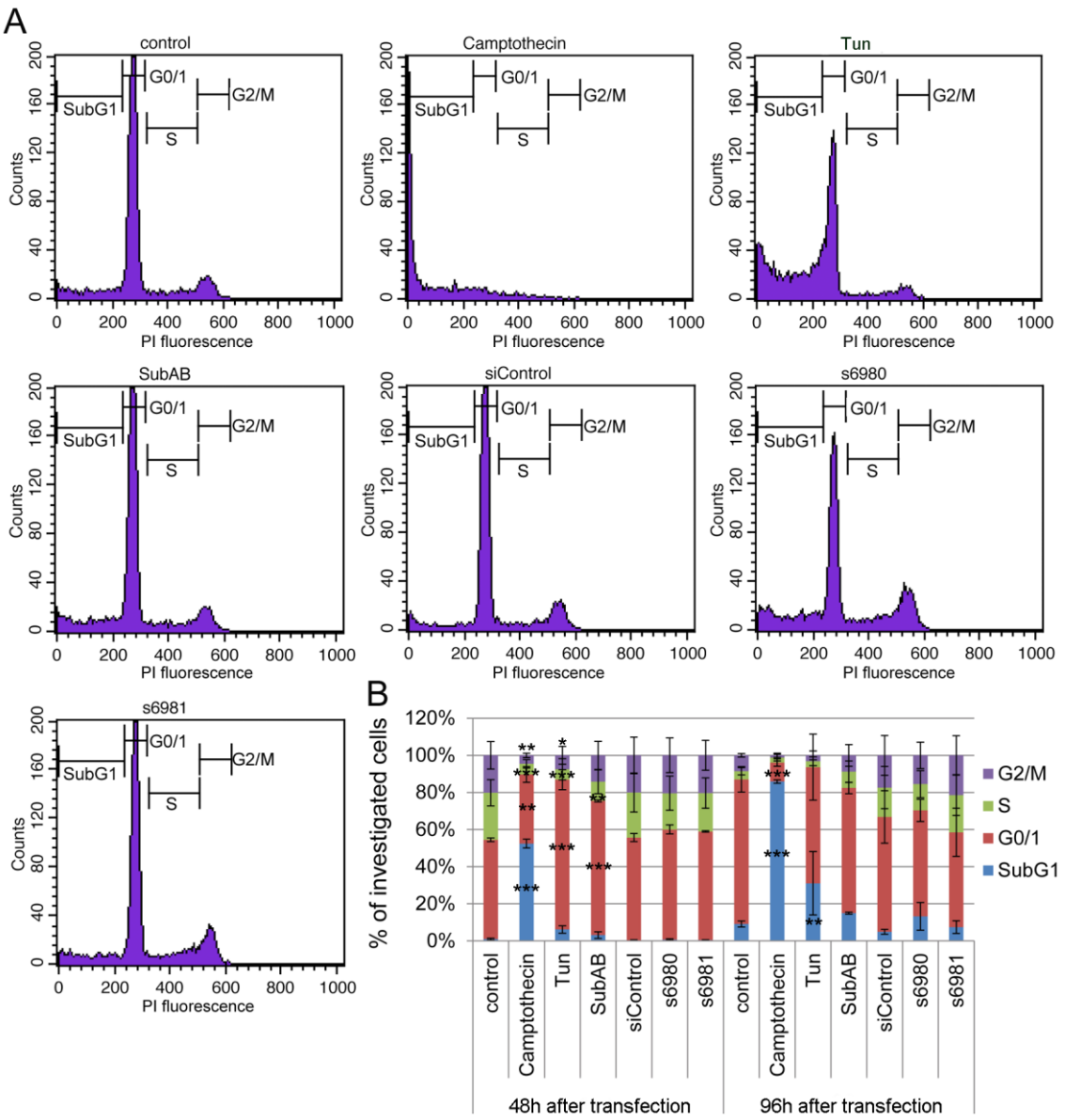

Fig. 18: Distribution of cell cycle phases in populations of BiP down-regulated cells.

Cells were fixed 48h and 96h after transfection of HUVEC with siRNA molecules to down-regulate BiP and control siRNA. As positive control, cells were treated with 6 µM camptothecin for 24h (48h sample) and 48h (96h sample) to induce apoptosis. To activate ER stress, cells were treated with 2 µg/ml tunicamycin for 24h (48h sample) and 48h (96h sample). To cross-check for BiP down-regulation, cells were treated with 100 ng/ml SubAB toxin for 24h (48h sample) and 48h (96h sample). Fixed cells were stained with PI and fluorescence was measured via FACS. Results of analyzed and gated samples 96h after transfection are presented in the form of histograms. The intensity of fluorescent signal correlated with DNA content of the cells and conclusions were drawn about cell cycle phases, SubG1, G0/1, S and G2/M (A). Histogram statistics permitted illustration of distribution of cell cycle phases presented as % of investigated cells (B, means ± SDs; statistics: two-way ANOVA *p≤0.05, **p≤0.01, ***p≤0.001, data compared to particular control; n=3).

The histogram statistics of three different donors support previously shown results (Fig. 18). Significant changes in distribution of cell populations in G0/1, S and G2/M phases were detected in tunicamycin-treated cells after 48h compared to control. Also after 96h, a significant increase of apoptotic cells was measured in tunicamycin-treated

cells. Depletion of BiP due to SubAB treatment led to a significant arrest of the cells in G0/1 phase after 48h. After 96h, the percentage of apoptotic cells increased, although this was not statistically significantly different from the control. The occurrence of apoptotic cells in the control group and control siRNA-transfected cells was similar 48h and 96h after transfection. In addition, cells transfected with the siRNA molecules, s6980 and s6981, showed a similar percentage of apoptotic cells compared to controls. 48h after transfection 0.7% and 0.5% of total cells were apoptotic in s6980- and s6981-transfected cells. 13.2% of s6980-transfected and 7.4% of s6981-transfected cells appeared to be in an apoptotic stage 96h after transfection. The population of apoptotic cells in the siControl 96h after transfection accounted for 4.9%. These differences in apoptotic activity 96h after transfection were statistically non-significant. With regard to other cell cycle phases, the analysis indicated a similar distribution of cells in G0/1, S and G2/M of BiP down-regulated and control cells. Most of the cells stayed in G0/1 phase. The proportions of the cell population present in the S or G2/M phases were comparable between BiP down-regulated cells and the siControl.

In summary, the results from investigation of the cell cycle with regard to apoptosis were in agreement with the data from the annexinV staining study (see above). A slight apoptotic activity in BiP down-regulated cells was measured. However, the effect was not comparable to apoptotic agents or activation of high ER stress.

3.2.5 Glycosylation patterns on the cell membrane of BiP down-regulated cells

Activation of UPR signaling due to accumulation of unfolded proteins in the lumen of the ER leads to an inhibition of protein synthesis and processing (Lacour *et al.,* 2007). This also includes glycosylation of the proteins, a component of post-translational modification (Blom *et al.,* 2004). On account of this fact, BiP down-regulated cells were probed for glycosylation of membrane proteins. Fig. 19 A shows histograms of cells, stained with lectin PHA-L, an AlexaFluor 488-conjugated protein which binds to glycoresidues on the cell surface. For analysis, areas of non-fluorescent cells (M1), defined by unstained, untreated cells, and fluorescent cells (M2), defined by stained, untreated cells were delimited. For interpretation of the results cells possessing a high fluorescent signal were considered to have well-functioning glycosylation, whereas low fluorescence of the cells was taken to indicate deficits in the glycosylation process. Known as an inhibitor of N-glycosylation (Price and Tsvetanova, 2007), tunicamycin not only served as an inducer of ER stress but also as a positive control for defective glycosylation in this experiment.

The histograms in Fig. 19 A show that in control samples most of the cells were detected in the area of fluorescent cells. A comparable distribution was observed in the cells transfected with control siRNA molecules. However, the peak in the siControl was more stretched with less height. SubAB-treated cells also showed cells with a broad range of fluorescent intensities. Tunicamycin-treated cells as positive control, showed two peaks in the histogram, one located in M1 and one placed in the M2 area. Within this single experiment, approximately 33% of measured cells gave a low fluorescent signal, which could indicate defective glycosylation. The histogram of s6980-transfected cells was similar to the histogram of tunicamycin-treated cells. Here as well, a peak in the M1 area was detectable 96h after transfection. Both measured peaks appeared to be broader. Remarkably, cells transfected with s6981 molecules did not show any deficits in glycosylation according to this assay. 84% of the cells a showed high fluorescent signal. The analysis of histogram statistics of four different donors (Fig. 19 B) confirmed these observations. Already 48h after transfection, differences in percentages of fluorescent cells were detected. Tunicamycin-treated, SubAB-treated and BiP down-regulated cells exhibited less fluorescence compared to control samples, whereas ER stress-induced samples presented the lowest proportion of fluorescent cells, thus representing a significant decrease of glycosylation. Fluorescent signals of s6980- and s6981-transfected cells were also significantly decreased. 96h after transfection the effect of tunicamycin treatment and BiP down-regulation as a result of s6980 transfection was even higher compared to control. Only 55% of the cells in tunicamycin-treated samples and 72% in s6980-transfected samples represented a fluorescent signal which indicative of a well-functioning glycosylation. SubAB-treated and s6981-transfected samples showed fewer fluorescent cells 96h after transfection, but not to the extent of tunicamycin-treated and s6980-transfected cells.

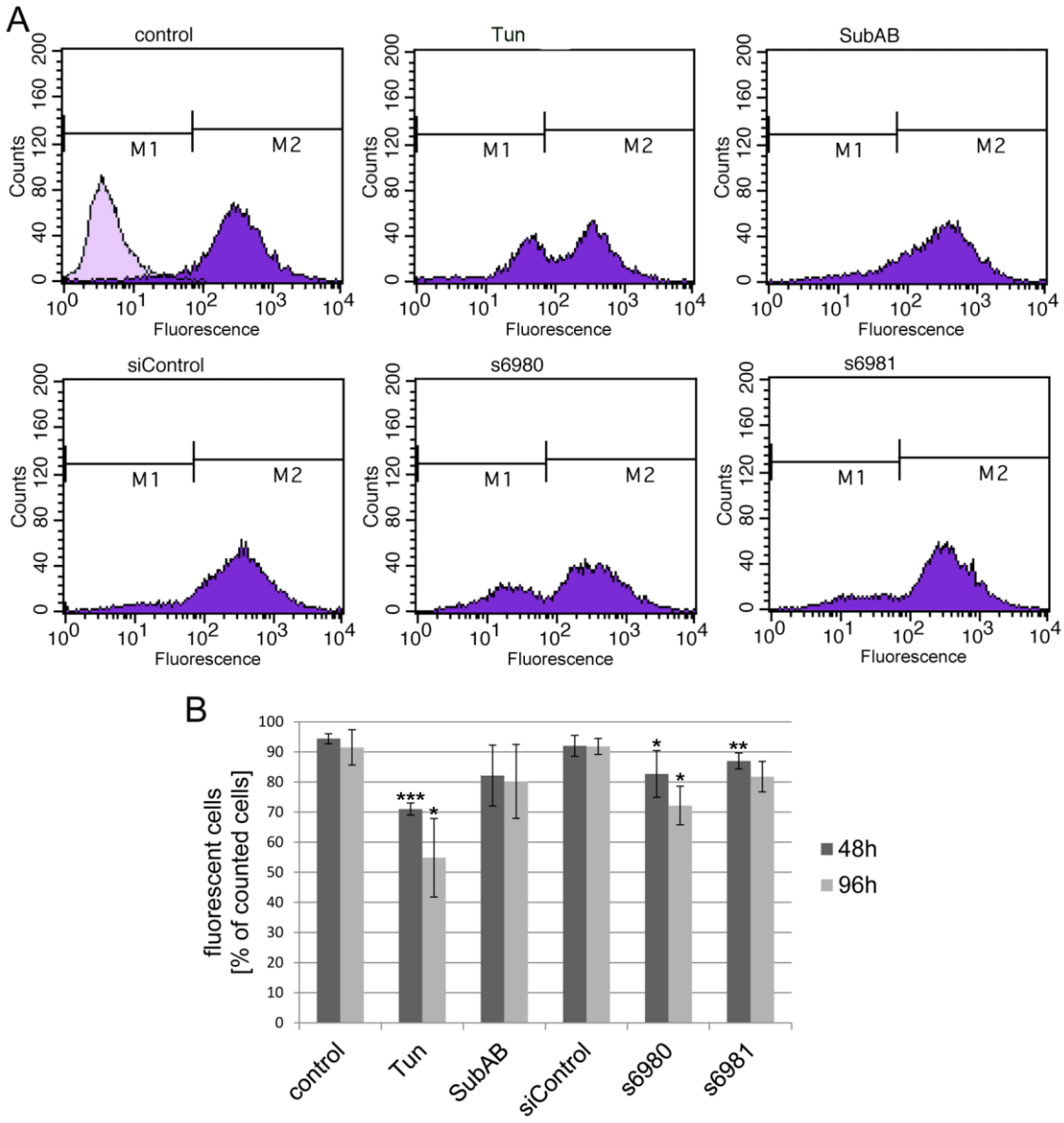

Fig. 19: Glycosylation of BiP down-regulated cells and cells under ER stress.

HUVEC transfected with siRNA molecules s6980 and s6981 to down-regulate BiP were investigated for degree of glycosylation. As positive control of inhibition of glycosylation cells were treated with 2 µg/ml tunicamycin for 24h (48h sample) and 48h (96h sample). Cells were treated with SubAB (100 ng/ml) for 24h (48h sample) and 48h (96h sample) to cross-check BiP down-regulation by disassembly of the protein by the toxin. Cells were stained using lectin PHA-L, an AlexFluor 488 conjugated protein, which binds to glycoresidues presented on the cell surface. Intensity of fluorescence was determined using FACS analysis. Histograms show distribution of fluorescent cells in relation to counted cells 96h after transfection (A). Areas of low fluorescent (M1) and high fluorescent (M2) cells were defined on the basis of fluorescent intensity of stained, untreated cells (control, M2 in purple) and unstained, untreated cells (control, M1 in light purple). Evaluation of histogram statistics is shown in B and presents percentages of highly fluorescent cells as a measure of well-functioning glycosylation, determined 48h and 96h after transfection (means ± SDs; statistics: paired t-test, data compared to respective control *p≤0.05, **p≤0.01, ***p≤0.001; n=4).

3.2.6 Xbp1-splicing following BiP down-regulation

Due to the fact that BiP is not only a mediator in the ER stress signaling pathway but also a chaperone with the function of protein folding, the effects resulting from BiP down-regulation could have different causes. To determine if BiP down-regulation leads to an activation of UPR, the samples were tested for Xbp1-splicing (Fig. 20). As a result of UPR activation and subsequent auto-phosphorylation of IRE1α, mRNA of Xbp1 is spliced by endonuclease activity of the receptor. After translation to protein, Xbp1 acts as an active transcription factor. Hence, splicing of Xbp1 mRNA is used as an indicator for UPR activation (Schadewijk *et al.,* 2012). The spliced form of the Xbp1 mRNA was detectable in cells treated with tunicmaycin in an u/s (unspliced/spliced) experimental approach detecting both variations simultaneously. Remarkably, in BiP down-regulated cells transfected with siRNA molecules and SubAB-treated cells the spliced form of Xbp1 was detectable. In particular, SubAB-treated cells showed high amounts of the spliced form of Xbp1. The lower band (spliced form) was more intensive compared to the upper band (unspliced form) and compared to UPR-activated and siRNA-transfected cells. Three different donors were tested and in all of them splicing of Xbp1 mRNA was observed as in the above-mentioned samples. This indicates activation of the UPR in cells with deficiency of the protein BiP.

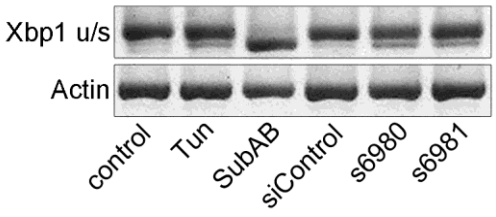

Fig. 20: Splicing of transcription factor Xbp1 mRNA in response to BiP down-regulation.
HUVEC were transfected with control siRNA, s6980 and s6981. To activate UPR signaling pathway, cells were treated with 2 µg/ml tunicamycin. To cross-check BiP down-regulation, cells were treated with 100 ng/ml SubAB toxin. 48h after transfection splicing of transcription factor Xbp1 mRNA was investigated with the help of RT PCR. Amplicons were separated on 2% agarose gel and detected using ethidium bromide. Actin was detected as reference.

3.2.7 Effect of BiP down-regulation on expression of other UPR members

UPR involves three individual signaling pathways. Xbp1 is a transcription factor in the IRE1α pathway. In addition, the expression of further members of the UPR pathway was investigated in BiP down-regulated HUVEC at mRNA level (Fig. 21). The expression of ATF4, a transcription factor of the signaling pathway, was slightly increased in all the samples compared to control but statistically non-significant. ATF6, another transcription factor, was not up-regulated on tunicamycin treatment or down-regulation of BiP, or by SubAB treatment or siRNA transfection. Moreover, expression

of the UPR receptors PERK and IRE1α was not increased under the above-mentioned experimental conditions.

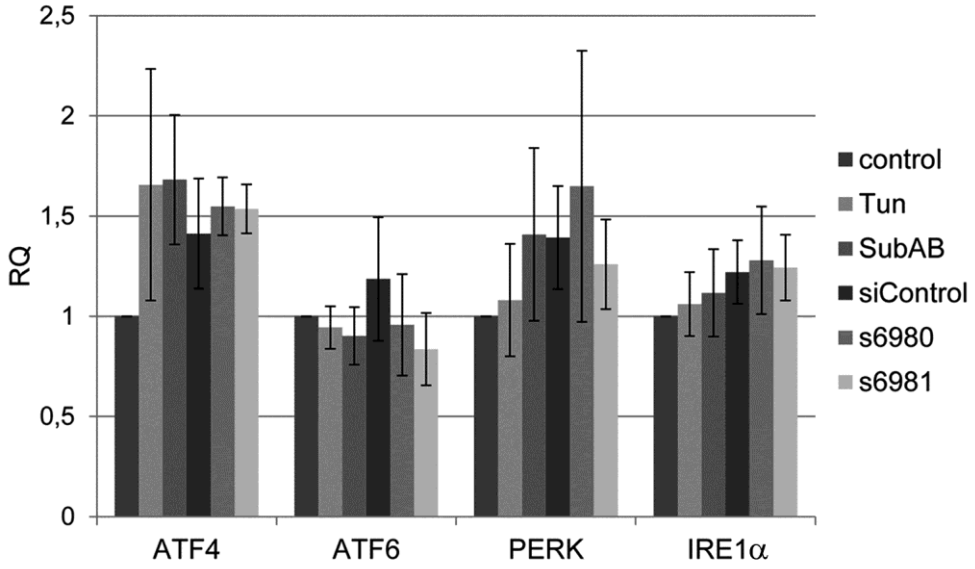

Fig. 21: Expression of UPR members ATF4, ATF6, PERK and IRE1α in BiP down-regulated cells at mRNA level.

HUVEC were transfected with control siRNA, s6980 and s6981 and RNA was isolated 48h after transfection. For positive control of UPR activation cells were treated with tunicamycin (2 µg/ml). For cross-checking of BiP down-regulation, cells were treated with 100 ng/ml SubAB toxin. Gene expression was analyzed by real time PCR. Data are shown as relative quantification (RQ). Untreated control was set as 1 (means ± SDs; n=4).

3.3 Inflammatory response of BiP down-regulated endothelial cells

Endothelial cells play an important role in inflammation. In order to elucidate a possible role of BiP in the early stage of the inflammatory process, secretion of cytokines and expression of adhesion molecules were investigated. With regard to wound healing-induced inflammation, the cytokines interleukin-8 (IL-8) and monocyte chemotactic protein 1 (MCP-1) are released to attract leukocytes during the initial inflammatory response (Bossink *et al.,* 1995; van Zee, K. J. *et al.,* 1991). In the depicted experiments, the release of cytokines IL-8 and MCP-1 was investigated under regular and pro-inflammatory conditions via ELISA.

BiP down-regulated cells showed a slight increase in IL-8 secretion, even without addition of a pro-inflammatory stimulant, whereas in cells transfected with s6981 siRNAs a higher release of IL-8 was observed compared to s6980-transfected cells (Fig. 22). To simulate an inflammatory process in endothelium, HUVEC were treated with TNFα. Two concentrations were chosen to investigate inflammatory responses of the cells. The values from non-transfected cells stimulated with 75 U/ml TNFα were set as 1 for normalization. Treatment with 75 U/ml TNFα led to a strong induction of the

inflammatory response and a high increase in IL-8 release. Comparing secretion of cytokines in control and siControl, no differences could be observed. Strikingly, a threefold increase of IL-8 release was noticed in TNFα-treated s6980-transfected cells compared to TNFα-treated control cells. BiP down-regulation due to s6981 led to an even higher rise in IL-8 i after TNFα treatment, namely 3.8-fold. Treatment of the cells with 300 U/ml TNFα caused a slight increase of IL-8 secretion compared to stimulation with 75 U/ml TNFα, but not significantly. Nonetheless, treatment of the s6980-transfected cells with 300 U/ml TNFα showed a strong effect on IL-8 release. Secretion of IL-8 rose to 3.9-fold. For s6981- transfected cells, an increase of IL-8 release was measured as 4.7-fold higher compared to control.

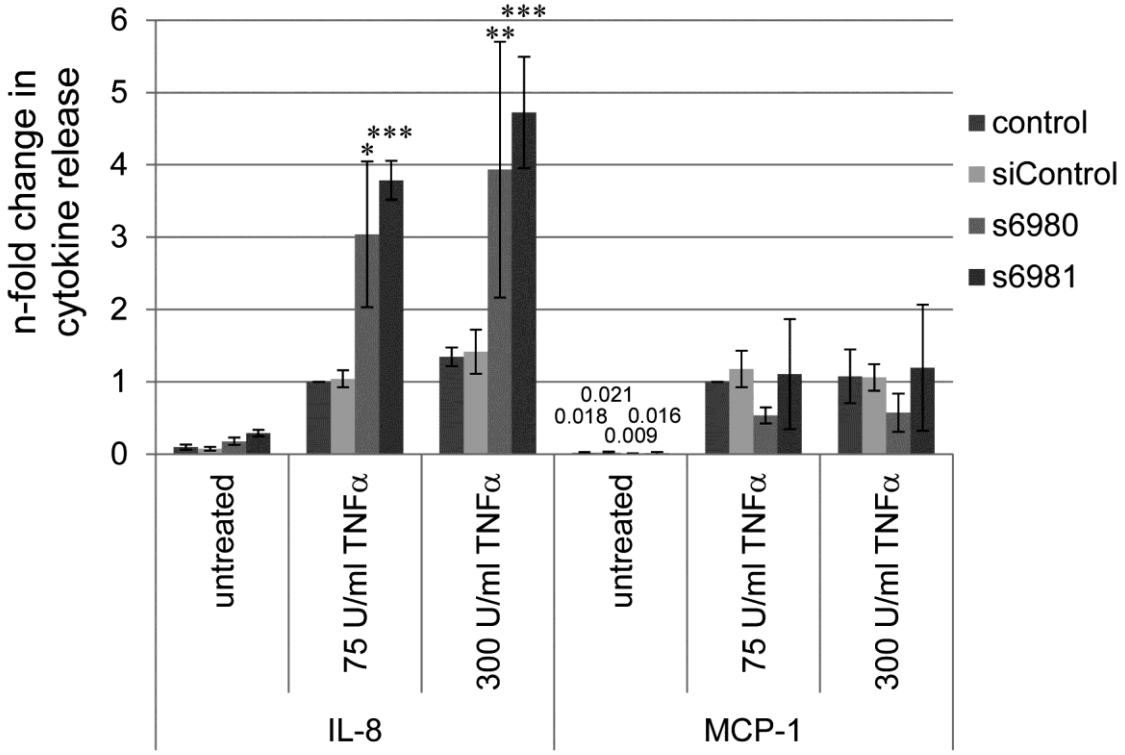

Fig. 22: Release of cytokines IL-8 and MCP-1 by BiP down-regulated cells upon pro-inflammatory activation.

48h after transfection of the cells with control siRNA (siControl), siRNA molecules s6980 and s6981, cells were stimulated with 75 U/ml or 300 U/ml TNFα for 24h to induce an inflammatory response. Release of IL-8 and MCP-1 was measured via ELISA. Results were normalized to untransfected control cells treated with 75 U/ml TNFα and illustrated as n-fold change in cytokine release. Data describing release of MCP-1 of untreated cells are additionally listed because of small bars on the scale (means ± SDs; statistics: two-way ANOVA, *p≤0.5, **p≤0.01, ***p≤0.001, data compared to particular control; n=3).

Remarkably, release of MCP-1 decreased in untreated cells, in which BiP was down-regulated using siRNA s6980. Cells transfected with s6981 showed similar release of the cytokine compared to control and siControl. Under inflammatory conditions, mean release of MCP-1 of s6981-transfected cells was comparable to secretion of control cells stimulated with 75 U/ml TNFα. In contrast, a reduction of MCP-1 release down to

50% was observed in BiP down-regulated cells transfected with s6980 siRNA. Treatment of s6980-transfected cells with 300 U/ml TNFα did not lead to a further inhibition of cytokine release compared to treatment of these cells with 75 U/ml TNFα. But the secretion of MCP-1 did not differ in control cells treated with 75 U/ml TNFα and 300 U/ml TNFα.

The next step in the inflammatory response is the presentation of adhesion molecules ICAM-1 and E-selectin on the outer aspect of the plasma membrane of endothelial cells. These molecules enable attachment of leucocytes attracted by the released cytokines to the vessel wall. Furthermore, they facilitate transmigration of the inflammatory cells to the site of inflammation (Peters *et al.,* 2003). On the basis of these important functions, expression of ICAM-1 and E-selectin was investigated under normal and inflammatory conditions (Fig. 23). With regard to ICAM-1 expression, no changes were observed between control cells and BiP down-regulated cells, if inflammation was not stimulated. On the other hand, a 1.7-fold increase of ICAM-1 expression was detected in HUVEC transfected with s6980 stimulated with 75 U/ml TNFα compared to untransfected control. Comparing control cells treated with 75 U/ml TNFα and s6981-transfected cells, the increase in ICAM-1 could also be observed but it was minor compared to s6980-transfected cells. Stimulation of the cells with 300 U/ml TNFα led to effects similar to ICAM-1 expression in the cells treated with 75 U/ml TNFα. The increase of ICAM-1 expression as a result of TNFα treatment in BiP down-regulated cells was statistically significant compared to the expression in control cells.

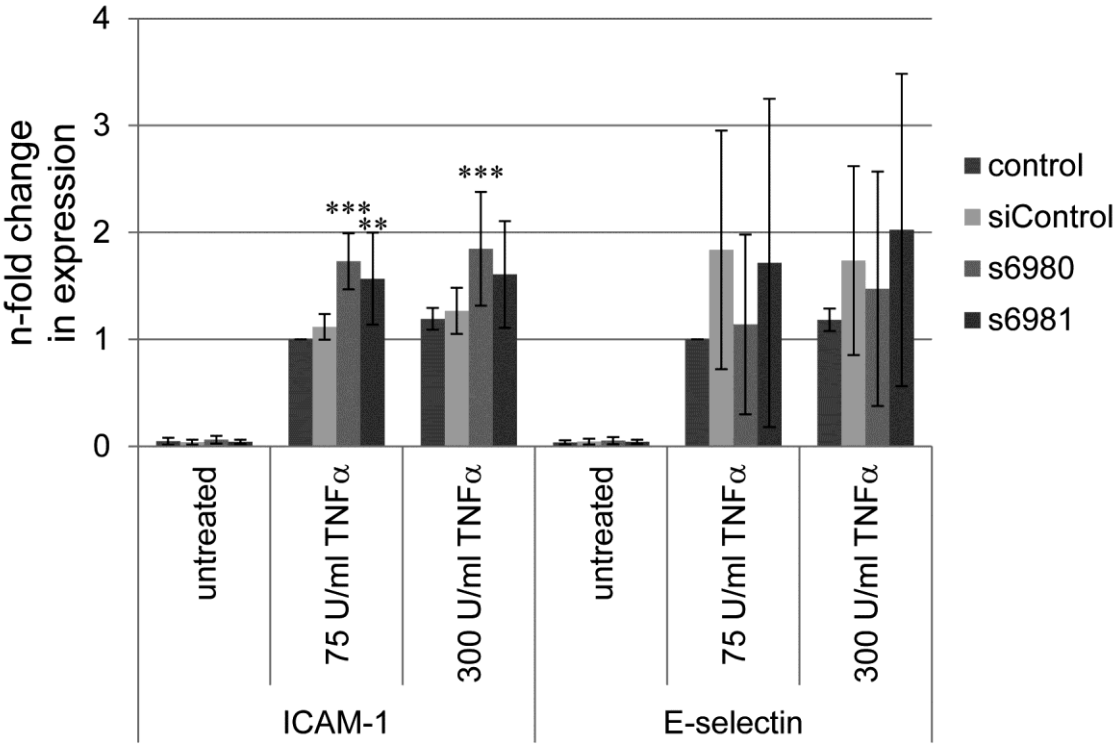

Fig. 23: Expression of adhesion molecules ICAM-1 and E-selectin in BiP down-regulated cells under inflammatory conditions.

48h after transfection of the cells with control siRNA (siControl), siRNA molecules s6980 and s6981, cells were stimulated with 75 U/ml or 300 U/ml TNFα for 24h (ICAM-1) or 4h (E-selectin) to induce an inflammatory response. Expression of inflammatory markers ICAM-1 and E-selectin was analyzed via EIA. Results were normalized to untransfected control cells treated with 75 U/ml TNFα and illustrated as n-fold change in expression (means ± SDs; statistics: two-way ANOVA, **p≤0.01, ***p≤0.001, data compared to particular control; n=5).

Considering expression of the adhesion molecule, E-selectin, a change in its expression was observed between control cells and cells transfected with control siRNA. High standard deviation in transfected samples could point to fluctuations in the expression. In this case, too, the higher concentration of TNFα did not lead to a higher expression of E-selectin. Significant differences in E-selectin expression were not detected in BiP down-regulated cells compared to control cells, neither as result of stimulation with 75 U/ml TNFα nor 300 U/ml TNFα. Nonetheless, an increase of expression was observed in case of inducing inflammatory response in control and transfected cells compared to untreated cells.

3.4 The effects of BiP on angiogenic activity of endothelial cells

Besides their role in inflammation, endothelial cells play an important part in angiogenesis, in which new blood vessels are formed from the pre-existing microvasculature (Sumpio *et al.,* 2002). Thus, experiments were carried out to investigate the behavior of BiP down-regulated cells in angiogenic assays *in vitro*.

3.4.1 Migration behavior of BiP down-regulated cells

Migration of endothelial cells constitutes a basic process in angiogenesis (Lamalice *et al.,* 2007; Ausprunk and Folkman, 1977). In a modified scratch assay, migration of BiP down-regulated cells was investigated.

In Fig. 24, the migration behavior of control cells and BiP down-regulated cells is shown over a time period of 32h. 48h after transfection, the time point of maximum down-regulation, the insert was removed and the pictures of the gap were taken (time point 0h). 8h after removing the insert, migration of the cells into the gap was observed. At this time point the migration behavior of control cells and s6980- and s6981-transfected cells was similar. However, 24h after the experiment started, differences in migration of the cells were observed. The migration of BiP down-regulated cells was inhibited compared to control cells, which bridged the gap almost completely. Of the BiP down-regulated cells, s6981-transfected cells migrated faster than s6980-transfected ones. This inhibition of migration in BiP down-regulated cells persisted up to 32h. The assay was performed with three different donors and images were quantified by Wimasis Image Analysis. The percentage of the cell covered area was determined by pseudocolour representation. Results were evaluated and illustrated in histogram form in Fig. 25. In the first 8h after the insert was removed the quantification indicated the onset of cell migration. After 24h control and siControl cells exhibited a cell covered area of nearly 100 %. No difference between the control cells and control siRNA-transfected cells could be detected. Strikingly, s6980-transfected cells were inhibited in migration as early as after 8h. After 24h the inhibition was even more obvious, with migration of the down-regulated cells being significantly slower than the migration of control cells. Remarkably, 32h after the insert was removed s6980-transfected cells showed a cell covered area comparable to starting conditions. S6981-transfected cells closed the gap gradually, but the cells migrated much slower compared to control cells.

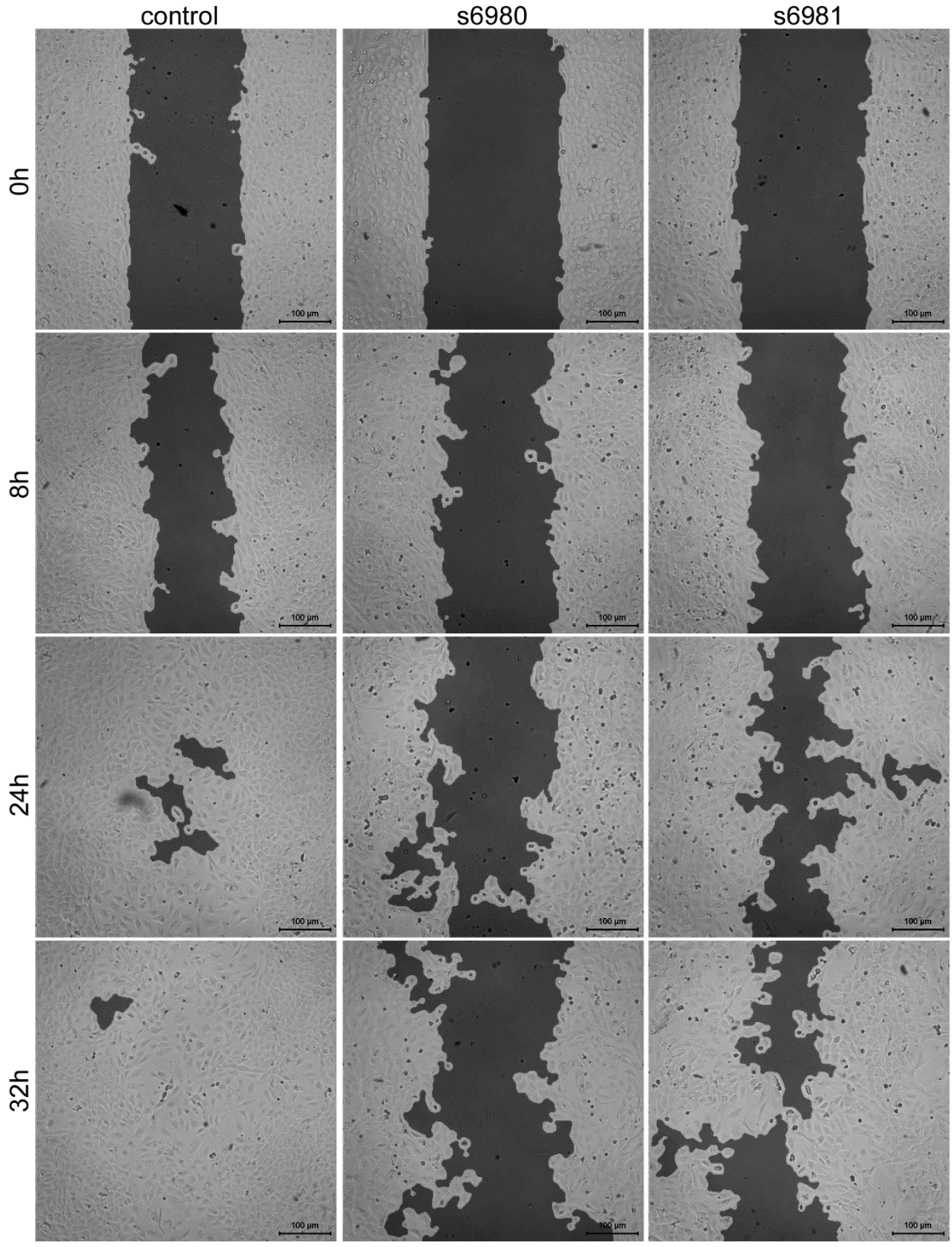

Fig. 24: Migration of BiP down-regulated cells.

In a modified scratch assay migration of control cells, s6980- and s6981-transfected cells was observed. About 48h after transfection, when the cells had reached confluency, the insert, which separated two cell chambers, was removed. Images of the gap were taken 0h, 8h, 24h and 32h after removing the insert. Images are presented in black and white, whereby light-colored area represented cell covered area (scale bar: 100 µm).

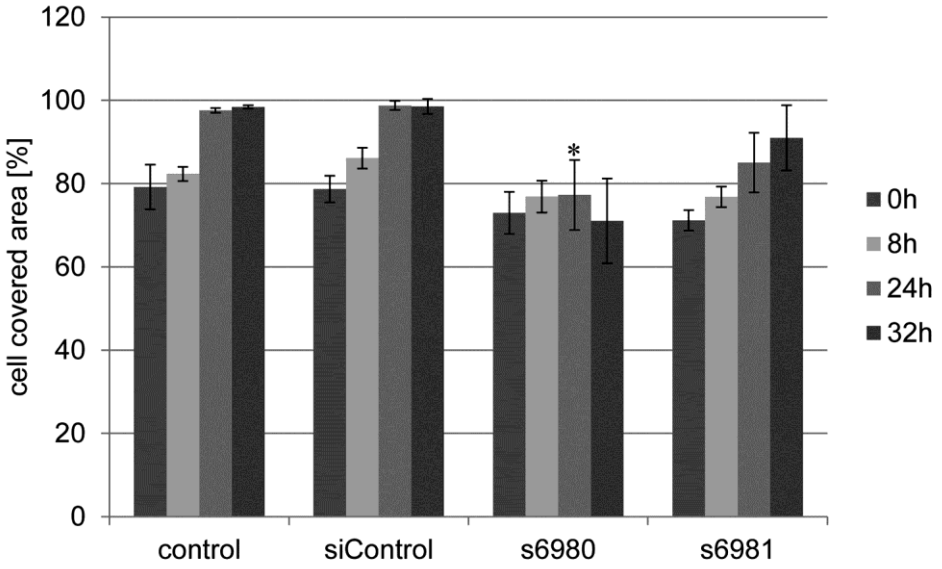

Fig. 25: Evaluation of modified scratch assay.

Images of migration assay were quantified as percentage of cell-covered area determined with help of the WimScratch application by Wimasis. Results of three different donors were summarized and statistical analysis was performed (means ± SDs, statistics: paired t-test, *p≤0.05; n=3).

In addition, cells were treated with the toxin SubAB, to support result of the modified migration assay with BiP down-regulated cells following siRNA transfection (Fig. 26 A). In addition to untreated cells used as a control, cells were treated with the mutated form of the toxin $SuBA_{A272}B$, which has no effect on BiP protein levels. Both untreated cells and cells treated with $SuBA_{A272}B$ showed similar migration behavior. Already after 8h the cells migrated into the gap and after 24h the gap was closed nearly completely. SubAB-treated cells started to migrate within the first 8h, but the migration was slower than in the control cells. 24h after the insert was removed migration of BiP-depleted cells was significantly inhibited. Additionally, the modified scratch assay was carried out with endothelial cells treated with tunicamycin, a potent ER-stressor and activator of the UPR. Results of tunicamycin-treated cells were similar to SubAB-treated cells. Thus, after 8h cells started to migrate slowly, but 24h after the insert was removed, cells treated with tunicamycin showed a significant reduction in migration (Fig. 26 B).

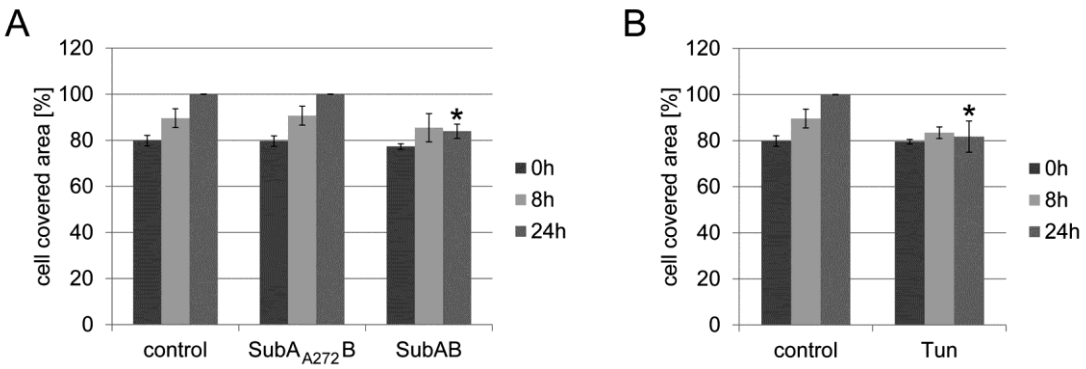

Fig. 26: Migration of primary endothelial following depletion of the chaperone BiP and under ER stress.

In a modified scratch assay, migration behavior of HUVEC was investigated after treatment of the cells with 100 ng/ml SubAB, which led to the depletion of BiP. Untreated cells were used as control. As a second control group, cells were treated with 100 ng/ml SubA$_{A272}$B (A). To induce ER stress, cells were treated with 2µg/ml tunicamycin (B). After 18h of treatment, the insert was removed and migration of the cells into the gap was observed. Images were taken after 0h, 8h and 24h and the cell-covered area was quantified via pseudocolour representation of WimScratch application by Wimasis. Data are presented as percentage of cell-covered area (means ± SDs, statistics: paired t-test, *p≤0.05; n=3).

3.4.2 Role of BiP in formation of capillary-like structures

In order to elucidate the effect of BiP down-regulation on the formation of capillary-like structures, angiogenesis assays were performed. Initially, cells were transfected and 32h after transfection a collagen gel was put on top of the confluent cell layer. Pro-angiogenic growth factors, VEGF and bFGF, were applied to stimulate tube formation (Fig. 27). Subsequently, after 24h of culturing, capillary-like structures were formed in samples with cells transfected with control siRNA. A formation of angiogenic structures was also detected in non-transfected cells (data not shown). Compared to both control groups, s6980-transfected cells formed shorter tubes. Additionally, capillary-like structures were not well connected compared to the siControl. Formation of capillary-like structures in s6981-transfected cells was similar to s6980-transfected cells.

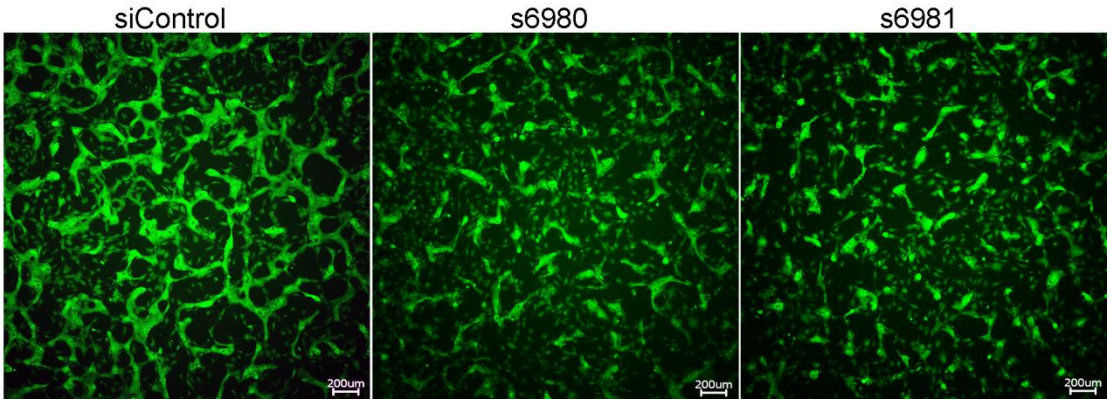

Fig. 27: Formation of capillary-like structures of BiP down-regulated endothelial cells in a 2D angiogenic assay.

A confluent layer of HUVEC, transfected with control siRNA and BiP down-regulating siRNAs s6980 and s6981, was covered with a collagen gel 32h after transfection. 24h later, cells were visualized with calcein-AM (scale bar: 200 µm).

In vivo, extracellular matrix (ECM) serves as a three-dimensional malleable scaffold for endothelial cells and plays a very important role in angiogenesis (Senger and Davis, 2011). Furthermore, collagen I, an essential component of the ECM, is known to stimulate spindle-shaped morphology of endothelial cells *in vivo* (Montesano *et al.,* 1983; Sweeney *et al.,* 1998). Hence, a 3D *in vitro* angiogenesis assay was performed to mimic a more *in vivo*-like situation. Therefore, cells were transfected with the BiP down-regulating siRNA molecules, s6980 and s6981, and 48h after transfection, the time-point of maximum BiP down-regulation, seeded into the collagen-fibrin gel. Pro-angiogenic factors were applied to the medium covering the gels. After 48h of culturing, the formation of capillary-like structures was observed (Fig. 28 A). After calcein-AM staining, well-branched angiogenic structures could be observed in the siControl. Importantly, s6981-transfected cells showed less capillary-like structures than control cells. Formation of short tubes, which were rarely branched, was monitored in cells transfected with siRNA s6980. Data could be supported by quantification of tube formation of four different donors (Fig. 28 B). With regard to the amount of total tubes s6980-transfected cells showed a significant decrease in tube formation, compared to the amount of total tubes in siControl. S6981-transfected cells formed 15% less tubes than control cells. Total tube length also significantly decreased to 21% in cells transfected with s6980, compared to control. The total length of the tubes was also lower in s6981-transfected cells but did not differ significantly. 82% of total tube length was reached, compared to control cells. Finally, as a result of BiP down-regulation, 29% less branching points were formed in s6981-transfected cells and 93% in s6980-transfected cells compared to control samples. In summary, formation of capillary-like structure network was significantly inhibited in BiP down-regulated cells.

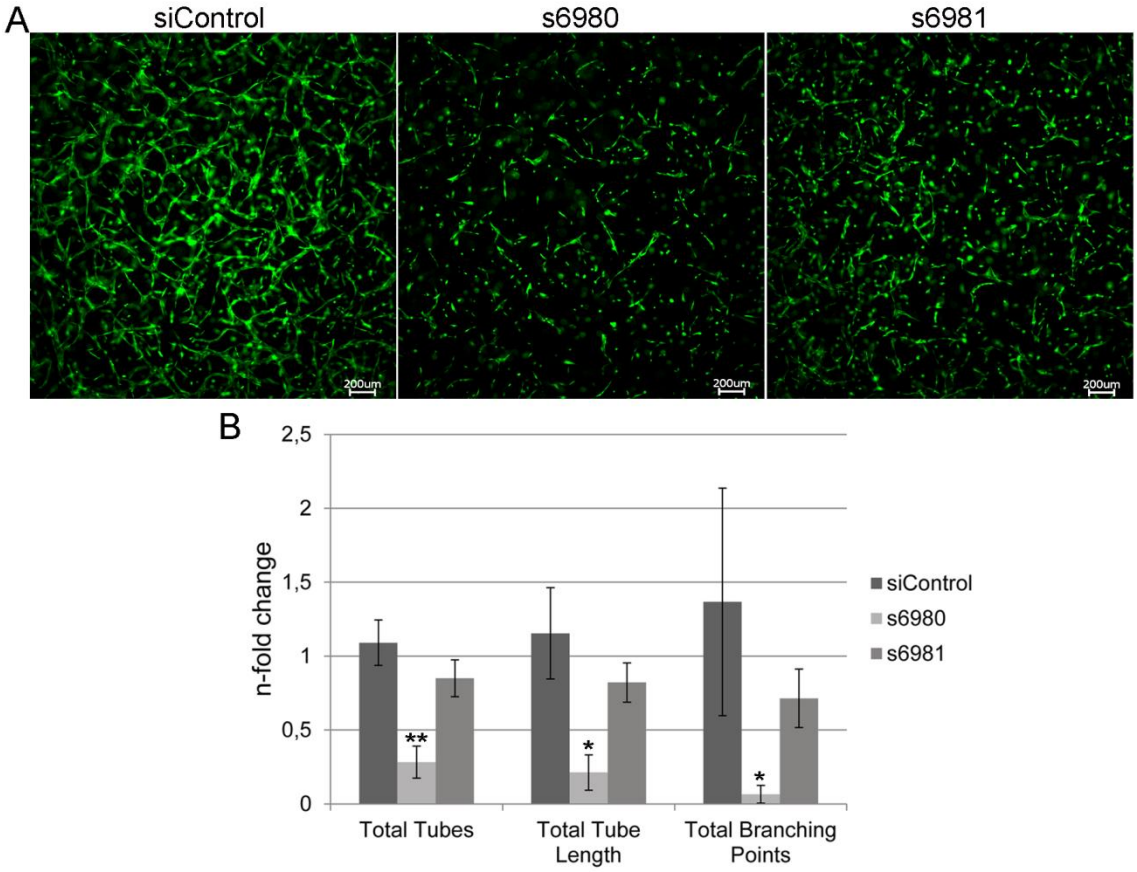

Fig. 28: Angiogenic structure formation of BiP down-regulated cells in a 3D *in vitro* angiogenesis assay.

Cells transfected with control siRNA and siRNAs s6980 and s6981 were embedded in a collagen-fibrin gel 48h after transfection. After 48h of culturing, cells were stained with calcein-AM (A, scale bar: 200 µm). Images, taken from assays performed with four different donors, were quantified using WimTube application by Wimasis in respect to total tubes, total tube length and total branching points (B). For normalization, non-transfected cells were set as 1 (means ± SDs, statistics: paired t-test, *p≤0.05, **p≤0.01; n=4).

Additional experiments were carried out in which the formation of capillary-like structures during the process of BiP down-regulation was observed. Hence, cells were embedded into the collagen-fibrin gels directly after transfection. Growth factors VEGF and bFGF were applied to the cell culture medium to induce tube formation. After 48h and 96h of culturing the cells in the collagen-fibrin gel, they were visualized by calcein-AM staining (Fig. 29). Within the first 48h after transfection, in which the BiP level slowly decreased in s6980- and s6981-transfected cells, cells formed capillary-like structures in control samples, but also in the down-regulated samples s6980 and s6981. Formed tubes were comparably long and branched. Formed tubes in siControl after 96h of culturing were stretched and the branches were well constituted. In contrast, 96h after transfection it was observed that the tubes formed in BiP down-regulated samples were retracted. S6981-transfected cells showed a decrease of formed capillary-like structures, but individual tubes and some branches were still

preserved. Previously formed angiogenic structures were totally regressed in s6980-transfected cells as a result of the low BiP protein level between 48h and 96h after transfection. To avoid possible assay-associated differences between angiogenic setups stained with calcein-AM at 48h and 96 h after transfection, the formation of capillary like network in the 96h sample was also documented by light microscopy at the 48h time point (data not shown).

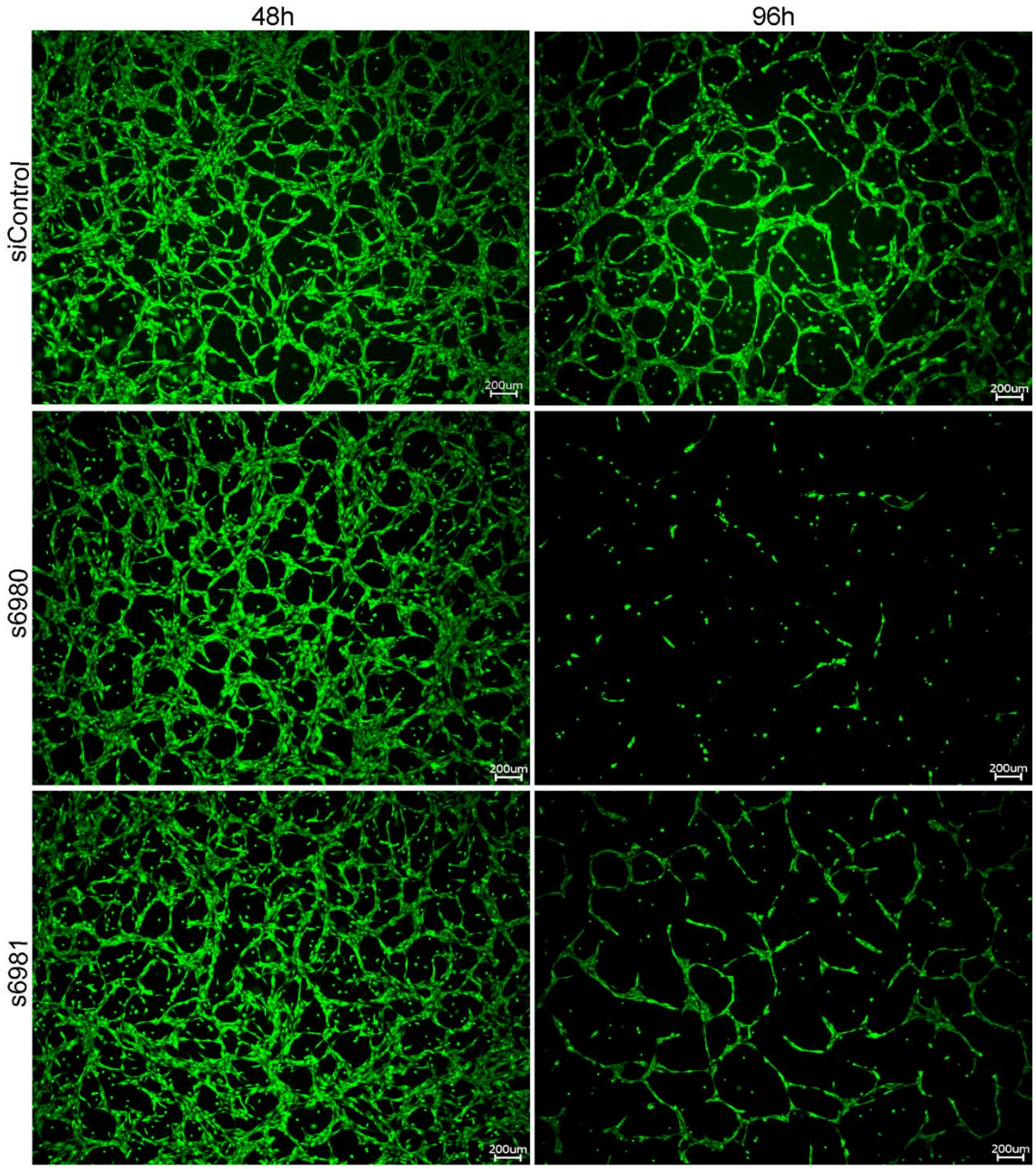

Fig. 29: Tube formation of BiP down-regulated cells seeded in a collagen-fibrin gel directly after transfection.

HUVEC, transfected with control siRNA and BiP down-regulating siRNA molecules s6980 and s6981 were embedded into a collagen-fibrin gel directly after transfection to observe tube formation during the process of BiP down-regulation. Growth factors VEGF and bFGF were added to the culture medium to stimulate tube formation. After 48h and 96h of culturing, samples were stained with calcein-AM to visualize the cells (scale bar: 200 µm).

The tube formation assay mentioned above was executed using three different donors, and images were quantified with the help of the WimTube application from Wimasis. Results are represented as n-fold change in total tube length, the amount of total tubes and total branching points (Fig. 30). Within the first 48h after transfection siControl cells, s6980- and s6981-transfected cells formed similar amounts of total tubes, as well as branching points. Samples were also similar with regard to tube length. Based on the fact that 48h after transfection a maximum of BiP down-regulation was reached and the level of the protein stayed very low until the time point 96h after transfection, images of samples were analyzed 96h after transfection. All samples showed a decline in all three capillary parameters. Thus, 70% of total tubes were detected in siControl 96h after transfection compared to 48h after transfection. Total tube length was retracted to 81% of tube length 96h after transfection and branching points fell to 75% comparing siControl 48h and 96h after transfection. Nevertheless, the retraction observed in BiP down-regulated samples was much stronger than in the siControl group. Remarkably, a significant decrease was observed in samples with s6980-transfected cells with regard to the amount of total tubes. The quantity of tubes decreased to 26% compared to the siControl (48h) 96h after transfection, whereas the amount of total tubes diminished to 47% in s6981-transfected cells compared to siControl (48h) at the same time point. With regard to total tube length, a drop to 34% in s6980-transfected cells was observed. Tubes in s6981-transfected samples still reached 59% of the tube length in controls 48h after transfection. The capability to form networks also decreased, as was reflected in 18% total branching points detected 96h after transfection with s6980, compared to control (48h). S6981-transfected cells exhibited 49% of formed branching points 96h after transfection, compared to the control group.

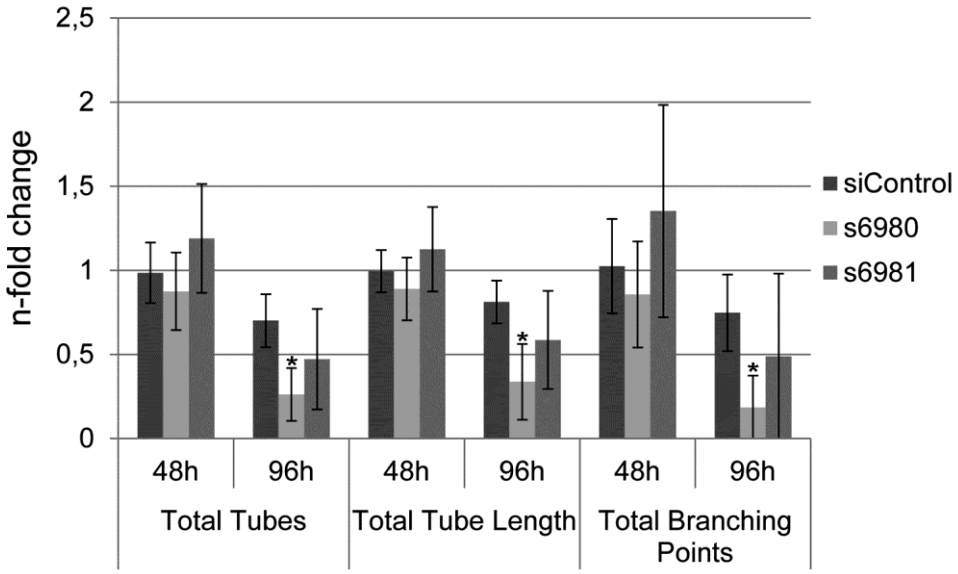

Fig. 30: Quantification of 3D tube formation assay using cells embedded in the collagen-fibrin gel directly after transfection.

HUVEC transfected with control siRNA, s6980 and s6981 were seeded into collagen-fibrin gels directly after transfection. VEGF and bFGF were applied for angiogenic stimulation of the endothelial cells. After 48h and 96h, cells were stained with calcein-AM and images were quantified via the WimTube application by Wimasis with regard to total tubes, total tube length and total branching points. For each parameter, data were normalized to non-transfected cells 48h after transfection. Results are presented as n-fold change (means ± SDs, statistics: paired t-test, *p≤0.05; n=3).

Similar experiments were also performed with cells treated with SubAB to confirm the results generated with siRNA-transfected cells. Besides untreated cells, $SubA_{A272}B$, was also used as an additional control. First, cells were pretreated with the toxins for 18h and then seeded into collagen-fibrin gels. In this experiment the capability to form capillary-like structures after BiP depletion was investigated. After 48h of culturing of the cells in the gel, they were subsequently visualized with calcein-AM (Fig. 31 A). The formation of capillary-like structures by untreated cells and the cells treated with $SubA_{A272}B$ was clearly seen. In contrast, SubAB-treated cells were totally rounded. No formation of angiogenic structures could be detected. Cells from a subsequent donor showed similar results.

In the second experiment cells were directly seeded into the collagen gel. Treatment of the cells with SubAB and the mutated form $SubA_{A272}B$ followed directly after embedding in the hydrogel. Hence, experimental design was comparable to the experiment presented in Fig. 29. Formation of capillary-like structures was analyzed 48h and 96h after seeding (Fig. 31 B). 48h after embedding, initial formation of tubes was observed in control samples and in samples treated with $SubA_{A272}B$. Samples treated with SubAB showed rounded cells. No capillary-like structures were formed at all. 96h after transfection angiogenic structures were also well-developed in control

samples. Additionally, tubes formed a well-branched network. Even after 96h of culturing, cells treated with SubAB did not form any angiogenic structures. These results could be supported by an angiogenesis assay using another donor.

To accomplish comparison of SubAB-treated cells and BiP down-regulated cells via siRNAs, the reduction of capillary-like structures was investigated. Cells were seeded into collagen-fibrin gel and angiogenesis was stimulated in the usual manner with the growth factors, VEGF and bFGF. After 72h of culturing, samples were treated with SubAB or $SubA_{A272}B$ for 24h and subsequently stained with calcein-AM. Fig. 31 C shows a well-branched network of capillary-like structures in a control sample and in the sample treated with $SubA_{A272}B$. The already formed capillary-like structures started to regress in SubAB-treated samples. Branching points were dissolved and tubes reformed as a result of BiP depletion. Experiment, executed with a second donor, supported shown data.

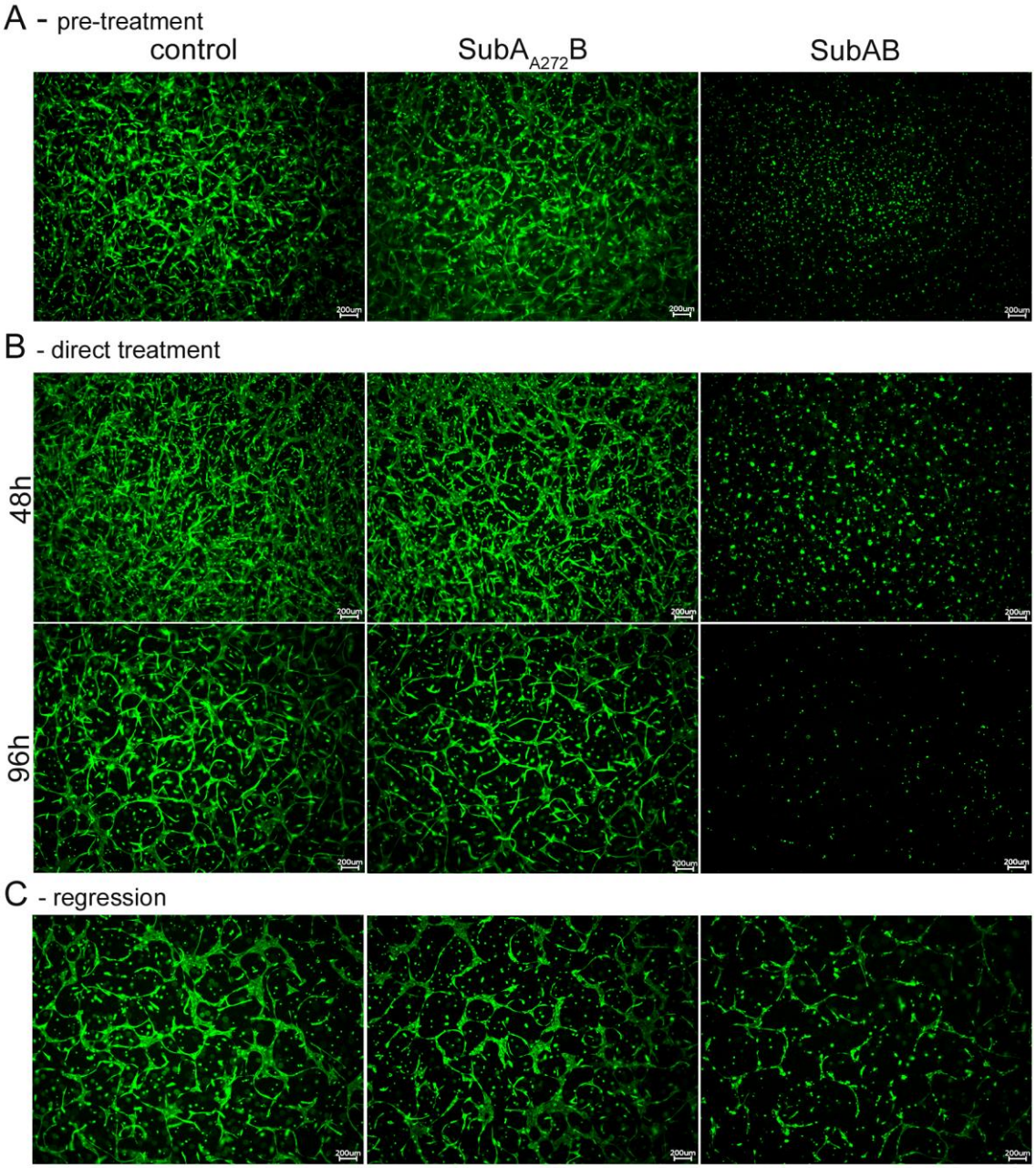

Fig. 31: Formation of capillary-like structures of BiP depleted cells.

HUVEC were treated with 100 ng/ml SubAB for BiP depletion. Untreated cells were used as control. In addition, cells were treated with 100 ng/ml of the mutated form of the toxin SubAB in a second control approach, named SubA$_{A272}$B. Cells were pre-treated for 18h with SubAB or SubA$_{A272}$B and seeded into collagen-fibrin gels. Cells were stained with calcein-AM after 48h of culture in the gel (A). In a second experimental design, cells were embedded in collagen-fibrin gels and treated with the agents directly after seeding. Samples were then visualized 48h and 96h after seeding (B). In addition, cells were seeded in the gels and 72h after embedding cells were treated with SubAB and SubA$_{A272}$B. After a further 24h period, cells were stained with calcein-AM (C, scale bar 200 µm).

To investigate the effect of ER stress on formation of capillary-like structures, experiments were performed once again with tunicamycin-treated cells. For comparative purposes the experiments were performed in the same manner as experiments with SubAB-treated cells. Thus, cells were pre-treated with tunicamycin for 18h. Subsequently, the stressed cells were cultured for 48h embedded in a collagen-fibrin gel and subsequently stained with calcein-AM. UPR-activated cells were not able to form angiogenic structures. Some of the tunicamycin-treated cells showed an elongated morphology, but tubes were not formed (Fig. 32 A).

Additionally, cells were seeded in the collagen-fibrin gels and treated directly with tunicamycin (Fig. 32 B). 48h after embedding, formation of capillary-like structures was observed in control samples, whereas cells with activated UPR following tunicamycin treatment showed rounded morphology. The formation of capillary-like structures was not observed. In samples treated with tunicamycin few cells were detectable 96h after seeding, presumably due to a toxic effect of the UPR stimulating agent or possibly to activation of the apoptotic pathway as a result of the prolonged ER stress.

The regression of capillary-like structures was also analyzed. Already-formed tubes were exposed to ER stress by tunicamycin treatment (Fig. 32 C). UPR-activated cells lost pre-formed angiogenic structures. The already-formed structures were not preserved. Similar to BiP-depleted cells, pre-formed tubes and branching points disappeared.

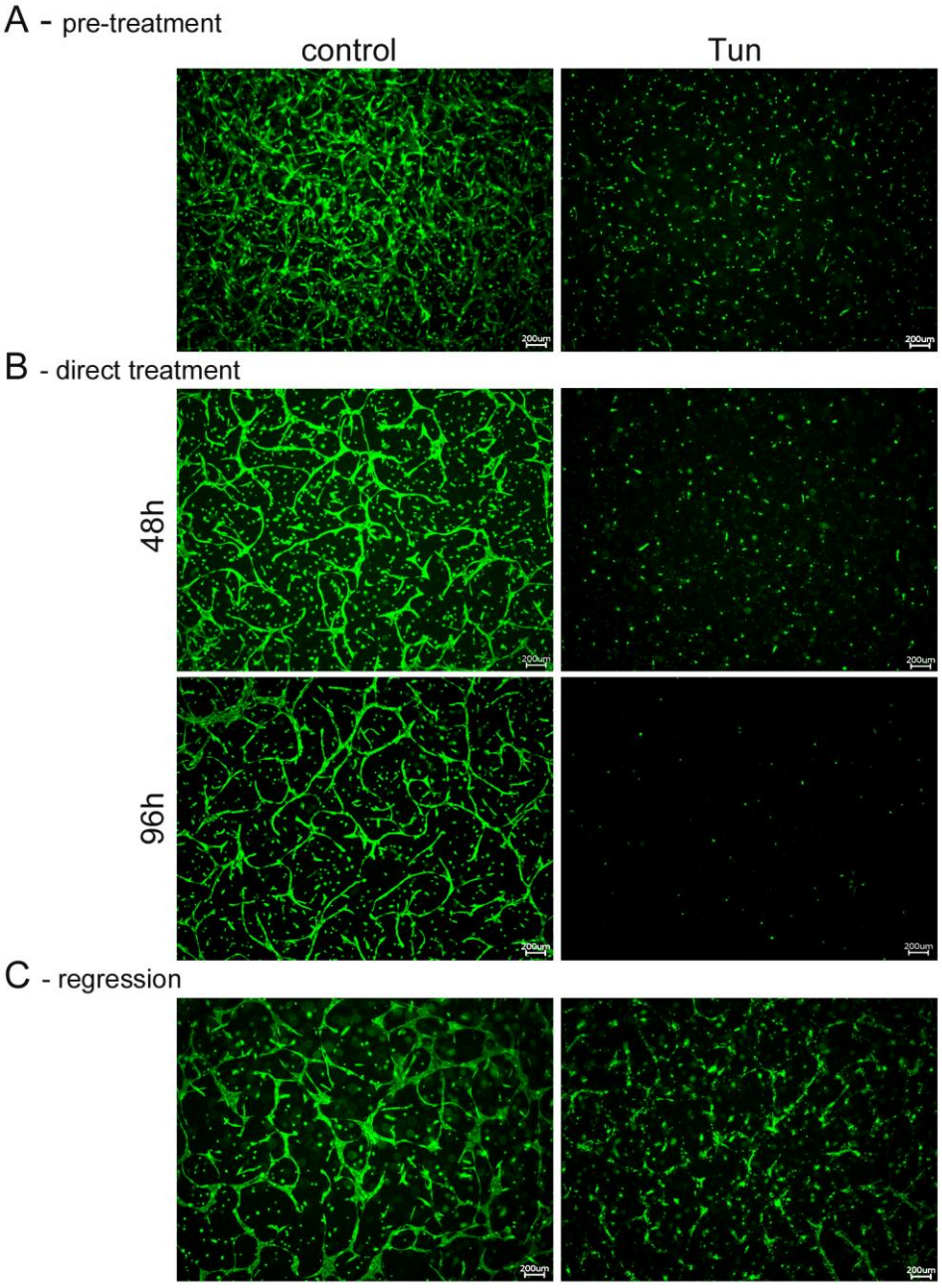

Fig. 32: Formation of capillary-like structures as a result of ER stress.

HUVEC were treated with 2 µg/ml tunicamycin to induce ER stress. As control, untreated cells were used. Cells were pre-treated with tunicamycin for 18h and seeded afterwards into collagen-fibrin gels. After a further 48h period, cells were stained with calcein-AM (A). Additionally, cells were embedded in collagen-fibrin gels and treated directly after seeding with the stress-stimulating agent. 48h and 96h after embedding, cells were visualized (B). In a third experimental procedure, regression of already-formed tubes due to ER stress was investigated. 72h after embedding, cells were treated with tunicamycin and stained after a further 24h of culture (C, scale bar 200 µm).

3.4.3 UPR receptors and their roles in angiogenesis

In the experiments with BiP down-regulated cells with inhibited migration, loss of the capability to form capillary-like structures and regression of already-formed angiogenic structures were observed. UPR-activated cells showed similar results. To understand the connection between BiP down-regulation and UPR activation, migration assays and 3D *in vitro* angiogenesis assays were performed with UPR receptor down-regulated cells. Receptors PERK and IRE1α were down-regulated using siRNA molecules (s18102 for PERK down-regulation: PERK↓ and s200432 for IRE1α down-regulation: IRE1α↓). First, migration behavior of the transfected cells was analyzed. As can be seen in Fig. 33 A, no differences in migration behavior could be observed between UPR receptor down-regulated and control cells, this being confirmed in three different donors. With regard to the capability to form capillary-like structures similar results were established (Fig. 33 B). Cells were embedded into the collagen-fibrin gel directly after transfection. PERK down-regulated cells formed well-branched tubes 48h after transfection and even 96h after transfection already-formed angiogenic structures were sustained. IRE1α down-regulated cells presented well-formed tubes 48h and 96h after transfection as well.

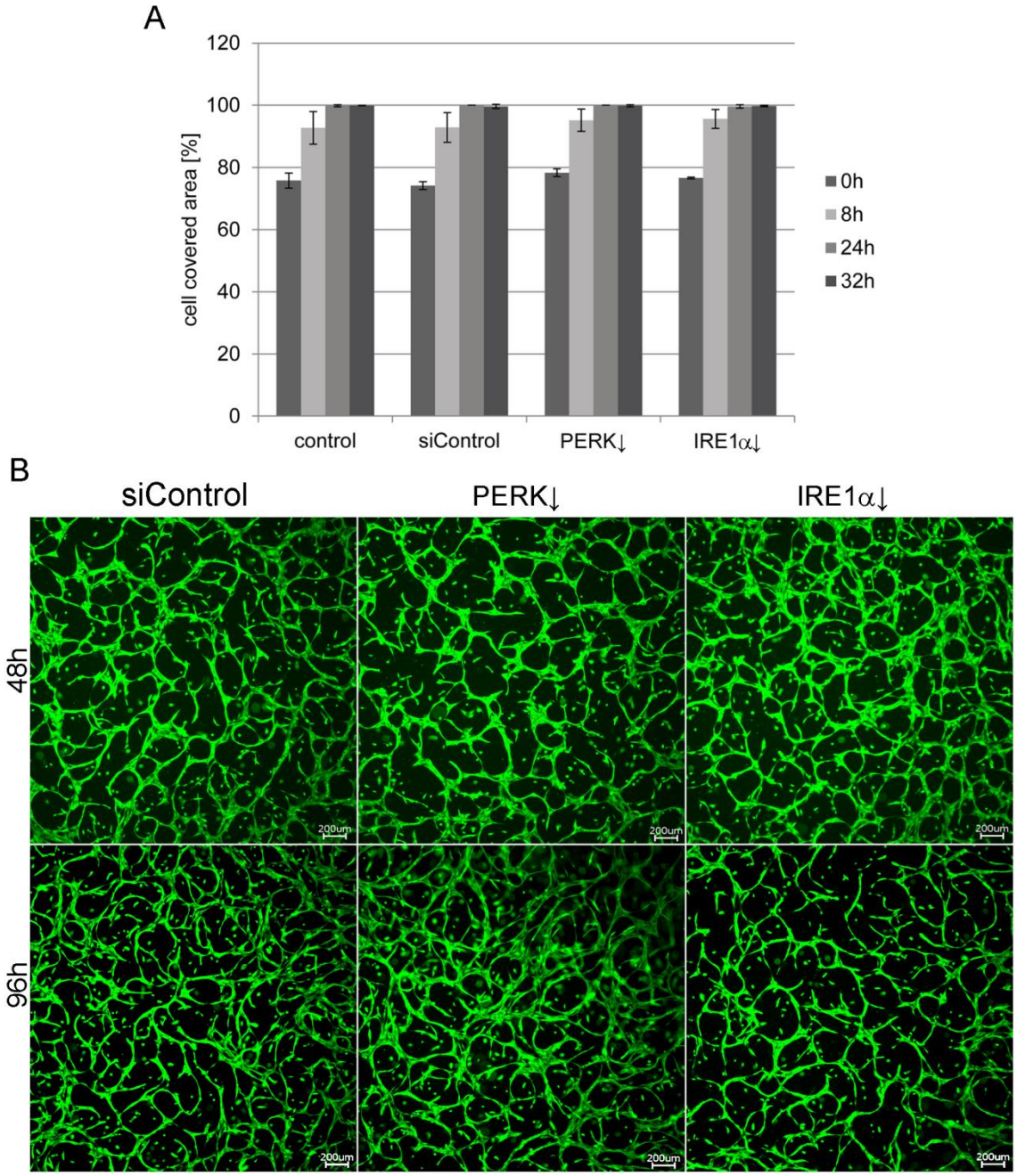

Fig. 33: Migration and tube formation of PERK and IRE1α down-regulated cells.

HUVEC were transfected with siRNA molecules s18102 to down-regulate PERK (PERK↓) and s200431 to down-regulate IRE1α (IRE1α↓). Transfected cells were applied in a migration assay and 48h after transfection the insert was removed. Images were taken after 0h, 8h, 24h and 32h. Quantification of migration was performed using the WimTube application by Wimasis via pseudocolour representation (A, means ± SDs, statistics: paired t-test; n=3). In addition, cells were seeded into collagen-fibrin gels with VEGF and bFGF, and visualized by calcein-AM 48h and 96h after transfection to investigate formation of capillary-like structures (B, scale bar: 200 µm).

3.4.4 Expression of VEGF receptors in BiP down-regulated cells

Due to the fact that BiP down-regulated cells showed a deficiency in tube formation and a regression of already-formed tubes, a possible mechanism was investigated in more detail. The growth factor, VEGF is one the most important stimuli for angiogenesis (Carmeliet *et al.,* 1996; Folkman, 1998). The signal of VEGF is mainly transduced by its receptors, KDR and Flt-1 (Zachary, 2003; Olsson *et al.,* 2006). Thus, the expression pattern of VEGF receptors was analyzed in BiP down-regulated cells. BiP was down-regulated using the siRNA molecules, s6980 and s6981. 48h and 72h after transfection the VEGF receptors, KDR and Flt-1, were detected at protein level via SDS-Page and Western Blot methodology. Additionally, cells were treated with tunicamycin so that the expression of VEGF receptors in endothelial cells could also be analyzed under ER stress. Regarding Western Blot results, the expression level of KDR was similar in control cells and in cells of the siControl, whereas protein level decreased in s6980- and s6981-transfected cells 48h after transfection (Fig. 34 A). In tunicamycin-treated cells, just a single band was detectable. 72h after transfection, extremely weak KDR bands were recognized in cells treated with tunicamycin or in BiP down-regulated cells. Control samples showed a similar protein level of KDR compared to 48h after transfection. Quantification of Western Blot of three different donors showed a significant decrease of KDR expression in tunicamycin-treated cells 48h after transfection (Fig. 34 B). A slight decrease was also recognized in s6980- and s6981-transfected cells compared to the control at this time point. 72h after transfection quantification showed a significant inhibition of KDR expression in tunicamycin-treated and in BiP down-regulated cells. A down-regulation of 82% was recognized in cells treated with tunicamycin compared to control. S6981-transfected cells exhibited residual KDR expression of 25% and, remarkably, KDR expression in cells transfected with s6980 was decreased to 11%. In contrast, no differences were observed with regard to Flt-1 expression in BiP down-regulated cells compared to control cells (Fig. 34 C). The protein expression pattern of three different donors was quantified and a minor decrease of Flt-1 detected in cells under ER stress, although this was not significant (Fig. 34 D).

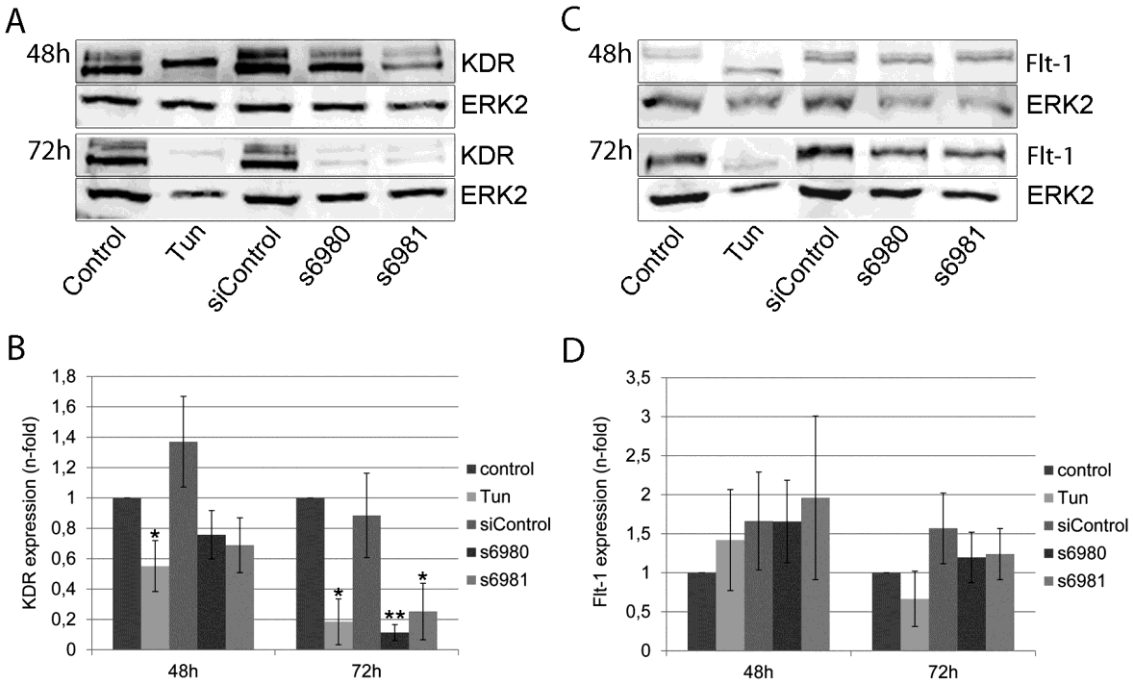

Fig. 34: Protein expression profile of VEGF receptors Flt-1 and KDR in BiP down-regulated and UPR activated cells.

HUVEC were transfected with control siRNA and BiP down-regulating siRNAs s6980 and s6981. To induce ER stress, cells were treated with 2 µg/ml tunicamycin (Tun). As additional control, untreated cells were used. After 48h and 72h VEGF receptors KDR (A) and Flt-1 (C) were detected at protein level using SDS-Page and Western Blot. ERK2 was detected as reference protein. Protein expression level of KDR (B) and Flt-1 (D) was quantified, normalized to the respective control and statistically analyzed (means ± SDs; statistics: paired t-test; *p<0.05, **p<0.01; n=3).

The expression profile of the VEGF receptors was also investigated at mRNA level to establish if the decreased protein level of KDR resulted from inhibited gene expression or translation. Additionally, the expression of VEGF was also investigated. VEGF was neither up-regulated nor down-regulated in BiP down-regulated cells at mRNA level (Fig. 35). Moreover, the expression of Flt-1 did not differ in the down-regulated cells compared to control. Remarkably, in contrast to the results at protein level, KDR mRNA expression did not decrease in s6980-transfected cells. In s6981-transfected cells a decrease of KDR was detected at mRNA level, but it was moderate and not statistically significant.

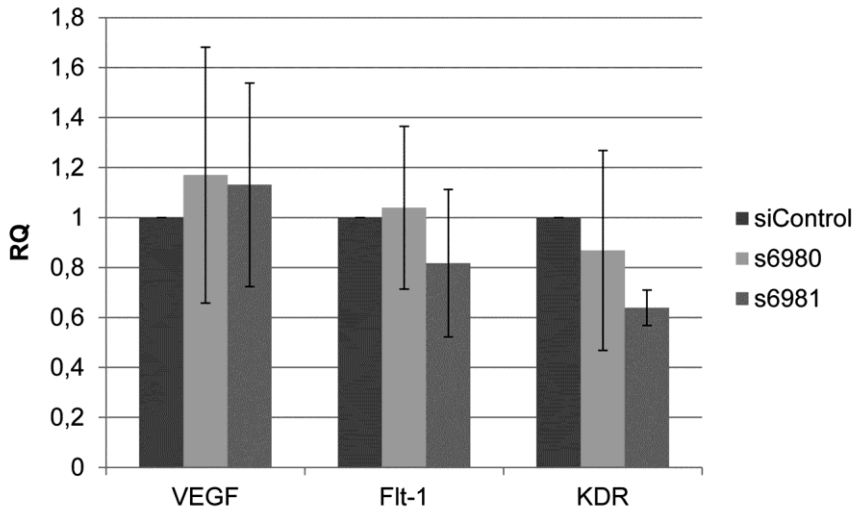

Fig. 35: Overview of expression patterns of the proteins VEGF, Flt-1 and KDR at mRNA level in s6980- and s6981-transfected endothelial cells.

HUVEC were transfected with control siRNA and siRNAs s6980 and s6981. Using real time qPCR expression of VEGF, Flt-1 and KDR was investigated at mRNA level. Data were normalized to the control (means ± SDs; statistics: Wilcoxon n=3).

As it is known that collagen I influences the expression of KDR in endothelial cells (Murota *et al.,* 2000) KDR expression was analyzed in cells embedded in the collagen-fibrin gel. Non-transfected cells, as well as BiP down-regulated cells were seeded into the collagen-fibrin gel. After the formation of capillary like structures, RNA was isolated. Using real time PCR the expression of KDR was investigated at RNA level 48h and 96h after transfection. As Fig. 36 shows, the expression of KDR did not vary in BiP down-regulated cells compared to control cells. In addition, the expression of matrix metalloproteases (MMPs) was analyzed in HUVEC under *in vivo*-like conditions, as these enzymes play an important role in the degradation of the ECM during angiogenesis. Especially MMP2 and MMP9, two important gelatinases, are known to be responsible for degradation of various collagens, as well as gelatin (Visse and Nagase, 2003). However, the expression of MMP2 and MMP9 did not change in BiP down-regulated cells 48h and 96h after transfection, compared to the corresponding control. With regard to different states of BiP down-regulation, changes in expression of the enzymes were also not observed. The maximum of BiP down-regulation and prolonged down-regulation did not affect the expression of MMP2 and MMP9.

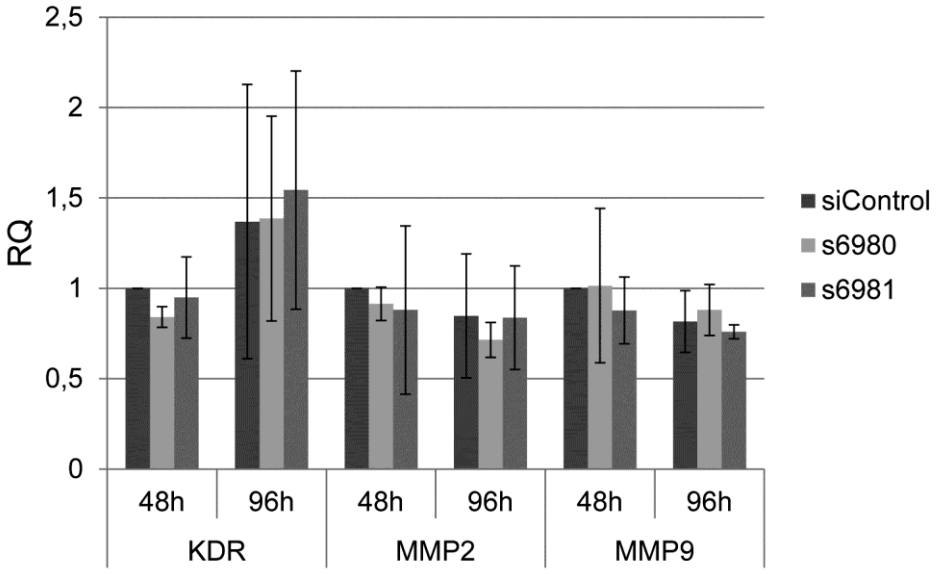

Fig. 36: Expression patterns of KDR and matrix metalloproteases 2 and 9 in BiP down-regulated endothelial cells.

HUVEC were transfected with siRNAs s6980 and s6981 to down-regulate BiP. As control, cells were transfected with control siRNA. Transfected cells were embedded in collagen-firbrin gels. RNA was isolated 48h and 96h after transfection, when cells had already formed capillary-like structures. The expression of KDR, MMP2 and MMP9 was analyzed using real time PCR. Results were normalized to siControl 48h after transfection and represented as RQ (means ± SDs; statistics: Wilcoxon n=3).

3.5 UPR activation in endothelial cells

Various stressors lead to accumulation of unfolded proteins in the lumen of the ER and UPR is activated to counteract the stress situation. BiP has been shown to play a role in the inflammatory and angiogenic responses of endothelial cells, as presented above. Following on from these observations, several inflammatory and angiogenic stimuli were tested for the activation of UPR at different levels of the signaling pathway in HUVEC.

3.5.1 Xbp1-splicing under pro-inflammatory and pro-angiogenic stimuli

Based on and the central role of endothelial cells in inflammation, pro-inflammatory stimuli were tested for UPR activation, analyzed by the investigation of Xbp1-splicing using PCR. Both forms of Xbp1 mRNA, the unspliced and the spliced variant were detected simultaneously, named u/s. To support the results additional experiments were performed, in which the unspliced form (Xbp1u) and the spliced form (Xbp1s) were detected separately. Stimulation of the cells with tumor necrosis factor α (TNFα) showed an inducible effect on Xbp1-splicing after 18h and 40h of treatment (Fig. 37), similar to the positive control, in which cells were treated with tunicamycin. More Xbp1s was detectable in these samples and the spliced form could also be obtained with the

u/s experimental approach. By contrast, treatment with interleukin 1β (IL1β), interferon γ (IFNγ) and LPS (lipopolysaccharide) did not activate Xpb1-splicing and consequently UPR. Bands of Xbp1s were comparable to control bands. These data could be supported by results using the u/s approach, in which no spliced form was detectable. Actin was used as reference gene to exclude differences in global mRNA amounts.

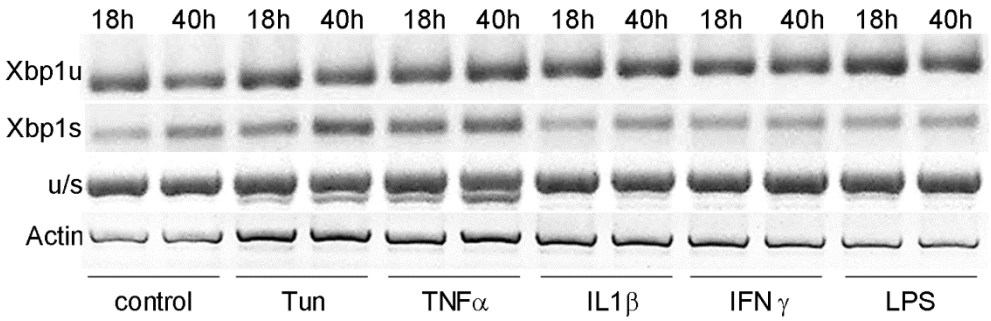

Fig. 37: Xbp1-splicing in response to inflammatory stimulation.

HUVEC were treated with pro-inflammatory stimuli 300 U/ml TNFα, 10 U/ml IL1β, 500 U/ml IFNγ and 1 µg/ml LPS for 18h and 40h. tunicamycin (2 µg/ml) stimulation was used as a positive control. Unspliced (Xbp1u) and spliced (Xbp1s) forms of Xbp1-mRNA molecule were detected using PCR. In experimental approach u/s both forms were detected. Actin was used as a reference gene. Amplicons were separated via electrophoresis (2% agarose gel).

Due to the role of endothelial cells in angiogenesis, HUVEC were treated with pro-angiogenic stimuli. Thus, cells were incubated in medium containing VEGF, bFGF or both stimulants. Based on the fact that signals triggered by VEGF are rapidly transferred, Xbp1-splicing was investigated after 4h and 8h of stimulation in addition to later time points (18h and 40h). As a further stimulus, cells were cultured under anoxic conditions, since lack of oxygen is known to induce angiogenesis. Already after 4h of stimulation with tunicamycin UPR is activated via the IRE1-Xbp1 pathway, resulting in Xbp1-splicing. Bands of the spliced form of Xbp1 were clearly seen after 4h and 8h of treatment, and were also still detectable after 18h and 40h of stimulation (Fig. 38). In PCR using primers which amplify both forms of Xbp1 RNA, a single lower band could be detected after 4h and 8h of treatment, which indicated the amplification of only the spliced form of Xbp1 RNA molecules. After tunicamycin treatment for 18h and 40h, both forms were detectable. In samples with pro-angiogenic stimuli a slight increase of the bands of the spliced form of Xbp1 was observed only after 4h and 8h of incubation. In contrast, culturing of the cells under anoxic conditions induced Xbp1-splicing after 40h. A double band in the u/s approach and one band in PCR using a XBP1s-specific primer were clearly seen.

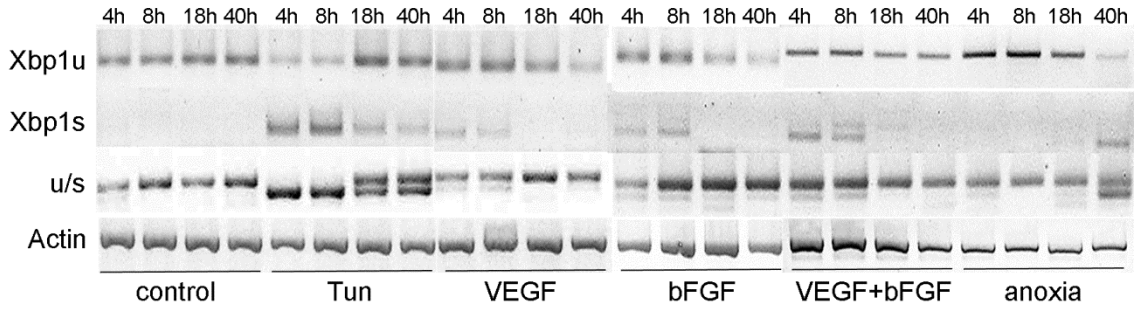

Fig. 38: Xbp1-splicing in response to pro-angiogenic stimuli.

Xbp1u, Xbp1s or both forms were amplified in RNA samples isolated from HUVEC treated with 50 ng/ml VEGF, 5 µg/ml bFGF or both in combination for 4h, 8h, 18h and 40h. For hypoxic treatment an anaerobic pouch system was used for cell culture. Stimulation with tunicamycin (2 µg/ml) was used for UPR activation and served as positive control. Actin was used as reference gene. Amplicons were separated via electrophoresis (2% agarose gel).

3.5.2 Chaperone expression

Based on the fact that BiP plays a role in inflammation and angiogenesis, UPR activation in response to pro-inflammatory and pro-angiogenic stimulation was analyzed at both protein and mRNA levels, with the emphasis on chaperone BiP as well as Grp94.

Using real time PCR, gene expression of mRNA for BiP and Grp94 was investigated (Fig. 39). UPR activation following tunicamycin treatment lead to a strong up-regulation of both chaperones, BiP and Grp94 18h after stimulation. After 40h of stimulation the mRNA expression was decreased compared to 18h-stimulation, but was still up-regulated compared to control. Comparing gene expression of both chaperones, BiP up-regulation was stronger than Grp94 after 18h and 40h of treatment. Pro-inflammatory stimulation of the cells with TNFα, IL1β, IFNγ and LPS did not increase BiP or Grp94 expression. The chaperones were also not up-regulated at mRNA level in response to treatment of HUVEC with VEGF, bFGF or both in combination. However, deprivation of oxygen led to an up-regulation of BiP and Grp94 mRNAs after 40h of culturing under anoxic conditions. In this case, the intensity of up-regulation of the chaperones was similar.

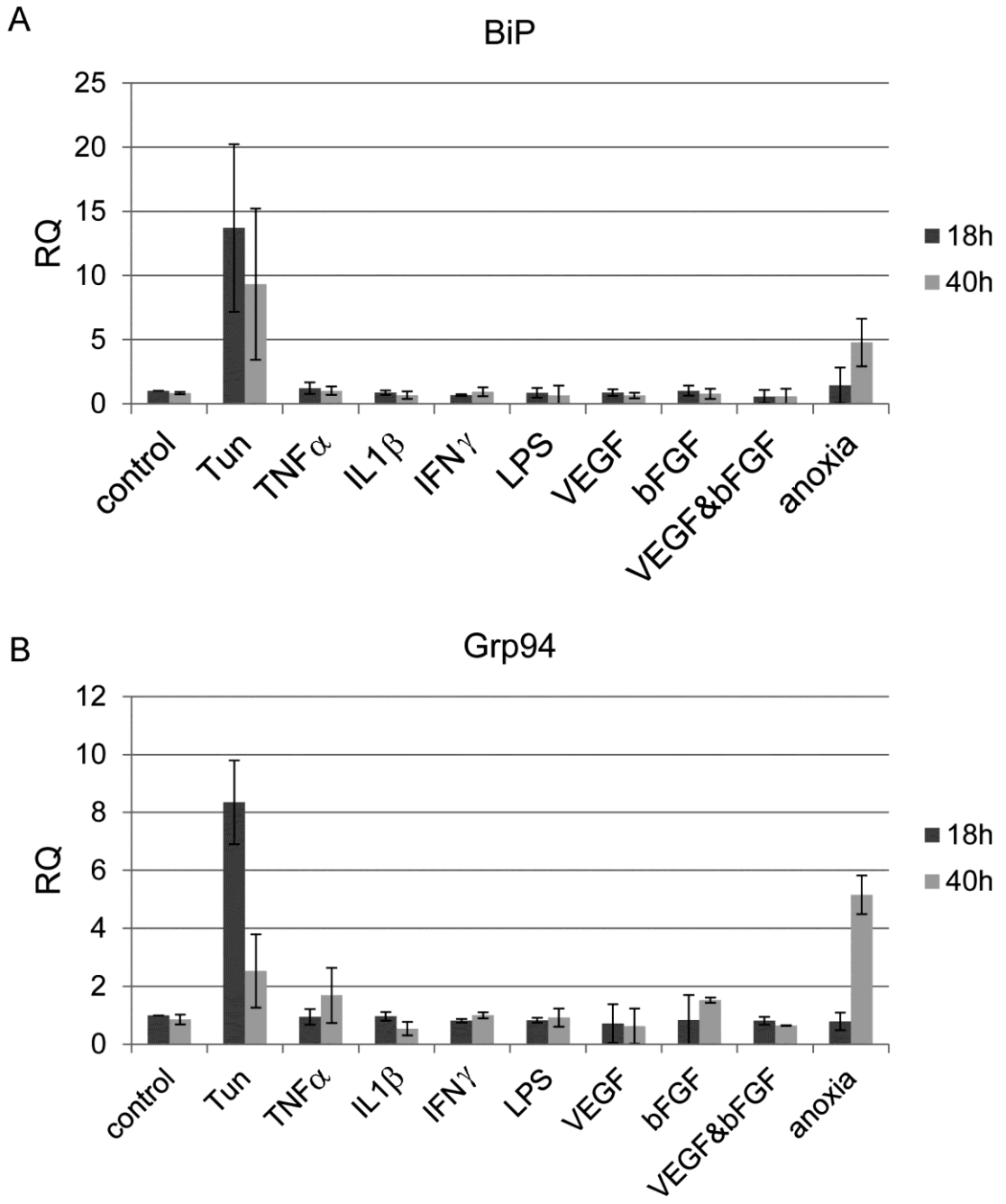

Fig. 39: Expression of BiP and Grp94 at mRNA level in response to pro-inflammatory and pro-angiogenic treatment.

Gene expression of chaperones BiP (A) and Grp94 (B) was investigated via qRT PCR using RNA isolated from HUVEC treated with pro-inflammatory (300 U/ml TNFα, 10 U/ml IL1β, 500 U/ml IFNγ and 1 µg/ml LPS) and pro-angiogenic (50 ng/ml VEGF, 5 µg/ml bFGF, both in combination, deprivation of oxygen) stimuli for 18h and 40h. Cells treated with 2 µg/ml tunicamycin (Tun) were used as positive control (means ± SDs; n=2-4).

At the protein level, activation of UPR signaling upon tunicamycin treatment led to an increased BiP expression already after 8h of treatment, whereas the treatment with pro-inflammatory stimuli did not induce BiP protein expression (Fig. 40 A). Shorter time periods of the treatments were also tested, but did not show any effect (data not

shown). Treatment of the cells with pro-angiogenic factors such as VEGF, bFGF or both for 4h, 8h, 18h and 40h did not cause an increase of BiP level. However, if the cells were cultured under deprivation of oxygen for 40h, BiP expression was up-regulated (Fig. 40 B). The expression pattern of Grp94 was similar to BiP expression at protein level (data not shown).

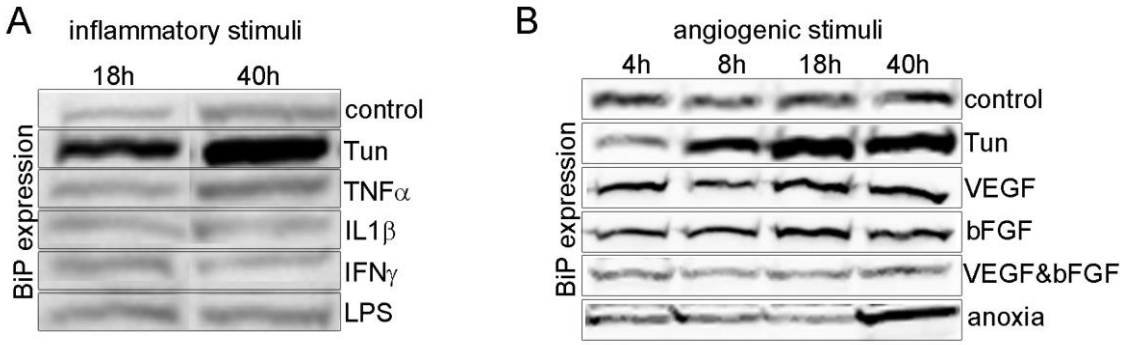

Fig. 40: Protein expression of chaperone BiP in response to pro-inflammatory and pro-angiogenic stimulation.

HUVEC were treated with pro-inflammatory stimuli (300 U/ml TNFα, 10 U/ml IL1β, 500 U/ml IFNγ and 1 µg/ml LPS) for 18h and 40h. (A). Additionally, the cells were stimulated with pro-angiogenic agents (50 ng/ml VEGF, 5µg/ml bFGF, both in combination (VEGF&bFGF) or under anoxic conditions) for 4h, 8h, 18h and 40h. Protein expression of BiP was analyzed via Western Blot (B). Stimulation with 2 µg/ml tunicamycin (Tun) was used as positive control for UPR activation.

3.5.3 Reporter gene assay

To study if the investigated agents could act directly on the expression of BiP, a reporter gene assay was performed. Cells transfected with a reporter gene vector carrying a BiP-promoter sequence were stimulated with pro-inflammatory and pro-angiogenic stimuli. Reporter gene activity was measured at several time points. Early response to stimulation was analyzed after 15 min, 30 min, 1 h, 2 h and 4 h, whereas luciferase activity was investigated after 8 h and 24 h for late response. Transfection of primary cells with the plasmid proved to be complicated. Therefore, three different cell lines were tested in the experiment:

- endothelial cell line ISO-HAS-1
- endothelial cell line HPMEC-ST1
- cervix cancer cell line HeLa

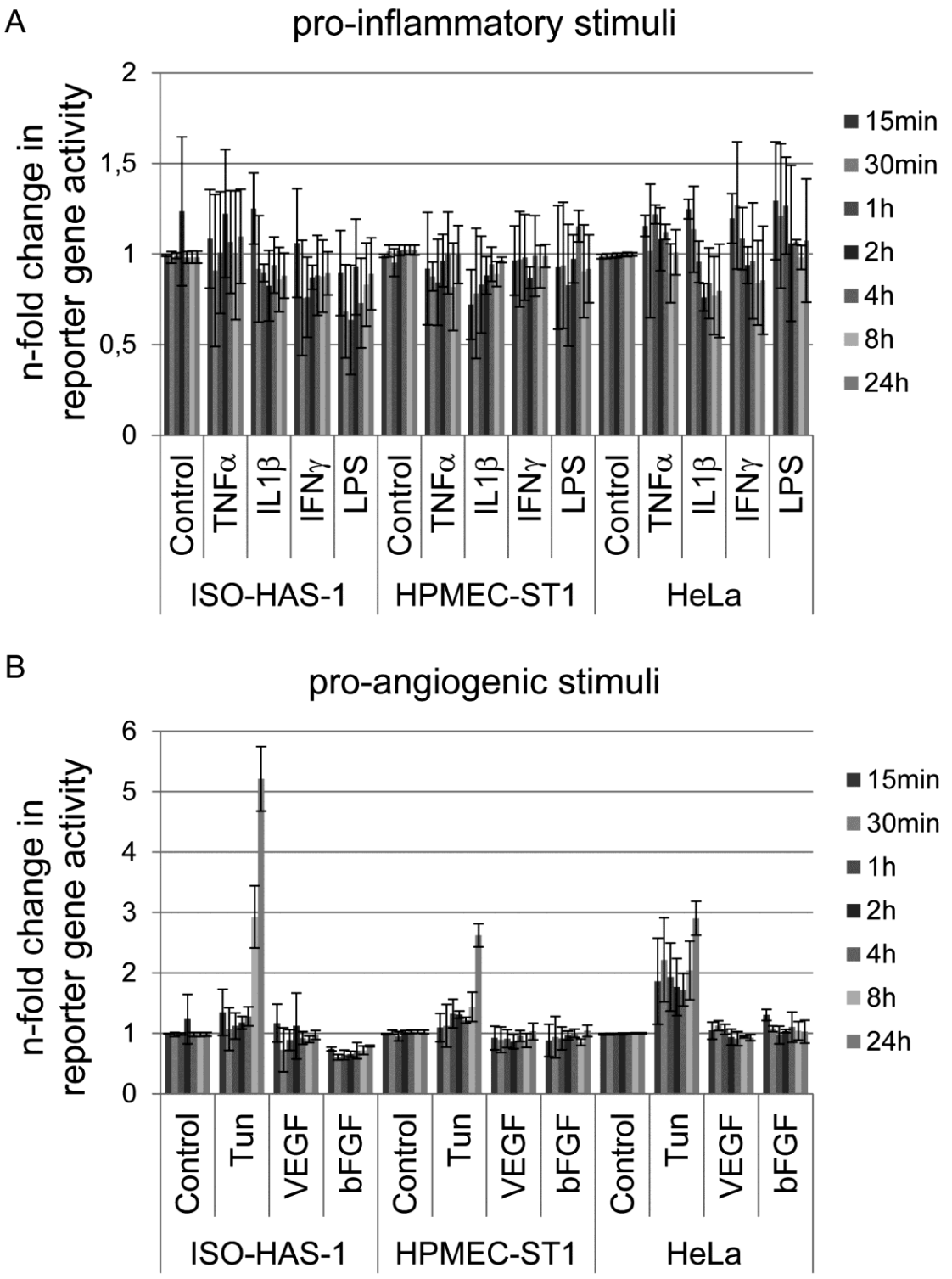

Fig. 41: BiP promoter activity in response to inflammatory and angiogenic stimulation measured via reporter gene assay.

Cell lines ISO-HAS-1, HPMEC-ST1 and HeLa were transfected with a reporter gene vector carrying a BiP-promoter and secreted luciferase as reporter gene. Cells were treated with pro-angiogenic (A) or pro-inflammatory (B) stimuli. Luciferase activity was measured after several time points to investigate early and late promoter induction. Cells treated with 2 µg/ml tunicamycin were used as a positive control for UPR activation and as a control of successful transfection. Results are shown as n-fold change in promoter gene activity (means ± SDs; statistics: paired t-test; n=3).

Pro-inflammatory stimulation did not induce activation of the BiP promoter. Signals triggered by the tested cytokines TNFα, IL1β, IFNγ and LPS did not lead to an increased expression of luciferase and therefore no increase in bioluminescence was detected (Fig. 41 A). All three cell lines, ISO-HAS, HPMEC-ST1 and HeLa behaved in the same way. Similar results were observed when the cells were treated with pro-angiogenic stimuli. The growth factors, VEGF and bFGF, did not induce BiP promoter activity and luciferase secretion. In contrast, activation of UPR in response to tunicamycin treatment led to a marked induction of promoter activity. After 8 h of incubation a threefold increase in reporter gene activity was measured compared to the control in ISO-HAS-1. Maximum activation was reached after 24 h of incubation. Induction of promoter activity upon tunicamycin treatment was detectable in HPMEC-ST1 cells after 24 h of incubation. Compared to control cells, HeLa cells showed twofold induction of reporter gene activity already after 30 min of incubation, which decreased over time to 1.5-fold induction after 8 h of stimulation and raised to a final threefold increase in luciferase activity after 24 h of stimulation of the cells with tunicamycin (Fig. 41 B).

3.6 Regulation of microRNA expression

Under normal conditions, cells of the vascular endothelium are in a quiescent state due to balanced levels of pro- and anti-angiogenic factors (Anand and Cheresh, 2011). However, under certain conditions an imbalance of pro- and anti-angiogenic factors can arise in the environment of the endothelial cells. These events lead to comprehensive changes in gene expression, which are highly regulated (Chen *et al.,* 2010). MicroRNAs play an important role in the regulation of gene expression at posttranscriptional level (Kuehbacher *et al.,* 2007) and their role has been demonstrated in endothelial cells as well as in UPR. This prompted a study of the effects of UPR activation and BiP deficiency in response to tunicamycin and SubAB treatment, respectively, on microRNA expression in endothelial cells. With the help of a microRNA expression array, based on Northern Blot methodology, changes in expression of 132 of the best studied microRNAs were analyzed. The cells were treated with the above-mentioned compounds, total RNA, including small RNA molecules, was isolated and the arrays were performed. For analysis, data were first normalized to array-containing positive controls and additionally to an internal control named RNU46, to guarantee application of the same amount of total RNA in every array membrane. Of the 132 regulatory microRNAs, 78 turned out to be up-regulated as a result of SubAB treatment, whereas 19 miRNAs were down-regulated. 35 of 132 miRNAs were not regulated following BiP deficiency (Fig. 42 A). ER stress also

affected the expression of microRNAs with 43 of 132 miRNAs being shown to be up-regulated. Equally, the expression of 43 miRNAs was down-regulated under ER stress, whereas the expression of 46 miRNAs did not change compared to controls (Fig. 42 B). Interestingly, in a study of expression patterns of intersecting sets in SubAB- and tunicamycin-treated cells, 40 miRNAs turned out to be up-regulated under ER stress and BiP deficiency (Fig. 42 C), for example miR-221, miR-222, miR-296 or miR-192. Most of the regulated miRNAs as a result of BiP deficiency were also up-regulated under ER stress. In contrast, 26 miRNAs were down-regulated exclusively in endothelial cells under ER stress. 17 microRNAs were down-regulated under both conditions, e.g. miR-196a or miR-19a (Fig. 42 D).

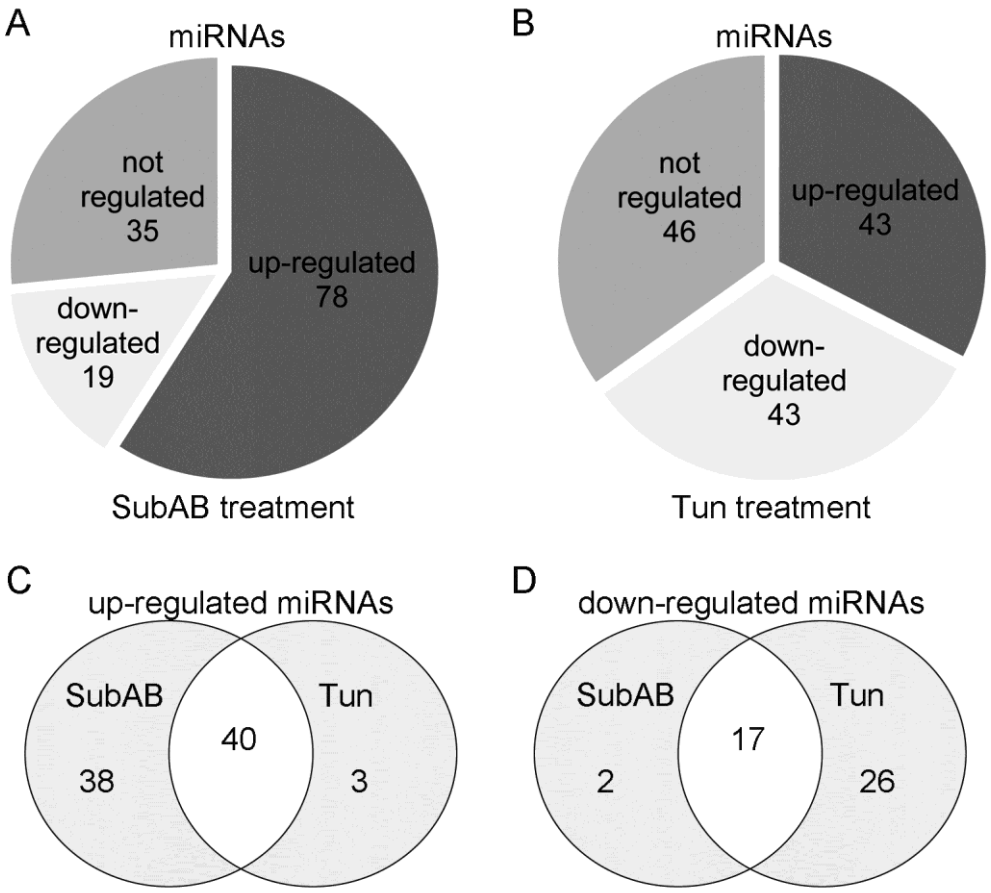

Fig. 42: Effect of SubAB and tunicamycin treatment on microRNA expression.

HUVEC were treated with 100 ng/ml SubAB, a toxin which disassembles BiP to create BiP deficiency, and 2 µg/ml tunicamycin to induce ER stress. After 18h of treatment, total RNA, including small RNAs, was isolated and microRNA arrays performed. The expression pattern of 132 miRNAs was analyzed. Results of the array were normalized to included positive controls and afterwards to an internal control. Subsequently, results were compared to the expression level in untreated cells. Data for SubAB (A) and tunicamycin (B) treatment were represented as not regulated, up-regulated and down-regulated miRNAs, compared to controls. Intersecting sets of up-regulated or down-regulated miRNAs due to both treatments are presented in C and D.

3.7 Expression of UPR components in skin pathology

In order to investigate the role of BiP and other UPR components in physiological and pathological processes, the expression of several UPR proteins (chaperone BiP, UPR receptors PERK and IRE1α and transcription factor ATF4) was analyzed in biopsies of human skin. Five different physiological and pathological types of skin were selected: embryo-fetal skin, adult skin, granulation tissue, haemangioma and angiosarcoma. To compare developmental stage with mature tissue, embryo-fetal skin and adult skin were analyzed. In addition, the expression of UPR components was analyzed in granulation tissue to investigate the possible role of UPR in wound healing processes. Furthermore, the expression of UPR components in two pathological cases, a benign vascular tumor (haemangioma) and a malignant vascular tumor (angiosarcoma), was analyzed.

Immunohistochemical staining of the biopsies was performed for several donors and the Immunoreactive Remmele Score (IRS) evaluated as described by Remmele and Stegner (1987). An overview of the expression of UPR components in endothelium and stromal cells of different tissues is presented in Tab. 7.

Expression of the chaperone BiP was classified as negative in embryo-fetal skin, in mature adult skin, as well as in granulation tissue, both in endothelial cells (Fig. 43) and in stromal cells. Remarkably, in comparison with the pathological cases of haemangioma and angiosarcoma (Fig. 44), an increase of expression was clearly seen in the malignant vascular tumor. According to IRS, BiP expression was negative in haemangioma. However, the staining intensity of BiP in stromal cells in granulation tissue was moderately positive with an IRS of 6.3.

The expression signal in IHC staining of the UPR receptor, PERK, was negative in endothelium and stromal cells of embryo-fetal and adult skin, whereas granulation tissue showed a weak positive signal, additionally illustrated in Fig. 43. Notably, comparing expression in vascular tumors, moderate positive expression was recognized in the angiosarcoma biopsies (Fig. 44). The expression pattern was negative for endothelium in haemangioma. It was also striking that in stromal cells mean expression of PERK was up-regulated in granulation tissue and slightly down-regulated in angiosarcoma.

Tab. 7: Expression pattern of UPR components BiP, PERK, IRE1α and AFT4 in different human tissues.

Biopsies of five different tissues, namely embryo-fetal skin, adult skin, haemangioma, angiosarcoma and granulation tissue, were stained for UPR components. Evaluation of immunohistochemical (IHC) staining was executed using the semi-quantitative method as described by Remmele and Stegner (1987). Data are represented as Immunoreactive Remmele Score (IRS; mean of IRS from 4-7 different donors) in endothelium and in stromal cells. IRS was defined as: 0-2 negative, 3-5 weakly positive, 6-8 moderately positive, 9-12 strongly positive.

Endothelium				
	BiP	PERK	IRE1α	ATF4
embryo-fetal skin	1	1.6	6	4.4
adult skin	0.9	1	12	3
granulation tissue	1.3	3.5	12	7
haemangioma	1.7	2	7.3	4.2
angiosarcoma	8.8	6	8	6.8
Stromal cells				
	BiP	PERK	IRE1α	ATF4
embryo-fetal skin	2.8	1.2	7.6	10.2
adult skin	2.7	1.3	12	5.4
granulation tissue	6.3	4.3	12	7.8
haemangioma	2	2.2	7.3	5.7
angiosarcoma	8.8	5.3	8	6.8

Conspicuously, the second receptor of the signaling pathway, IRE1α, studied here showed the highest expression level of the investigated proteins in the human tissues. Remarkably, IRS in adult skin and granulation tissue reached maximum expression in the endothelium, a similar expression occurring also in stromal cells. In contrast to expression in adult skin, embryo-fetal skin showed just moderately positive staining for the receptor in endothelial as well as in stromal cells. Importantly, in both cell types, no differences in expression between haemangioma and angiosarcoma were observed. A selection of IHC-P samples stained for IRE1α is presented in Fig. 43 and Fig. 44.

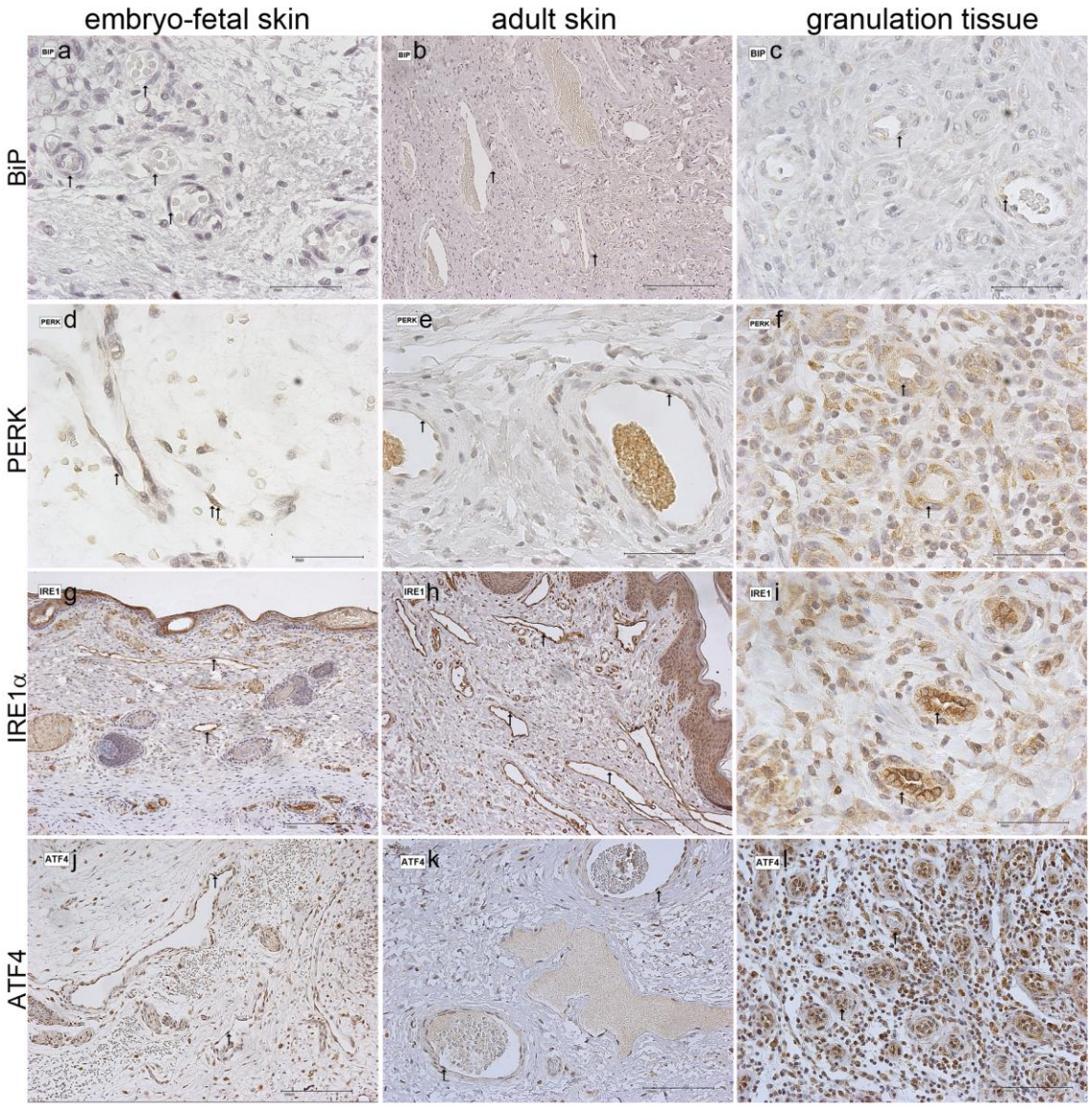

Fig. 43: Expression of UPR components, in embryo-fetal skin, adult skin and granulation tissue.

IHC-P staining of various tissues for BiP, PERK, IRE1α and ATF4. Arrows mark staining of endothelial cells (scale bar: a, c-f, l 50 µm; g,k, l 100 µm; b, h, j 200 µm).

A weak positive staining of ATF4 was detected in all samples (Fig. 43 and Fig. 44). Expression of the transcription factor showed a slight increase exclusively in granulation tissue and angiosarcoma. Both endothelial and stromal cell types were affected. Notably, staining of stromal cells of embryo-fetal skin was strongly positive.

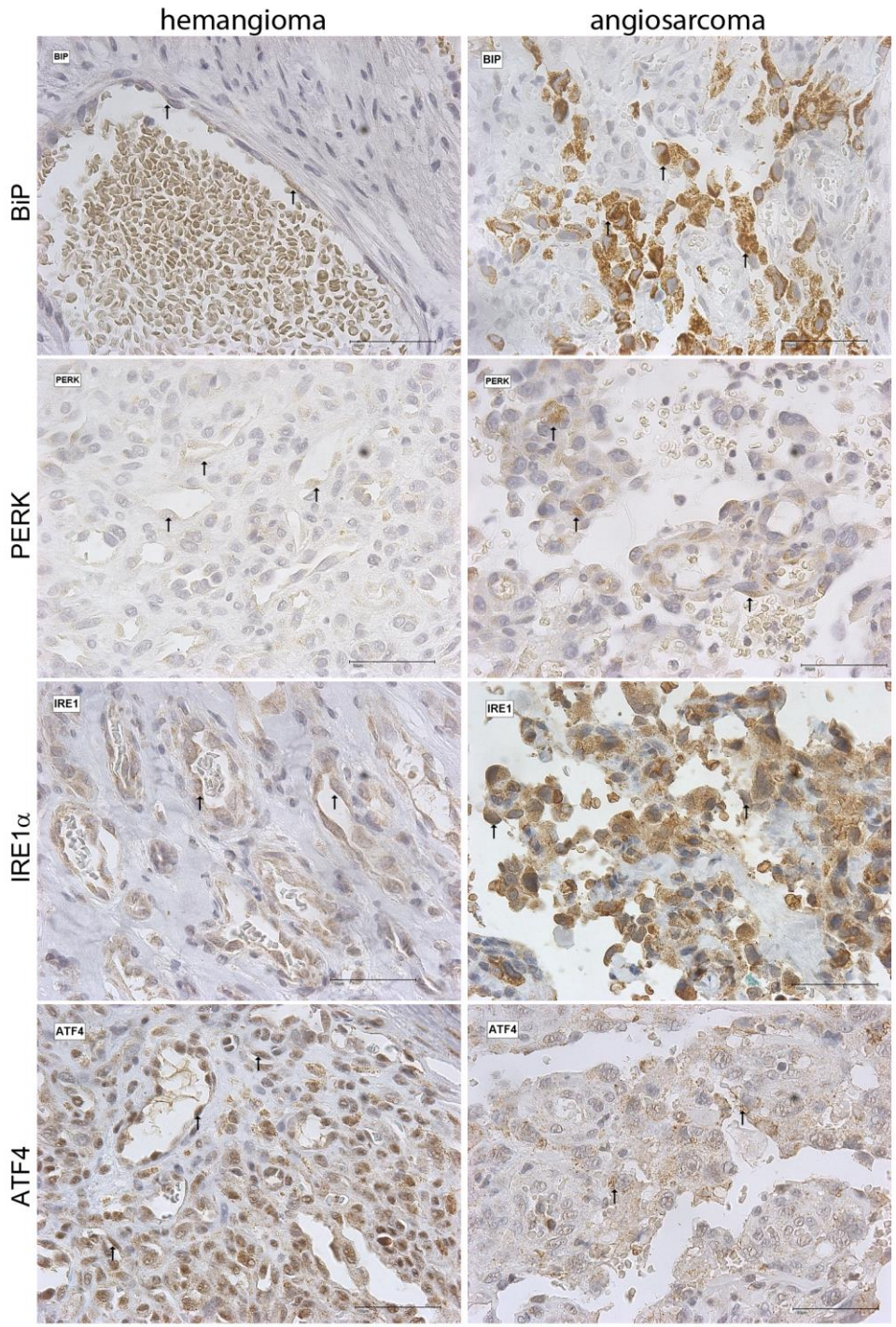

Fig. 44: BiP, PERK, IRE1α and ATF4 expression in haemangioma and angiosarcoma.

IHC-P staining for named UPR components in benign and malignant tumor tissue. Arrows mark staining of endothelial cells (scale bar: 50 µm).

4 Discussion

Highly regulated processes like inflammation and angiogenesis are accompanied by a high protein synthesis rate and are regulated by multiple signaling pathways to maintain homeostasis. This present study underlines the participation of the ER stress pathway UPR in inflammation and, importantly, also in angiogenesis. With regard to the ER-resident chaperone and stress sensor protein, Binding immunoglobulin Protein (BiP), an important role of protein folding functionality in the regulation of angiogenesis is demonstrated and possible targeting for the regulation of vascularization is discussed.

4.1 UPR and down-regulation of BiP in endothelial cells

Regardless of whether a situation is physiological or pathological, cellular responses to stress are highly regulated and intricately intertwined. During processes such as inflammation and particularly angiogenesis, numerous proteins are synthesized in order to transmit further signals. This high synthesis rate can elicit a stress response in the cell as a result of the accumulation of unfolded proteins in the lumen of the endoplasmatic reticulum (ER). ER stress comprises both physiological stress, originating from increased secretory load, and pathological stress, induced for example by the presence of mutated proteins, which are improperly folded. In addition, the presence of proteins inhibiting glycosylation or formation of disulfide bounds causes pathological stress (Lin *et al.,* 2008). The cell response to counteract ER stress is the activation of the UPR, resulting in reduced translation, enhanced protein folding capacity and the clearance of misfolded proteins (Diehl *et al.,* 2011). In general, UPR is believed to contribute to the decision between cell survival or cell death under a stress situation, which therefore represents a link to many diseases (Lin *et al.,* 2008). Combined output of the three activated pathways involved in the UPR results in a balanced level of survival and apoptotic factors. A higher stability of the pro-survival factors at mRNA as well as protein level promotes the survival of the cells within a stress situation. The preferred activation of single pathways of the UPR also presents a crucial step in cell fate decisions. Activation of the PERK-mediated pathway, for example, leads to the induction of apoptosis, whereas IRE1α-mediated UPR activation confers a pro-survival response (Lin *et al.,* 2007). Nonetheless, various diseases can be associated with persistent ER stress responses reflected in a decreased capability to fold proteins and to recognize misfolded or unfolded proteins, the exhaustion of ER

loading capacity by misfolded proteins or the specific activation of apoptosis via UPR signaling (Lin *et al.,* 2008).

Diabetes mellitus type II is an example of such ER-stress-associated disease. It is characterized by resistance of the peripheral tissue to insulin. Consistently high blood sugar levels induce elevated insulin production with the consequence of hypersecretion of the hormone from the pancreatic β islet cells, which induces ER stress. Hence, continuous UPR signaling induces apoptosis in pancreatic cells. Especially the PERK-mediated pathway is activated during this condition, as reported by Harding and group. Thus, they showed development of diabetes mellitus in *Perk*$^{-/-}$ knockout mice (Harding *et al.,* 2001). In a special form of diabetes in humans, the Wolcott-Rallison-Syndrom, a mutation in the *Perk* gene was verified (Delepine *et al.,* 2000). Furthermore, several viruses use UPR for their own reproduction. Herpes simplex virus (HSV) and hepatitis C virus (HCV) induce ER stress via their envelope proteins. Thus, translation of host proteins is stopped and the translation machinery is used for viral replication (Mulvey *et al.,* 2007; Pavio *et al.,* 2003). Another strategy of HSV is the use of homologous proteins, for example GADD36, the mediator of eIF2α phosphorylation, which also results in the inhibition of host proteins translation (Chou and Roizman, 1994). In retinitis pigmentosa (RP), patients lose the sense for light due to a mutation in rhodopsin, a photoreceptor in the eye. The mutation causes misfolding, which leads to an accumulation of the protein in the lumen of the ER and thus to activation of the UPR (Liu *et al.,* 1996; Ryoo *et al.,* 2007). UPR activation was also recognized in Alzheimer's disease. Misfolded β-amyloid, found in plaques, reflects cytotoxicity in UPR activation (Hoozemans, J. J. M. *et al.,* 2005).

UPR is also involved in tumor growth and metastasis. The UPR chaperone BiP and the transcription factor Xbp1 are demonstrably up-regulated in cancer cells (Jamora *et al.,* 1996; Romero-Ramirez *et al.,* 2004). Expression of the tumor suppressor p53 is down-regulated as a result of prolonged ER stress (Pluquet *et al.,* 2005). Hypoxic conditions, present in tumors above a certain size (Gimbrone *et al.,* 1972), can cause dysbalance of the oxidative environment in the ER and inhibit oxygen-dependent enzymes, leading to protein misfolding and UPR activation (Bi *et al.,* 2005). Furthermore, ER stress is known to modulate the effects of chemotherapeutic agents, for example via reduction of the therapeutic effects of topoisomerase inhibitors, which should interfere with DNA-replication of tumor cells (Lin *et al.,* 2008). On the other hand, the usage of cisplatin, a widely used component of chemotherapeutics, leads to misfolding of proteins, UPR activation and finally to cell death. In this manner, the therapeutic effect of cisplatin is enhanced via UPR activation (Obeng *et al.,* 2006). Numerous impacts of the ER stress signaling pathway in pathological cases are known, but only a few are fully understood.

Therefore, better knowledge is needed to understand disease mechanisms and thus develop adequate therapeutic strategies.

In a general sense, the UPR signaling pathway acts as a mechanism to adapt cells to microenvironmental stresses such as hypoxia, nutrient deprivation, as well as changes in redox status. In particular, all of the listed conditions appear in cancer (Atkins *et al.,* 2013). The combined occurrence of tumor growth, metastasis and formation of new blood vessels was observed a long time ago. Already in the early 70s, Gimbrone and group did first experiments linking tumor size to angiogenic activation (Gimbrone *et al.,* 1972). For tumor survival, neovascularization represents the limiting factor. Fortunately, questions arose about the nature of angiogenic switches, which were also transferred to other disease states, including age-related macular degeneration (AMD) and ischemia in chronic wounds. Obviously, the UPR became an interesting pathway to investigate the possible association between angiogenesis and ER stress. Several studies implicated the role of UPR in angiogenesis. It was shown for several cell lines that pro-angiogenic factors were up-regulated due to activated UPR triggered by known ER stress inducers such as tunicamycin and thapsigargin or hypoxia (Pereira *et al.,* 2010). Furthermore, it was reported that the transcription factor Xbp1 is involved in the regulation of angiogenesis in human pancreatic adenocarcinoma (Romero-Ramirez *et al.,* 2009). Dysregulation of angiogenesis in association with UPR activation was shown in AMD (Salminen and Kauppinen, 2010) as well as in kidney epithelium under ischemic stress (Bouvier *et al.,* 2012). Remarkably, a master regulator of the UPR, the ER-resident chaperone BiP, was reported to be involved in angiogenic processes during tumor development (Dong *et al.,* 2011; Wang *et al.,* 2009). However, the precise mechanisms of UPR effects on angiogenesis under pathological and normal conditions are not characterized in detail. Therefore, this study focused on the effects of UPR signaling and, in particular, UPR sensor and chaperone BiP in endothelial cells.

Besides its functionality as a chaperone, BiP is the master regulator protein of the UPR. The quantitative measurement of the protein is considered as a marker for ER stress (Shang, 2005). The up-regulation of BiP as a result of ER stress has been known since 1988 (Kozutsumi *et al.,* 1988). In addition, the increase of the expression of the chaperone is linked with high protein synthesis (Brewer and Diehl, 2000). Detection of BiP is applied in medical diagnostics as well. Cell-free BiP is present in synovial fluid of RA patients (Corrigall *et al.,* 2004). Accordingly, it is known to stimulate TNFα, IL-10 and TNFR release via the MAPK pathway and, in addition, the extracellular protein activates immunomodulatory and anti-inflammatory pathways (Corrigall *et al.,* 2004). In 1998, BiP was identified on the cell surface of several cell types (Delpinoi *et al.,* 1998). The signal, transferred via membrane-bound BiP is known

to promote cell survival and proliferation (Misra and Pizzo, 2010). Due to the fact that the BiP level is low on the cell surface of endothelial cells (Davidson *et al.,* 2005) the membrane-bound form of the protein was not investigated separately in this study.

In summary, BiP plays an important role in cell signaling and is essential on several fronts to establish and maintain an optimally functioning cell homeostasis. Therefore, BiP was chosen as the essential molecule in this study. It was down-regulated with RNAi technology in primary endothelial cells and its effects on inflammation and the formation of capillary-like structures were investigated. SiRNA molecules specifically target the mRNA level and RNAi is also referred to as post-transcriptional gene silencing (PTGS). Gene silencing was measurable at both the mRNA and protein level, as a result of reduced translation caused by mRNA degradation (Fig. 9). The degree of down-regulation was determined for each experiment. Experiments with a minimum of 50% of BiP down-regulation were included in the statistical evaluation. Down-regulation of BiP was stable for more than 96h. Additional ER stress, induced by tunicamycin treatment of siRNA-transfected cells, did not lead to an increase of BiP expression at protein level (Fig. 12). In addition, the protein was depleted using the toxin SubAB (Fig. 10) to support the results generated from cells with siRNA-silenced BiP. However, important differences were observed between toxin-treated and siRNA-transfected cells. Thus, in endothelial cells treated with SubAB it was observed that BiP expression was up-regulated at mRNA level. This effect was comparable to induction of BiP expression as a result of UPR activation by tunicamycin treatment. Activation of BiP expression was more powerful with a longer period of treatment (between 8 and 48h) (Fig. 11). An increase of BiP expression due to ER stress was reported previously (Nakamura *et al.,* 2013; Walter and Ron, 2011; Gething, 1999). It is a known outcome of an activated signaling pathway, shown to be mediated by IRE1α and ATF6, and it represents a negative feedback loop which increases protein folding capacity of the cell and reduces the UPR (Gething, 1999). It is possible that depletion of BiP with SubAB activates UPR receptors and leads to BiP upregulation in this feedback loop. This effect was not seen in siRNA-transfected cells, in which a residual amount of BiP is still present. However, UPR activation has also been shown in siRNA-transfected cells. Thus, by analyzing splicing of Xbp1 mRNA, a known method to investigate UPR activation (Hirota *et al.,* 2006), it was noticed that BiP down-regulation with siRNA molecules led to Xbp1-splicing (Fig. 20). Moreover, BiP depletion by SubAB treatment also resulted in a strong induction of the signaling pathway. Therefore, BiP down-regulation represents a complex system, in which ER folding capacity is reduced and UPR is simultaneously activated.

4.2 Role of BiP in inflammatory responses of endothelial cells

Endothelial cells play an important role in inflammatory processes. TNFα, one of the main mediators of inflammation, induces the secretion of IL-8 and MCP-1 in endothelial cells. These pro-inflammatory cytokines are responsible for leukocyte attraction and for the amplification of the inflammatory signal. In addition, presentation of the cell-cell interaction proteins, E-selectin and ICAM-1, on the cell surface is increased as a result of pro-inflammatory stimulation. Both mediate the attachment and adhesion of leukocytes to the endothelial cells (Peters *et al.,* 2003). In order to elucidate alterations in the release and expression of inflammatory marker proteins of endothelial cells, the inflammatory response was investigated in BiP down-regulated HUVEC. As expected, expression of ICAM-1 and E-selectin increased in non-transfected cells stimulated with TNFα (Fig. 23). No changes in E-selectin expression were observed after BiP down-regulation, although strong fluctuations in E-selectin expression occurred. High standard deviations in E-selectin expression which were noticed primarily in transfected cells, siControl included, may result from the transfection process itself. Nevertheless, BiP down-regulation had no influence on E-selectin expression. In contrast, expression of ICAM-1 was significantly up-regulated in BiP down-regulated TNFα treated cells compared to stimulated control. Due to the fact that down-regulation of BiP activates UPR signaling, it can be assumed, that ICAM-1 mRNA carries uORF, which leads to its preferred translation under UPR-activated conditions.

Regarding release of the pro-inflammatory agents, MCP-1 and IL-8, a shift of secretion pattern was observed (Fig. 22). In BiP down-regulated and TNFα-stimulated HUVEC, a moderately lower level of MCP-1 was measured in the supernatant compared to stimulated non-transfected cells, although this difference was not statistically significant. This could indicate that folding, processing and resulting secretion of the chemokine is dependent on BiP. It may be also possible that decrease in MCP-1 release originates from global translational inhibition, a result of UPR activation. Conversely, TNFα-induced IL-8 release increased markedly in BiP down-regulated cells. Differences were shown to be significant compared to stimulated, but non-transfected cells. It is possible that IL-8 mRNA also carries uORF, and thus is preferentially translated upon UPR activation. This hypothesis could be supported by the fact that IL-8 release was also increased in BiP down-regulated cells under non-inflammatory conditions, although to a lower extent compared to TNFα treatment. An increased release of IL-8 and also IL-6 mediated by UPR due to pro-inflammatory stimulation with phospholipolyzed LDL (low density protein) was previously described in HUVEC (Gora *et al.,* 2010). In addition, an increased IL-8 release due to ER stress of epithelial cells (Maguire *et al.,* 2011) and of several breast cancer cell lines (Marjon

et al., 2004) was also reported. Wolff et al. described an intracellular storage of IL-8 in the Golgi apparatus (Wolff *et al.,* 1998). This enables a high release of the cytokine for a fast response, which does not require *de novo* protein synthesis. In addition, IL-8 and other molecules (e.g. vWF and angiopoietin) are incorporated into so-called Weibel-Palade-bodies. Secretion of this cocktail as another mechanism of fast response supports processes in inflammation, coagulation, stem cell mobilization, vascular permeability and endothelial cell viability (Goligorsky *et al.,* 2009). A possible direct role of BiP in the storage of intracellular IL-8 could be suggested. However, a decreased BiP level would not be sufficient for IL-8 retention in the cell. Alternatively, it is possible that UPR activation as a result of BiP down-regulation stimulates IL-8 release from these intercellular storage units.

Glycosylation is a process of co- or post-translational processing of newly synthesized proteins and proceeds in the ER and in the Golgi (Blom *et al.,* 2004). Especially for proteins presented on the cell surface, it constitutes a crucial post-translational modification. Glycosylation is known to be involved in endothelial cell functionality, for example, by supporting survival of the cells (Croci *et al.,* 2014). Importantly, attachment of sugar chain structures is essential for the function of adhesion molecules involved in inflammatory processes (Lowe, 2003). In BiP down-regulated cells, less superficial glycosylation was measured compared to control cells (Fig. 19). Notably, these data are in contrast with the increase of ICAM-1 in BiP down-regulated cells. However, ICAM-1 mRNA could be preferentially expressed under UPR conditions, as suggested above, and properly glycosylated, as glycosylation was not inhibited completely in BiP down-regulated cells. Nonetheless, inhibition of superficial glycosylation was previously demonstrated in cells under ER stress (Lin *et al.,* 2007) and was associated with a decrease in VCAM-1 expression. The decrease of glycosylation on the cell surface in the present study could be attributed to activated UPR signaling as a result of BiP down-regulation, which can lead to inhibition of common translation, including translation of enzymes involved in post-translational modifications. On the other hand, the lack of chaperone functionality in BiP down-regulated cells without participation of the activated UPR pathway could contribute to reduced ER protein folding and maturation capacity and must be considered as well.

Since BiP influences pro-inflammatory response in endothelial cells, its expression could well be regulated during inflammation. Therefore, induction of chaperone expression was analyzed in response to pro-inflammatory stimuli. In addition, the expression of the chaperone Grp94, which is induced upon ER stress, in a similar fashion to BiP, was investigated as well. The pro-inflammatory factors tested in this study, including TNFα, IL-1β, IFNγ and LPS, are known inducers of pro-inflammatory

responses in endothelial cells (Peters *et al.,* 2003). However, none of the investigated agents induced expression of BiP or Grp94, either at mRNA (Fig. 39), or protein level (Fig. 40 A). Furthermore, BiP expression was examined using a reporter gene assay in order to obtain insight into whether the stimuli have a direct effect on BiP promoter activity. Similar to mRNA and protein expression, pro-inflammatory treatment did not show any effect on BiP promoter activity (Fig. 41).

Interestingly, treatment of HUVEC with the cytokine TNFα led to splicing of the Xbp1 mRNA molecule, a sign of UPR activation via the IRE1α-mediated pathway, whereas IL-1β, IFNγ and LPS did not exert an effect on Xbp1-splicing (Fig. 37). Inflammatory processes triggered by TNFα and resulting in Xbp1-splicing were observed in murine fibroblasts as well (Xue *et al.,* 2005). Signals mediated by TNFα are known to influence the endothelial cytoskeleton by regulating the organization of actin within the cell, to affect common protein synthesis and to induce apoptosis. This study describes the activation of the UPR signaling pathway triggered by TNFα via the IRE1α-mediated pathway in endothelial cells. However, TNFα did not up-regulate BiP expression. Therefore, it is possible, that BiP contributes to a pro-inflammatory response without an increase of its expression. Basal BiP expression could be important for folding, storage and release of pro-inflammatory molecules, as shown by the effects of BiP down-regulation on ICAM-1 and IL-8 in TNFα-treated endothelial cells. Additionally, as mentioned above, UPR activation, as a result of BiP down-regulation could contribute to the effects of BiP on inflammation.

4.3 The effects of chaperone BiP on angiogenesis

It is known that the expression and functionality of chaperone BiP could be associated with angiogenesis in tumor cells (Dong *et al.,* 2008; Katanasaka *et al.,* 2010). This part of the study focused on the role of BiP in angiogenesis by investigating migration of endothelial cells and the formation of capillary-like structures *in vitro*. Migration of endothelial cells plays a crucial role, especially in the wound healing process, when endothelial cells enter the granulation tissue to build up new vessels, as well as in sprouting angiogenesis (Lamalice *et al.,* 2007; Reinhart-King; Wang *et al.,* 2009). Hence, the migration behaviour of BiP down-regulated cells was investigated. Remarkably, in a modified scratch assay, a significant inhibition in migration of s6980-transfected cells was observed after 24h (Fig. 25). Deceleration of migration was also seen in s6981-transfected cells, but the level of inhibition was not significant. Whilst control cells nearly closed the gap, a clear defect could still be recognized in BiP down-

regulated cells (Fig. 24). Cells which lack BiP as a result of SubAB treatment gave the same results, with migration significantly slower compared to control cells (Fig. 26). Notably, 32h after the experiment started, the cell-covered area detected in s6980-transfected cells was lower compared to the percentage of the starting point.

In order to clarify this observation, metabolic activity and proliferation of the BiP down-regulated cells were analyzed. Transfection methodology did not influence metabolic activity. Control cells and siControl cells did not show a difference in conversion of MTS to formazan. Down-regulation of BiP with the help of siRNAs did not influence metabolic activity at the single cell level (Fig. 14). However, 72h after transfection, a significant inhibition of proliferation was detected in s6980-transfected cells compared to controls (Fig. 15). The observation of inhibited proliferation as a result of BiP down-regulation was previously reported for HUVEC (Katanasaka *et al.,* 2010). Furthermore, activated UPR is known to trigger the arrest of the cells in G1 phase of the cell cycle (Diehl *et al.,* 2011). Due to the fact that BiP down-regulation was shown to induce UPR signaling, this is a possible explanation for decreased proliferation as well. Besides a direct effect of BiP down-regulation on migration of endothelial cells, a low proliferation rate of BiP down-regulated cells can, therefore, contribute to inhibited migration observed in the modified scratch assay. UPR activation as a result of BiP down-regulation can also explain slow migration of BiP down-regulated cells. This hypothesis could be supported by results of the modified scratch assay performed with tunicamycin-treated cells (Fig. 26). Recently, this effect was also reported by Nakamura et al. They observed slower migration under high ER stress, but an increase of migration behavior due to mild ER stress, triggered by lower concentrations of tunicamycin (Nakamura *et al.,* 2013). Migration of endothelial cells represents one component of angiogenesis, which should end in the formation of new blood vessels to supply the surrounding tissue with oxygen and nutrients. Therefore, angiogenesis assays were performed to investigate the effects of BiP down-regulation on the capability of endothelial cells to form capillary-like structures.

Endothelial cells retain some angiogenic properties *in vitro*. In contact with a matrix which resembles ECM they are able to form capillary-like structures. This special feature was exploited to investigate tube formation of BiP down-regulated cells. In a 2D angiogenesis assay, in which collagen gel was placed on top of a confluent cell layer, fewer tubes were formed in cells with a down-regulated level of BiP (Fig. 27). In addition, the formation of less branching points in down-regulated cells was a striking feature. To establish more *in vivo*-like conditions for the cells a 3D angiogenesis assay was performed. Using this assay differences in the ability to form capillary-like structures in BiP down-regulated cells were even more distinct. The lack of cell-cell

contacts, which were present in the 2D assay, could explain the enhanced effect of BiP down-regulation in a 3D matrix. After BiP down-regulation had reached a maximum, cells were embedded in the collagen-fibrin gel. BiP down-regulated cells were not able to form capillary-like structures, an observation which was supported by quantification of the angiogenesis assay performed with cells from three different donors (Fig. 28). In parallel, the 3D angiogenesis assay was repeated with SubAB treatment. In this case, endothelial cells were also not able to form capillary-like structures (Fig. 31 A).

In a second setup of the experiment, cells were seeded directly into the collagen-fibrin gel after transfection. During the first 48h, in which the BiP level was not down-regulated to its maximum, capillary-like structures could be formed. Almost no differences between the down-regulated and the control cells were observed. By contrast, 96h after transfection regression of the tubes became obvious in BiP down-regulated cells, especially in s6980-transfected cells (Fig. 29). In order to support the role of BiP in the regression of formed tubes, cells were treated with SubAB 48h after embedding in the 3D gel. Reduction of capillary-like structures was apparent (Fig. 31 C) with fragmentation of the network leaving only a few tubes. In summary, BiP depletion in endothelial cells led to a strong inhibition of tube formation. Cells with reduced amount of BiP seemed to lose the capability to form capillary-like structures. In addition, low level of the chaperone led to regression of already formed tubes, which could not be sustained. To understand the fate of the cells with down-regulated BiP, they were tested for apoptotic activity.

First, cells were tested for caspase3 activity, which indicates apoptosis activation. The activated form of the enzyme was detected in tunicamycin-treated cells, which are known to undergo apoptosis as a result of high ER stress (Shiraishi *et al.,* 2006; Tabas and Ron, 2011). 72h after transfection, the activated form of caspase3 was also detectable in s6980-transfected cells and to a lower extent in s6981-transfected cells (Fig. 16). Since it was observed that BiP down-regulation induced UPR signaling, apoptotic activity, which was comparable to tunicamycin-treated cells, could result from UPR activation. Additionally, an apoptosis assay was performed in which phosphatidylserine (PS) was detected by fluorescent labeling. PS is translocated from the inner into the outer membrane in the early stages of apoptosis (Vermes *et al.,* 1995). As shown in Fig. 17, 48h after transfection no differences in apoptotic switch were detected in BiP down-regulated cells and control cells including the siControl. In addition, SubAB-treated cells showed a higher level of necrotic cells, but the apoptotic population was similar to the control. In contrast, cells under ER stress induced by tunicamycin treatment proved to have higher apoptotic activity than BiP down-regulated cells, especially 96h after transfection. To further support these results, another

apoptosis assay was performed. Within cell cycle measurement, cells with a lower DNA content than cells in G1 phase constitute so called SubG1 phase, populated mostly by apoptotic cells, which is attributed to the degradation of DNA during apoptosis. In this assay differences between BiP down-regulated and control cells were not observed (Fig. 18). In turn, cells under tunicamycin-induced ER stress undergo apoptosis, similar to the other assays performed before. Long-term treatment of the cells with SubAB also increased the population of cells with low DNA content, indicating that SubAB is more toxic than BiP down-regulation with siRNA. Although apoptosis measurements in early and late phase apoptosis, performed by the PS and SubG1 assays, did not indicate cell death in BiP down-regulated cells, the increase of activated caspase3 could indicate a certain level of apoptosis induction due to deficiency of BiP. In addition to reduced proliferation this could contribute to reduced formation of capillary-like structures. Apoptosis of endothelial cells assumes a regulatory role in development and adult neovascularization. Besides limiting angiogenesis to avoid e.g. the formation of tumors, apoptosis plays an important role in the remodeling of the vascular network (Dimmeler and Zeiher, 2000; Hughes and Chan-Ling, 2000). Therefore, ongoing apoptosis, which was detected in BiP down-regulated cells via caspase3 activity, is a possible explanation for the regression of capillary-like structures shown in Fig. 29 and triggered by UPR activity in transfected cells.

Another outcome of activated UPR is the arrest of cells in G1 phase (Diehl *et al.,* 2011), a resting phase between the cell divisions. Predominantly, cell cycle exit as an outcome of activated UPR is triggered by the PERK-mediated pathway (Brewer and Diehl, 2000) and allows a cell to stop proliferation to handle and counteract stress situation. In the current study, besides investigation of apoptosis in BiP down-regulated cells via cell cycle measurement, the cell population in G1 phase was determined as well. Cells under ER stress following tunicamycin treatment showed 27% higher numbers of cells in G0/G1 phase compared to control. BiP-depleted cells (SubAB-treated) exhibited 19% more cells in G0/G1 phase than control cells. S6980- and s6981-transfected cells showed only a slight increase of 4-5% in cell population in G0/G1 phase 48h after transfection. The data correlate with UPR activation in BiP down-regulated cells: high activation of UPR signaling in tunicamycin- and SubAB-treated cells and low activation in s6980- and s6981-transfected cells (Fig. 20). Decrease of proliferative activity in s6980-transfected cells and tunicamycin-treated cells also supports cell cycle arrest in G1 phase due to ER stress (Fig. 15).

In addition, formation of capillary-like structures under ER stress was investigated in this study. HUVEC were not able to form capillary-like structures, whether under pre-treatment with tunicamycin before seeding of the cells into the collagen-fibrin gel, or

due to direct treatment after cells were embedded. Regression of already-formed tubes could also be observed in cells treated with tunicamycin (Fig. 32). Notably, the effect of tunicamycin treatment on tube formation was stronger in comparison to the impact of BiP down-regulated cells and could be attributed to induction of a higher level of ER stress. High ER stress is known to decrease proliferation of capillary endothelial cells derived from bovine adrenal medulla (Banerjee *et al.,* 2011) and to induce apoptosis *in vitro* (Diehl *et al.,* 2011) as well as *in vivo* (Xu *et al.,* 2009). Both inhibition of proliferation and induction of apoptosis were also detected in the current study and represent a possible explanation for strong inhibition of tube formation due to ER stress and the regression of capillary-like structures. The inhibition of tube formation following ER stress initiated by tunicamycin treatment was previously reported in a murine oxygen-induced retinopathy model in association with ischemic retinal disease (Nakamura *et al.,* 2013). Moreover, the latter group recognized an acceleration of retinal neovascularization as a result of mild ER stress. In combination with data of this study, the present hypothesis of an association between angiogenesis and UPR signaling can be supported. Furthermore, the results provide additional evidence that loss of capability to form capillary-like structures in BiP down-regulated cells is a result of UPR activation and its consequences.

Conversely, in this study down-regulation of the UPR receptors PERK and IRE1α turned out to be irrelevant for migration and the formation of capillary-like structures (Fig. 33). In the literature IRE1α knockout is described as being lethal in mice (Chen and Brandizzi, 2013). IRE1α-mediated signaling is known to be highly involved in affecting cell fate with special regard to cell survival (Lin *et al.,* 2007). In cells of a malignant glioma IRE1α down-regulation led to a reduction of pro-angiogenic factors, as well as to an inhibition of vessel formation (Auf *et al.,* 2010). In addition, a decrease of approximately 40% of formed tubes was reported for primary bovine retinal microvascular endothelial cells with down-regulated IRE1α using RNAi methodology (Liu *et al.,* 2013). Studies on *Perk*$^{-/-}$ mouse embryonic fibroblasts (MEFs) showed inhibited angiogenesis, cell proliferation and in consequence a reduction of tumor growth (Bi *et al.,* 2005). Furthermore, PERK is targeted in anti-cancer therapies to suppress angiogenesis and tumor growth by inhibiting enzyme activity of the UPR receptor (Atkins *et al.,* 2013). Except the study reported by Liu et al, most of the studies show indirect effects of IRE and PERK on angiogenesis, i.e. in the cells with pro-angiogenic activity, such as tumor cells and fibroblasts. UPR includes three signaling pathways, therefore reduction of only one of them could be insufficient to alter overall UPR response and therefore has no effect on migration and tube formation in primary endothelial cells.

Since BiP has an effect on angiogenic activity of endothelial cells, pro-angiogenic stimuli were tested for their ability to induce UPR at the level of Xbp1-splicing as well as chaperone BiP and Grp94 expression. As expected, prolonged deprivation of oxygen, which is a known angiogenic stimulus, induced UPR as shown by Xbp1-splicing (Fig. 38). Hypoxic UPR activation was reported in many tumor cell lines mediated via the PERK-pathway (Mujcic *et al.,* 2009). Insufficient oxygen supply can disturb oxidative protein folding, thus resulting in UPR activation. This response of the cell to hypoxia is known to be a HIF-1α independent reaction (Rzymski and Harris, 2007). In this study, the expression of the chaperones BiP and Grp94 was increased in cells cultured under anoxic conditions, which are known to induce UPR activation. Hypoxia is a known ER stressor and induces an increase of chaperone expression, for example, in prostate cell lines or in the hepatocellular carcinoma cell line HepG2 (Ghosh *et al.,* 2010; Rzymski and Harris, 2007). Furthermore, pro-angiogenic stimulation triggered by VEGF and bFGF induced the signaling pathway, indicated by Xbp1-splicing (Fig. 38). Several studies concentrated on VEGF effects in tumor cells. This growth factor was shown to induce endothelial cell proliferation mediated by the IRE1α pathway in models of retinal vasculogenesis (Liu *et al.,* 2013; Zhang *et al.,* 2010). Karali et al. reported Xbp1-splicing in HUVEC following VEGF treatment (Karali *et al.,* 2014). They also demonstrated up-regulation of chaperone BiP at mRNA level in response to VEGF treatment. Although their results on Xbp1-splicing are in line with the current study, BiP up-regulation could not be supported, either at mRNA or protein level (Fig. 39; Fig. 40). Treatment of bFGF did not lead to an increase of BiP or Grp94 expression. In addition pro-angiogenic agents did not appear to activate the BiP promoter in the reporter assay (Fig. 41). In conclusion, within the scope of the present study the effects of hypoxia on UPR activation could be supported by Xbp1-splicing, as well as an increase of chaperone expression. Furthermore, VEGF could induce mild UPR activation, as seen by Xbp1-splicing.

To find a possible link between BiP functionality, ER stress and angiogenesis at molecular level, expression of Flt-1 and KDR was investigated. Both are known to be expressed in endothelial cells, whereby VEGF A-KDR-signaling is the most important pathway contributing to differentiation, proliferation and angiogenesis (Shalaby *et al.,* 1995; Waltenberger *et al.,* 1994). The KDR receptor is known to be up-regulated in the presence of VEGF (Shen *et al.,* 1998). The expression of the KDR protein in the present study showed a moderate but statistically insignificant decrease 48h after transfection of the cells with s6980 or s6981, whereas the expression profile of Flt-1 was unaltered at mRNA as well as at protein level in BiP down-regulated cells (Fig. 34 B, D; Fig. 35). Remarkably, 72h after transfection, expression of KDR was significantly

inhibited in BiP down-regulated cells at protein level, while Flt-1 was still unaltered (Fig. 34 A, C). Due to the fact that KDR plays an important role in signaling of the angiogenic switch, this could be a further explanation for inhibited tube formation. KDR expression was also down-regulated in cells under ER stress caused by tunicamycin treatment. However, the mechanisms could be different, since tunicamycin also induced changes in gel mobility of KDR. An ER stress-dependent down-regulation of KDR was also reported in capillary endothelial cells derived from bovine adrenal medulla (Banerjee *et al.,* 2011). Interestingly, KDR was not down-regulated at mRNA level in BiP down-regulated cells (Fig. 35). Hence, activated UPR and the subsequent inhibition of translation of KDR mRNA could be a reason for loss of capability to form capillary-like structures in BiP down-regulated cells. Similar results were generated by other groups investigating the expression of MMP13 in Perk$^{-/-}$ MEFs. The expression of MMP13 was similar in wild type and knock out cells at mRNA level, although the expression at protein level was decreased. The authors explained this effect by the inhibition of the ribosomal recruitment of MMP13 mRNA (Blais *et al.,* 2006). In addition, comparable KDR expression at mRNA level and decreased KDR protein could be explained by the lack of chaperone functionality in BiP down-regulated cells, as well. A study in a colon cancer cell line demonstrated a decrease in KDR as well as Flt-1 expression at both protein and mRNA level after BiP down-regulation (Kuo *et al.,* 2013). However, comparison of data generated from experiments using cell lines originating from cancer tissue and primary cells has to be regarded with caution. In contrast, other studies with HUVEC showed a decrease in phosphorylation of the receptor as a result of BiP down-regulation. However, the total quantity of the receptor was similar to control cells (Katanasaka *et al.,* 2010).

Interestingly, an up-regulation of KDR in endothelial cells was reported, if the cells were embedded in gels consisting of collagen I (Murota *et al.,* 2000). In this case collagen itself or changes in cell culture conditions, such as the embedding of the cells in a gel in which the cells are exposed to matrix in 3D, influenced the expression of the receptor. Beyond that, it is known that gene expression pattern changes in endothelial cells according to their phenotype, i.e. quiescent endothelial cell, tip cells or stalk cells (Jakobsson *et al.,* 2010; Siemerink *et al.,* 2012). Therefore, KDR expression was investigated in the *in vivo*-like situation of a 3D angiogenesis assay, involving isolation of RNA from the cells embedded in the collagen-gel after they formed capillary-like structures. No KDR up-regulation at mRNA level was observed in these cells (Fig. 35). Additionally, differences in expression of KDR between control and BiP down-regulated cells were also not detectablel. These data support the hypothesis mentioned above, namely that KDR expression was regulated post-transcriptionally in BiP down-

regulated cells. In this context, expression of MMP2 and MMP9 was also investigated in this study. Matrix metalloproteases play an important role in degradation of the ECM and this process represents a crucial step in angiogenesis. Notably, the expression of the enzymes MMP2 and MMP9 at mRNA level was not affected in BiP down-regulated cells (Fig. 36). However, it is still possible that protein expression of the active MMPs is regulated under these conditions, although this was not investigated in the scope of the present dissertation. Additionally, the expression of other proteins, which are involved in the degradation of the ECM, such as MMP13 or several integrins, could be impaired due to BiP down-regulation. Therefore, further investigations are necessary to understand the role of BiP in tube formation.

In summary, inhibition of the formation of capillary-like structures as a result of BiP down-regulation can be partially attributed to the decrease of KDR expression. Stimulation of angiogenesis via VEGF A-KDR signaling could not take place under these conditions. The angiogenic signal is blocked and the endothelial cells therefore do not form capillary-like structures. To understand whether the changes in KDR are caused by induced UPR or by lack of BiP chaperone activity will require further studies. The regression of already formed capillary-like structures in BiP down-regulated cells can be explained by UPR activation as a result of BiP down-regulation and the slightly increased apoptotic activity. Inhibited migration of BiP down-regulated cells can be traced back to the decrease of proliferation rate in BiP down-regulated cells. Due to the fact that VEGF A-KDR signaling is also involved in migration of endothelial cells by regulating stress fibers and lamellopodia formation (Lamalice *et al.,* 2004), the data also support the observation of inhibition of migration as a result of BiP down-regulation. The presented data indicate that KDR down-regulation is attributed to UPR signaling, activated by deficiency of the chaperone BiP.

4.4 miRNA expression in BiP down-regulated cells

Approximately one third of mammalian protein-coding genes is regulated by miRNAs (Yang *et al.,* 2011; Friedman *et al.,* 2008). In the last two decades, this mechanism of post-transcriptional regulation of gene expression has been intensively investigated. Increasing numbers of miRNA molecules were discovered and their targets and the effect of their regulatory outcome determined. Dysregulation of miRNAs expression is suggested to trigger several diseases, such as prostate cancer (Yang *et al.,* 2013), or psoriasis (Sonkoly *et al.,* 2007). On the other hand, mutations in the 3'UTR of target mRNAs, where miRNAs bind, lead to dysfunction of regulatory process. This is known

to be the case for asthma (Tan *et al.,* 2007) or rheumatoid arthritis (Stanczyk *et al.,* 2008). Moreover, circulating miRNAs were discovered in blood, helping to serve as biomarkers for several cancer types (Mitchell *et al.,* 2008) or cardiac hypertrophy in chronic hemodialysis patients (Wen *et al.,* 2014). Therefore, they represent new possible targets for drug development. The benefit of miRNA therapies is that they can regulate multiple target genes and are involved in a network of highly regulated processes. Currently, several strategies are being developed in miRNA therapies, for example, the delivery of nucleotide-linked liposomes, sponges or the application of miR-masks. Furthermore, nucleotide-expressing vectors are under investigation (Garzon *et al.,* 2010).

Several groups focussed on the role of miRNAs in the angiogenic switch apart from the specific process of tumor vascularization (Suarez and Sessa, 2009; Anand and Cheresh, 2011). The down-regulation of Drosha and Dicer, which resulted in the inhibition of miRNAs biogenesis, led to inhibited migration, reduced capillary sprouting and tube formation. Effects could also be shown *in vivo* (Kuehbacher *et al.,* 2007). Due to the fact that the expression of a number of miRNA molecules is known to be regulated by the UPR (Chitnis *et al.,* 2013; Bartoszewska *et al.,* 2013), the expression pattern of selected microRNAs was investigated in the present study. The association of UPR, BiP depletion and angiogenesis was analyzed. The performed expression array included 132 of the most studied miRNAs and their isoforms. Remarkably, many of them were shown to be regulated in response to ER stress or BiP depletion by SubAB treatment (Fig. 42). Interestingly, most of the investigated miRNAs were up-regulated by BiP deficiency. In contrast, in response to ER stress equal numbers of miRNAs were up- and down-regulated. Comparing both conditions, most of the miRNAs which were up-regulated following BiP depletion were also up-regulated under ER stress. Similar results were observed for down-regulated miRNAs. UPR activation as a result of BiP depletion, as discussed above, could explain these observations. However, several miRNAs seemed to be specific for each treatment. Thus, a number of miRNAs was down-regulated in tunicamycin-treated cells. It is possible that some genes involved in the process of stress reaction are regulated via miRNAs. Under normal conditions, translation of stress proteins could be inhibited by miRNAs, which is interrupted under stress. On down-regulation of miRNAs translation would be unblocked and stress proteins could be rapidly expressed. Conversely, up-regulated miRNAs could inhibit translation of proteins which are not essential for a cell during the stress response.

Several miRNAs regulated by SubAB or tunicamycin treatment were reported to be involved in angiogenesis regulation. Thus, miR-221 and miR-222 were up-regulated in

HUVEC in response to UPR activation, as well as after BiP depletion. These regulatory molecules are known to modulate angiogenic properties in HUVEC (Poliseno *et al.,* 2006; Suarez and Sessa, 2009). The overexpression of the miRNAs miR-221 and miR-222 leads to reduced expression of c-kit, a receptor involved in regulation of tube formation in endothelial cells (Suarez *et al.,* 2007). Furthermore, miR-296 was highly up-regulated following BiP depletion. The expression of this miRNA was shown to be stimulated by VEGF. The target is HGF, which is involved in the regulation of KDR expression (Ewan *et al.,* 2006). Moreover, contrary to the expression in primary human brain microvascular endothelial cells, the expression of miR-196a is reported to be up-regulated in the malignant tumor form of the cells (Würdinger *et al.,* 2008). In HUVEC this miRNA was down-regulated by activation of the UPR and BiP depletion. A number of regulated miRNAs in the present study, for example miR-192, miR-9-1 or miR-205, were shown to be associated with several cancer types (Pichiorri *et al.,* 2010; Lehmann *et al.,* 2008; Elgamal *et al.,* 2013). In the literature nothing is reported about BiP representing a possible target for miRNAs. Moreover, the effects of BiP on miRNA expression are not described. Therefore, association of BiP and UPR with miRNAs, especially those involved in angiogenesis, is of great interest. More detailed studies of the regulation of miRNA expression in connection with UPR and BiP are necessary and could provide both mechanistic and therapeutic insights.

4.5 The role of UPR components *in vivo*

In order to elucidate the influence of UPR signaling in endothelial cells *in vivo*, the expression level of the UPR components BiP, PERK, IRE1α and ATF4, was analyzed in histological samples. In this study, expression of these proteins was investigated in five different groups of skin samples obtained from biopsies of 5-7 patients. Data were evaluated using a semiquantitative method described by Remmele and Stenger in 1987 (Tab. 7). Expression of the UPR markers BiP, PERK, IRE1α and ATF4 was investigated during both developmental and mature stages, represented by embryo-fetal and adult skin respectively. Additionally, from a point of view of injured tissue and wound healing processes, expression of the UPR components was analyzed in granulation tissue. Finally, the expression of UPR proteins was examined in skin malformations, such as hemangioma, the benign form of a tumor with involvement of endothelial cells, and the malignant counterpart, angiosarcoma. Adult skin was used as the healthy control.

With regard to endothelium and BiP expression, no differences were observed in developmental and mature stages of skin, as well as in granulation tissue and hemangioma. Interestingly, expression of BiP was highly increased in angiosarcoma, both in endothelial and stromal cells (Fig. 44). Enhanced expression of the chaperone is widely reported, for example, in multiple myeloma or hepatocellular carcinoma (Obeng *et al.,* 2006; Shao *et al.,* 2012). Importantly, in most of the tissues, expression of the protein was comparable in benign and healthy tissue, whereas expression increased in malignant tumor cells, as reported for the lung (Uramoto *et al.,* 2005), breast (Fernandes *et al.,* 2000), prostate (Daneshmand *et al.,* 2007) and hepatocellular cancer (Shuda *et al.,* 2003). It is assumed that UPR is induced in the hypoxic, acidic and nutrient-deprived microenvironment of the tumor. This stress situation leads to an up-regulation of BiP and the tumor cells embrace the pro-survival features of the protein, for example, its role in blocking caspase activation. In the process of tumorigenesis, BiP up-regulation is maintained to inactivate the apoptotic pathway (Wang *et al.,* 2009). As a result of BiP overexpression in the tumor cells, a corresponding increase of autoantibodies against BiP in human serum was considered as a marker of hepatocellular carcinoma (Shao *et al.,* 2012). In contrast to endothelial cells, stromal cells of granulation tissue demonstrated a high expression of BiP in the present study. This can be attributed to a high protein synthesis rate in the participating stromal cells during the wound healing process. In the context of the present study, no differences in the expression patterns between embryo-fetal and adult skin could be detected. Development proceeds in a highly regulated fashion and the basal expression of BiP seems to be sufficient for the protein load during the development of the skin. Importantly, other studies showed phenotypically normal development in $BiP^{+/-}$ mice, whereas homozygotic knockout of the chaperone was lethal (Dong *et al.,* 2008; Luo *et al.,* 2006; Wang *et al.,* 2009).

The expression of the PERK receptor was quite similar in endothelial cells in developmental and mature stages of skin, as well as in benign tumors (Tab. 7). Nevertheless, an increased expression level of the receptor was detectable in endothelial cells of angiosarcoma. The expression pattern of the protein in endothelial cells and stromal cells was almost similar in each tissue. Knockout studies of $PERK^{-/-}$ mice reported reduced tumor growth (Blais *et al.,* 2006) which leads to the assumption of a dysregulation of PERK expression in malignant tumor cells. It was also reported that cells with a defective PERK-mediated signaling pathway are more sensitive to hypoxia *in vitro*. On account of this, the authors concluded thatt there was a higher hypoxic tolerance of tumors *in vivo* which showed up-regulation of PERK expression (Fels and Koumenis, 2006).

IRE1α, a receptor of the UPR, is expressed at similar level in adult skin and granulation tissue, whereas IRS (Tab. 7) is lower by half in embryo-fetal skin, compared to adult skin. Interestingly, the expression in tumor cells was decreased as well, but the pattern was similar in benign and malignant tumor cells. Moreover, stromal cells showed a similar expression level of IRE1α in the different pathological cases of the tissues, as was the case in endothelial cells. Although the IRE1α-mediated pathway is classified as the most prominent pro-survival pathway of the UPR (Lin *et al.,* 2007), it was recently discussed that apoptosis is also regulated by IRE1α. Continuous ER stress leads to the repression of adaptive responses via the IRE1α-mediated pathway. This signal finally ends in the activation of RIDD and following cell death (Chen and Brandizzi, 2013). This fact could explain the down-regulation of IRE1α in endothelial and stromal cells of angiosarcoma and haemangioma.

Additionally, the expression of a transcription factor of the UPR, ATF4, was analyzed. The expression pattern in endothelial cells of embryo-fetal skin, adult skin and haemangioma was similar. Increased expression of the transcription factor was observed in endothelial and stromal cells of granulation tissue and malignant angiosarcoma. Up-regulation of ATF4 has already been reported for several tumor cells, for example in human breast cancer or malignant melanoma (Li *et al.,* 2011; Ameri *et al.,* 2004). A possible explanation for ATF4 overexpression in tumor cells could be the capability of ATF4 to influence VEGF expression and, thus, promote angiogenesis and tumor growth. This transcription factor is able to bind directly to the VEGF promoter (Urra and Hetz, 2014). Tumor cells could exploit this feature to drive angiogenesis and subsequent tumor growth.

In summary, most of the tested UPR components are up-regulated in malignant angiosarcoma. It has been mentioned on several occasions that the deprivation of oxygen activates the UPR *in vitro*, which was shown in the current study as well. Such a hypoxic microenvironment occurs with increasing tumor growth. Furthermore, it is known that the response to oxygen deprivation via UPR is a HIF1α-independent process (Rzymski and Harris, 2007). In addition, VEGFA was reported to be up-regulated by ER stress in a prostate cancer cell line, a liver cancer cell line and in insulinoma cells (Ghosh *et al.,* 2010). These insights could explain the up-regulation of several UPR members in tumor tissue. Interestingly, BiP was shown to be highly regulated in endothelial cells, as well as in stromal cells.

Besides cancer, several diseases are associated with abnormal vasculature, for example AMD or reduced vascularization present, for example, in chronic ischemic wounds. Intensive research has concentrated on investigating anti-angiogenic

therapies to fight cancer, as well as pro-angiogenic therapies to combat e.g. cardiovascular diseases. Several studies are ongoing which are engaged with therapies involving targeting of growth factors like VEGF, but they present several limitations. The initial promise of trials with antisense-VEGF and dominant-negative KDR, but also the usage of KDR inhibitors unfortunately did not demonstrate obvious clinical benefit (Zadeh and Guha, 2003). Nevertheless, the anti-VEGF antibody drugs, Bevacizumab or Pazopanib, an inhibitor of tyrosine kinase receptors like KDR, PDGF receptor and FGF receptor, are currently under intensive investigation in cancer research (Oliver and McGuire, 2014; Numnum *et al.,* 2006). In clinical trials, Bevacizumab is often combined with standard therapies (Allegra *et al.,* 2013; Gramont *et al.,* 2012). However, recent studies showed that prolonged treatment with the anti-angiogenic agent may result in a more aggressive tumor phenotype (Mountzios *et al.,* 2014; Carmeliet and Jain, 2011). Recently, *in vitro* investigations on the effects of the anti-angiogenic drug, Sunitinib, revealed an increase of KDR expression in endothelial cells, indicating pro-angiogenic consequences (Norton *et al.,* 2014). With regard to pro-angiogenic therapies to induce blood vessel development, first concepts arose with growth factors like VEGF or bFGF to treat, for example, ischemic tissue directly by supporting the physiological reaction. Further studies followed involving gene therapy mechanisms, in which intramuscular gene transfer was investigated, demonstrating increased levels of VEGF in the ischemic tissue. Additionally, research on biomaterials regulating growth factor release received high attention (Folkman, 1998), but did not lead to the desired success. On account of these facts, it is important to find other strategies to trigger angiogenesis. Possessing several targets to regulate the process of new blood vessel formation may open new doors for pro- and anti-angiogenic therapies. Hence, investigation of angiogenic switchs concentrating on cell signaling pathways could represent a great step forward in treatment of diseases comprising defective vascularization. The UPR and its important role in stress management make it attractive to investigate the regulatory role of this signaling pathway in angiogenic processes.

Within the present study, an inhibitory effect on tube formation could be shown in endothelial cells after BiP down-regulation *in vitro*. Hence, this clearly indicates a regulatory role of the chaperone in angiogenesis. Particularly, BiP level showed a regulatory effect on KDR expression. Therefore, it could be assumed that higher levels of BiP, for example in malignant tumors, are accompanied by an increase of KDR expression, resulting in promoted angiogenesis. Transferring the results from the *in vitro* to the *in vivo* situation, it could be postulated that stable levels of BiP might regulate UPR activation and therefore have protective effects against dysregulation of

angiogenesis under physiological conditions. In contrast, up-regulation of BiP in malignant tumors would strongly block UPR activation, thus leading to survival and proliferation of endothelial cells, eventually resulting in uncontrolled angiogenesis. This hypothesis is substantiated by the observation of high angiogenic activity in endothelial cells in angiosarcoma with increased expression of BiP. In several other studies it was shown that BiP is up-regulated in various cancer types like lung, stomach, breast or prostate cancer (Uramoto *et al.,* 2005; Fernandes *et al.,* 2000; Pootrakul *et al.,* 2006; Zheng *et al.,* 2008). High levels of BiP could protect against UPR activation, which normally results in apoptosis of the cells, regression of blood vessels or the prevention of new blood vessel formation. In addition, the up-regulation of the chaperone BiP ensures continuation of a high protein synthesis rate in tumor cells by guaranteeing a proper folding of newly synthesized proteins. Moreover, Virrey et al. postulated that overexpression of BiP in malignant glioma is responsible for resistance of the cells to chemotherapeutic agents and described the chaperone as a possible target to sensitize the tumor cells for anti-cancer therapies (Virrey *et al.,* 2008).

In summary, the results of this study indicate that control of UPR by the chaperone BiP could be important for regulation of angiogenesis *in vivo*. Controlling BiP amount and regulation of UPR in general might represent a promising way to control angiogenesis.

5 Summary

Several diseases are accompanied by dysregulated vascularization. Commonly employed therapies, involving, for example, the targeting of VEGF, present several limitations. Therefore, new strategies for regulation of angiogenesis need to be evolved. Targeting novel signaling pathways to trigger or inhibit angiogenesis could prove to be promising. Angiogenesis is a highly regulated process associated with a high protein synthesis rate. Previously, angiogenesis was linked with the ER stress signaling pathway, the Unfolded Protein Response (UPR) (Zeng *et al.,* 2013; Bouvier *et al.,* 2012). In a histological examination in the present study, UPR components were shown to be dysregulated under pathological conditions *in vivo*. Remarkably, BiP, the major stress sensor protein of the UPR, was shown to be highly up-regulated in endothelial cells in angiosarcoma. Down-regulation of BiP *in vitro* with the help of the RNAi technique was shown to influence inflammatory responses and tube formation in endothelial cells. BiP down-regulation strengthened the inflammatory response of HUVEC, reflected in a significant increase in IL-8 release and ICAM-1 expression, this being attributable to UPR signaling, activated by BiP down-regulation. Moreover, the endothelial cell phenotype of BiP down-regulated cells was similar to non-transfected endothelial cells, analyzed by the investigation of the cytoskeleton and the expression of the endothelial cell-specific marker, CD31. In turn, glycosylation of membrane proteins in BiP down-regulated cells differed. The level of glycosylation resembled the status of UPR activation. Focussing on angiogenesis, reduced cell migration and inhibition of the formation of capillary-like structures in BiP down-regulated cells was very prominent. Importantly, KDR expression was strongly reduced in BiP down-regulated cells, while the expression of another VEGF receptor, Flt-1, remained unaltered. Characterization of the BiP down-regulated cells indicated that decreased expression of KDR could be attributed to UPR activation following BiP down-regulation. Alternatively, a deficiency of chaperone functionality in BiP down-regulated cells could be responsible for down-regulation of KDR. The results of this study indicate that stable levels of BiP contribute to regulated angiogenesis by controlling UPR signaling in physiological processes. Dysregulation of BiP levels, as in malignant tumors, could provide an advantage to tumor cells and involved endothelial cells by strong inhibition of UPR, eventually leading to aberrant vascularization. Therefore, BiP and the UPR pathway represent potential targets for the regulation of angiogenesis.

6 Zusammenfassung

Verschiedene Krankheiten gehen mit einer fehlerhaften Vaskularisierung einher. Allerdings ist der Erfolg der derzeitig vorhandenen Therapieansätze, die sich z.B. auf VEGF fokussieren, beschränkt. Aus diesem Grund ist es wichtig, neue Strategien zur Regulation der Angiogenese zu entwickeln. Hierbei stehen neue Signaltransduktionswege im Fokus, die sich als vielversprechend erweisen, um Angiogenese zu fördern oder zu inhibieren. Die Blutgefäßneubildung ist ein hochregulierter Prozess, der mit einer hohen Proteinsyntheserate verknüpft ist. Die Angiogenese wurde bereits mit dem ER-Stress Signaltransduktionsweg, der Unfolded Protein Response (UPR), in Verbindung gebracht (Zeng *et al.,* 2013; Bouvier *et al.,* 2012). Eine im Rahmen der vorliegenden Studie durchgeführte histologische Untersuchung konnte eine Fehlregulierung der Expression von UPR beteiligten Proteinen *in vivo* unter pathologischen Bedingungen gezeigt werden. Bemerkenswerter Weise war BiP, der Hauptsensor der UPR, in Endothelzellen von Angiosarkomen sehr stark exprimiert. In *in vitro* Experimenten wurde gezeigt, dass das Herunterregulieren von BiP mittels RNAi Einfluss auf die inflammatorische Antwort und die Bildung angiogener Strukturen in Endothelzellen nimmt. Das Herunterregulieren des Proteins BiP verstärkte die inflammatorische Antwort von HUVEC, was sich in einer gesteigerten Bildung von IL-8 und ICAM-1 äußerte und wurde auf die Aktivierung der UPR durch die verringerte Menge an BiP zurückgeführt. Der Phänotyp BiP-herunterregulierter Zellen entsprach dem untransfizierter Zellen, welcher durch das Cytoskelett und die Expression des endothelspezifischen Markers CD31 charakterisiert wurde. Im Gegensatz dazu änderte sich der Grad der Glykosylierung in transfizierten Zellen. Im Hinblick auf die Blutgefäßbildung, zeigten sich eine gehemmte Migration und eine inhibierte Bildung Gefäß-ähnlicher Strukturen in BiP-herunterregulierten Zellen. In diesen Zellen war die Expression von KDR auffallend stark inhibiert, wohingegen die Flt-1 Expression sich als gleichbleibend herausstellte, was ebenfalls auf die Aktivierung der UPR zurückgeführt werden konnte. Alternativ wäre der reduzierte Level des Proteins BiP im Hinblick auf die Funktion als Helferenzym in der Proteinfaltung eine mögliche Erklärung für die gehemmte Expression von KDR. Die Ergebnisse dieser Studie deuten darauf hin, dass stabile Spiegel von BiP die Regulierung der Angiogenese durch die Kontrolle der UPR in physiologischen Prozessen unterstützen könnte. Eine Fehlregulierung von BiP durch Unterdrückung der UPR, wie z.B. in malignen Tumoren, könnte Tumorzellen und beteiligten Endothelzellen einen Vorteil verschaffen und zu einer gestörten Vaskularisierung führen. Somit stellt das Stresssensorprotein BiP und die UPR einen potentiellen Angriffspunkt für die Regulation der Angiogenese dar.

7 References

Agapitov AV and Haynes WG (2002). Role of endothelin in cardiovascular disease. *J Renin Angiotensin Aldosterone Syst.* **3:** 1.

Allegra CJ, Yothers G, O'Connell MJ, Sharif S, Petrelli NJ, Lopa SH and Wolmark N (2013). Bevacizumab in Stage II-III Colon Cancer: 5-Year Update of the National Surgical Adjuvant Breast and Bowel Project C-08 Trial. *Journal of Clinical Oncology.* **31:** 359–364.

Almagro S, Durmort C, Chervin-Petinot A, Heyraud S, Dubois M, Lambert O, Maillefaud C, Hewat E, Schaal JP, Huber P and Gulino-Debrac D (2010). The Motor Protein Myosin-X Transports VE-Cadherin along Filopodia To Allow the Formation of Early Endothelial Cell-Cell Contacts. *Molecular and Cellular Biology.* **30:** 1703–1717.

Alon R and Feigelson S (2002). From rolling to arrest on blood vessels: leukocyte tap dancing on endothelial integrin ligands and chemokines at sub-second contacts. *Seminars in Immunology.* **14:** 93–104.

Alon T, Hemo I, Itin A, Pe'er J, Stone J and Keshet E (1995). Vascular endothelial growth factor acts as a survival factor for newly formed retinal vessels and has implications for retinopathy of prematurity. *Nat Med.* **1:** 1024–1028.

Ameri K, Lewis CE, Raida M, Sowter H, Hai T and Harris AL (2004). Anoxic induction of ATF-4 through HIF-1-independent pathways of protein stabilization in human cancer cells. *Blood.* **103:** 1876–1882.

Anand S and Cheresh DA (2011). MicroRNA-mediated regulation of the angiogenic switch. *Current Opinion in Hematology.* **18:** 171–176.

Asahara T, Murohara T, Sullivan A, Silver M, van der Zee, R., Li T, Witzenbichler B, Schatteman G and Isner JM (1997). Isolation of Putative Progenitor Endothelial Cells for Angiogenesis. *Science.* **275:** 964–966.

Atkins C, Liu Q, Minthorn E, Zhang S, Figueroa DJ, Moss K, Stanley TB, Sanders B, Goetz A, Gaul N, Choudhry AE, Alsaid H, Jucker BM, Axten JM and Kumar R (2013). Characterization of a Novel PERK Kinase Inhibitor with Antitumor and Antiangiogenic Activity. *Cancer Research.* **73:** 1993–2002.

Auf G, Jabouille A, Guerit S, Pineau R, Delugin M, Bouchecareilh M, Magnin N, Favereaux A, Maitre M, Gaiser T, Deimling A von, Czabanka M, Vajkoczy P, Chevet E, Bikfalvi A and Moenner M (2010). Inositol-requiring enzyme 1 is a key regulator of

angiogenesis and invasion in malignant glioma. *Proceedings of the National Academy of Sciences.* **107:** 15553–15558.

Ausprunk DH and Folkman J (1977). Migration and proliferation of endothelial cells in preformed and newly formed blood vessels during tumor angiogenesis. *Microvascular Research.* **14:** 53–65.

Banerjee A, Lang J, Hung M, Sengupta K, Banerjee SK, Baksi K and Banerjee DK (2011). Unfolded Protein Response Is Required in nu/nu Mice Microvasculature for Treating Breast Tumor with Tunicamycin. *Journal of Biological Chemistry.* **286:** 29127–29138.

Bartel DP (2009). MicroRNAs: Target Recognition and Regulatory Functions. *Cell.* **136:** 215–233.

Bartoszewska S, Kochan K, Madanecki P, Piotrowski A, Ochocka R, Collawn JF and Bartoszewski R (2013). Regulation of the unfolded protein response by microRNAs. *Cell Mol Biol Lett.* **18:** 555–578.

Bertolotti A, Zhang Y, Hendershot LM, Harding HP and Ron D (2000). Dynamic interaction of BiP and ER stress transducers in the unfolded-protein response. *Nature Cell Biology.* **2:** 326–332.

Bi M, Naczki C, Koritzinsky M, Fels D, Blais J, Hu N, Harding HP, Novoa I, Varia M, Raleigh J, Scheuner D, Kaufman RJ, Bell J, Ron D, Wouters BG and Koumenis C (2005). ER stress-regulated translation increases tolerance to extreme hypoxia and promotes tumor growth. *Seminars in Immunology.* **24:** 3470–3481.

Blair P and Flaumenhaft R (2009). Platelet α-granules: Basic biology and clinical correlates. *Blood Reviews.* **23:** 177–189.

Blais JD, Addison CL, Edge R, Falls T, Zhao H, Wary K, Koumenis C, Harding HP, Ron D, Holcik M and Bell JC (2006). Perk-Dependent Translational Regulation Promotes Tumor Cell Adaptation and Angiogenesis in Response to Hypoxic Stress. *Molecular and Cellular Biology.* **26:** 9517–9532.

Blom N, Sicheritz-Pontén T, Gupta R, Gammeltoft S and Brunak S (2004). Prediction of post-translational glycosylation and phosphorylation of proteins from the amino acid sequence. *PROTEOMICS.* **4:** 1633–1649.

Blum Y, Belting H, Ellertsdottir E, Herwig L, Lüders F and Affolter M (2008). Complex cell rearrangements during intersegmental vessel sprouting and vessel fusion in the zebrafish embryo. *Developmental Biology.* **316:** 312–322.

Bossink AW, Paemen L, Jansen PM, Hack CE, Thijs LG and van Damme J (1995). Plasma Levels of the Chemokines Monocyte Chemotactic Proteins 1 and 2 are Elevated in Human Sepsis. *Blood.* **86:** 3841–3847.

Bouvier N, Fougeray S, Beaune P, Thervet E and Pallet N (2012). The Unfolded Protein Response Regulates an Angiogenic Response by the Kidney Epithelium during Ischemic Stress. *Journal of Biological Chemistry.* **287:** 14557–14568.

Brewer JW and Diehl JA (2000). PERK mediates cell-cycle exit during the mammalian unfolded protein response. *PNAS.* **97:** 12625–12630.

Buchner J (2002). Introduction: the cellular protein folding machinery. *CMLS (Cellular and Molecular Life Science).* **59:** 1587–1588.

Bussmann J, Wolfe SA and Siekmann AF (2011). Arterial-venous network formation during brain vascularization involves hemodynamic regulation of chemokine signaling. *Development.* **138:** 1717–1726.

Carman CV and Springer TA (2004). A transmigratory cup in leukocyte diapedesis both through individual vascular endothelial cells and between them. *The Journal of Cell Biology.* **167:** 377–388.

Carmeliet P, Ferreira V, Breier G, Pollefeyt S, Kieckens L, Gertsenstein M, Fahrig M, Vandenhoeck A, Harpal K, Eberhardt C, Declercq C, Pawling J, Moons L, Collen D, Risau W and Nagy A (1996). Abnormal blood vessel development and lethality in embryos lacking a single VEGF allele. *Nature.* **380:** 435–439.

Carmeliet P and Jain RK (2011). Principles and mechanisms of vessel normalization for cancer and other angiogenic diseases. *Nat Rev Drug Discov.* **10:** 417–427.

Cesarman-Maus G and Hajjar KA (2005). Molecular mechanisms of fibrinolysis. *Br J Haematol.* **129:** 307–321.

Chappell JC, Taylor SM, Ferrara N and Bautch VL (2009). Local Guidance of Emerging Vessel Sprouts Requires Soluble Flt-1. *Developmental Cell.* **17:** 377–386.

Chen S, Xue Y, Wu X, Le C, Bhutkar A, Bell EL, Zhang F, Langer R and Sharp PA (2014). Global microRNA depletion suppresses tumor angiogenesis. *Genes & Development.* **28:** 1054–1067.

Chen Y, Banda M, Speyer CL, Smith JS, Rabson AB and Gorski DH (2010). Regulation of the Expression and Activity of the Antiangiogenic Homeobox Gene GAX/MEOX2 by ZEB2 and MicroRNA-221. *Molecular and Cellular Biology.* **30:** 3902–3913.

Chen Y and Brandizzi F (2013). IRE1: ER stress sensor and cell fate executor. *Trends in Cell Biology.* **23:** 547–555.

Chitnis N, Pytel D and Diehl JA (2013). UPR-inducible miRNAs contribute to stressful situations. *Trends in Biochemical Sciences.* **38:** 447–452.

Chomczynski P and Sacchi N (1987). Single-step method of RNA isolation by acid guanidinium thiocyanate-phenol-chloroform extraction. *Analytical Biochemistry.* **162:** 156–159.

Chou J and Roizman B (1994). Herpes simples virus 1 g1-34.5 gene function, which blocks the host response to infection, maps in the homologous domain of the genes expressed during growth arres and DNA damage. *Proc Natl Acad Sci.* **91:** 5247–5251.

Chowdhary S and Townend JN (2001). Nitric oxide and hypertension: not just an endothelium derived relaxing factor! *Journal of Human Hypertension.* **15:** 219–227.

Cinamon G, Shinder V, Shamri R and Alon R (2004). Chemoattractant Signals and 2 Integrin Occupancy at Apical Endothelial Contacts Combine with Shear Stress Signals to Promote Transendothelial Neutrophil Migration. *The Journal of Immunology.* **173:** 7282–7291.

Clark R (1990). Fibronectin Matrix Deposition and Fibronectin Receptor Expression in Healing and Normal Skin. *The Journal of Investigative Dermatology.* **94:** 128–134.

Clemetson KJ (2012). Platelets and Primary Haemostasis. *Thrombosis Research.* **129:** 220–224.

Corrigall VM, Bodman-Smith MD, Brunst M, Cornell H and Panayi GS (2004). Inhibition of antigen-presenting cell function and stimulation of human peripheral blood mononuclear cells to express an antiinflammatory cytokine profile by the stress protein BiP: Relevance to the treatment of inflammatory arthritis. *Arthritis & Rheumatism.* **50:** 1164–1171.

Croci DO, Cerliani JP, Dalotto-Moreno T, Méndez-Huergo SP, Mascanfroni ID, Dergan-Dylon S, Toscano MA, Caramelo JJ, García-Vallejo JJ, Ouyang J, Mesri EA, Junttila MR, Bais C, Shipp MA, Salatino M and Rabinovich GA (2014). Glycosylation-Dependent Lectin-Receptor Interactions Preserve Angiogenesis in Anti-VEGF Refractory Tumors. *Cell.* **156:** 744–758.

Daneshmand S, Quek ML, Lin E, Lee C, Cote RJ, Hawes D, Cai J, Groshen S, Lieskovsky G, Skinner DG, Lee AS and Pinski J (2007). Glucose-regulated protein GRP78 is up-regulated in prostate cancer and correlates with recurrence and survival. *Human Pathology.* **38:** 1547–1552.

Davidson DJ, Haskell C, Majest S, Kherzai A, Egan DA, Walter KA, Schneider A, Gubbins EF, Solomon L, Chen Z, Lesniewski R and Henkin J (2005). Kringel 5 of Human Plasminogen Induces Apoptosis of Endothelial and Tumor Cells through Surface-Expressed Glucose-Regulated Protein 78. *Cancer Research.* **65:** 4663–4672.

Deanfield JE, Halcox JP and Rabelink TJ (2007). Endothelial Function and Dysfunction: Testing and Clinical Relevance. *Circulation.* **115:** 1285–1295.

Delepine M, Nicolino M, Barrett T, Golamaully M, Lathrop GM and Julier C (2000). EIF2AK3, encoding translation initiation factor 2-a kinase 3, is mutated in patients with Wolcott-Rallison syndrome. *nature genetics.* **25:** 406–409.

Delpinoi A, Piselli P, Vismara D, Vendetti S and Colizzi V (1998). Cell surface localization of the 78 kD glucose regulated protein (GRP 78) induced by thapsigargin. *Molecular Membrane Biology.* **15:** 21–26.

Desmouliere A, Chaponnier C and Gabbiani G (2005). Tissue repair, contraction, and the myofibroblast. *Wound Repair and Regeneration.* **13:** 7–12.

Dey S, Baird TD, Zhou D, Palam LR, Spandau DF and Wek RC (2010). Both Transcriptional Regulation and Translational Control of ATF4 Are Central to the Integrated Stress Response. *Journal of Biological Chemistry.* **285:** 33165–33174.

Diehl JA, Fuchs SY and Koumenis C (2011). The Cell Biology of the Unfolded Protein Response. *Gastroenterology.* **141:** 38–41.e2.

Dimmeler S and Zeiher AM (2000). Endothelial Cell Apoptosis in Angiogenesis and Vessel Regression. *Circulation Research.* **87:** 434–439.

Dinarello CA (2000). Proinflammatory Cytokines. *CHEST.* **118:** 503–508.

Dong D, Ni M, Li J, Xiong S, Ye W, Virrey JJ, Mao C, Ye R, Wang M, Pen L, Dubeau L, Groshen S, Hofman FM and Lee AS (2008). Critical Role of the Stress Chaperone GRP78/BiP in Tumor Proliferation, Survival, and Tumor Angiogenesis in Transgene-Induced Mammary Tumor Development. *Cancer Research.* **68:** 498–505.

Dong D, Stapleton C, Luo B, Xiong S, Ye W, Zhang Y, Jhaveri N, Zhu G, Ye R, Liu Z, Bruhn KW, Craft N, Groshen S, Hofman FM and Lee AS (2011). A Critical Role for GRP78/BiP in the Tumor Microenvironment for Neovascularization during Tumor Growth and Metastasis. *Cancer Research.* **71:** 2848–2857.

Douglas RS, Tarshis AD, Pletcher CH, Nowell PC and Moore JS (1995). A simplified method for the coordinate examination of apoptosis and surface phenotype of murine lymphocytes. *Journal of Immunological Methods.* **188:** 219–228.

Doyle B, Metharom P and Caplice N (2006). Endothelial Progenitor Cells. *Endothelium.* **13:** 403–410.

Dvorak AM and Feng D (2001). The Vesiculo-Vacuolar Organelle (VVO): A New Endothelial Cell Permeability Organelle. *Journal of Histochemistry & Cytochemistry.* **49:** 419–431.

Eilken HM and Adams RH (2010). Dynamics of endothelial cell behavior in sprouting angiogenesis. *Current Opinion in Cell Biology.* **22:** 617–625.

Elgamal OA, Park J, Gusev Y, Azevedo-Pouly, Ana Clara P., Jiang J, Roopra A, Schmittgen TD and Guan X (2013). Tumor Suppressive Function of mir-205 in Breast Cancer Is Linked to HMGB3 Regulation. *PLoS ONE.* **8:** e76402.

Ellis RJ and van der Vies SM (1991). Molecular Chaperones. *Annu. Rev. Biochem.* **60:** 321–347.

Eren E, Yilmaz N and Aydin O (2013). Functionally Defective High-Density Lipoprotein and Paraoxonase: A Couple for Endothelial Dysfunction in Atherosclerosis. *Cholesterol.* **2013:** 1–10.

Ewan LC, Jopling HM, Jia H, Mittar S, Bagherzadeh A, Howell GJ, Walker JH, Zachary IC and Ponnambalam S (2006). Intrinsic Tyrosine Kinase Activity is Required for Vascular Endothelial Growth Factor Receptor 2 Ubiquitination, Sorting and Degradation in Endothelial Cells. *Traffic.* **7:** 1270–1282.

Fels DR and Koumenis C (2006). The PERK/eIF2a/ATF4 Module of the UPR in Hypoxia Resistance and Tumor Growth. *Cancer Biology & Therapy.* **5:** 723–728.

Fernandes PM, Tabbara SO, Jacobs LK, Manning, F. C. R., Tsangaris TN, Schwartz AM, Kennedy KA and Patierno SR (2000). Overexpression of the glucose-regulated stress gene GRP78 in malignant but not benign human breast lesions. *Breast Cancer Research and Treatment.* **59:** 15–26.

Fischer C, Mazzone M, Jonckx B and Carmeliet P (2008). FLT1 and its ligands VEGFB and PlGF: drug targets for anti-angiogenic therapy? *Nat Rev Cancer.* **8:** 942–956.

Folkman J (1998). Therapeutic Angiogenesis in Ischemic Limbs. *Circulation.* **97:** 1108–1110.

Fong G, Rossant J, Gertsenstein M and Breitman ML (1995). Role of the Flt-1 receptor tyrosine kinase in regulating the assembly of vascular endothelium. *Nature.* **376:** 66–70.

Fonseca SG, Gromada J and Urano F (2011). Endoplasmic reticulum stress and pancreatic β-cell death. *Trends in Endocrinology & Metabolism.* **22:** 266–274.

Friedman RC, Farh KK, Burge CB and Bartel DP (2008). Most mammalian mRNAs are conserved targets of microRNAs. *Genome Research.* **19:** 92–105.

Furie B and Furie BC (2008). Mechanisms of Thrombus Formation. *N Engl J Med.* **359:** 938–949.

Garzon R, Marcucci G and Croce CM (2010). Targeting microRNAs in cancer: rationale, strategies and challenges. *Nat Rev Drug Discov.* **9:** 775–789.

Gerhardt H, Golding M, Fruttiger M, Ruhrberg C, Lundkvist A, Abramsson A, Jeltsch M, Mitchell C, Alitalo K, Shima D and Betsholtz C (2003). VEGF guides angiogenic sprouting utilizing endothelial tip cell filopodia. *The Journal of Cell Biology.* **161:** 1163–1177.

Gething M (1999). Role and regulation of the ER chaperone BiP. *Cell & Developmental Biology.* **10:** 465–472.

Geudens I and Gerhardt H (2011). Coordinating cell behaviour during blood vessel formation. *Development.* **138:** 4569–4583.

Ghosh R, Lipson KL, Sargent KE, Mercurio AM, Hunt JS, Ron D, Urano F and Blagosklonny MV (2010). Transcriptional Regulation of VEGF-A by the Unfolded Protein Response Pathway. *PLoS ONE.* **5:** e9575.

Gillies RJ, Didier N and Denton M (1986). Determination of cell number in monolayer cultures. *Analytical Biochemistry.* **159:** 109–113.

Gimbrone MA, Leapmen SB, Cotran RS and Folkman J (1972). Tumor dormancy in vivo by prevention of neovascularization. *The Journal of Experimental Medicine.* **136:** 261–276.

Goligorsky MS, Patschan D and Kuo M (2009). Weibel–Palade bodies—sentinels of acute stress. *Nat Rev Nephrol.* **5:** 423–426.

Gora S, Maouche S, Atout R, Wanherdrick K, Lambeau G, Cambien F, Ninio E and Karabina S (2010). Phospholipolyzed LDL induces an inflammatory response in endothelial cells through endoplasmic reticulum stress signaling. *The FASEB Journal.* **24:** 3284–3297.

Gramont A de, van Cutsem E, Schmoll H, Tabernero J, Clarke S, Moore MJ, Cunningham D, Cartwright TH, Hecht JR, Rivera F, Im S, Bodoky G, Salazar R, Maindrault-Goebel F, Shacham-Shmueli E, Bajetta E, Makrutzki M, Shang A, André T and Hoff PM (2012). Bevacizumab plus oxaliplatin-based chemotherapy as adjuvant treatment for colon cancer (AVANT): a phase 3 randomised controlled trial. *The Lancet Oncology.* **13:** 1225–1233.

Greenhalgh DG (1998). The role of apoptosis in wound healing. *The International Journal of Biochemistry & Cell Biology.* **30:** 1019–1030.

Haas IG and Wabl M (1983). Immunoglobulin heavy chain binding protein. *Nature.* **306:** 387–389.

Harding HP, Zeng H, Zhang Y, Jungries R, Chung P, Plesken H, Sabatini DD and Ron D (2001). Diabetes Mellitus and Exocrine Pancreatic Dysfunction in Perk−/− Mice Reveals a Role for Translational Control in Secretory Cell Survival. *Molecular Cell.* **7:** 1153–1163.

Harding HP, Zhang Y, Bertolotti A, Zeng H and Ron D (2000). Perk Is Essential for Translational Regulation and Cell Survival during the Unfolded Protein Response. *Molecular Cell.* **5:** 897–904.

He L and Hannon GJ (2004). MicroRNAs: small RNAs with a big role in gene regulation. *Nat Rev Genet.* **5:** 522–531.

Hellström M, Phng L, Hofmann JJ, Wallgard E, Coultas L, Lindblom P, Alva J, Nilsson A, Karlsson L, Gaiano N, Yoon K, Rossant J, Iruela-Arispe ML, Kalén M, Gerhardt H and Betsholtz C (2007). Dll4 signalling through Notch1 regulates formation of tip cells during angiogenesis. *Nature.* **445:** 776–780.

Hetz C (2012). The unfolded protein response: controlling cell fate decisions under ER stress and beyond. *Nat Rev Mol Cell Biol.* **13:** 89–102.

Hetz C and Glimcher LH (2009). Fine-Tuning of the Unfolded Protein Response: Assembling the IRE1α Interactome. *Molecular Cell.* **35:** 551–561.

Hirota M, Kitagaki M, Itagaki H and Aiba S (2006). Quantivtative measurement of spliced XBP1 mRNA as an indicator of endoplasmatic reticulum stress. *The Journal of Toxicological Sciences.* **31:** 149–156.

Hollien J and Weissman JS (2006). Decay of Endoplasmic Reticulum-Localized mRNAs During the Unfolded Protein Response. *Science.* **313:** 104–107.

Hoozemans, J. J. M., Veerhuis R, Van Haastert, E. S., Rozemuller JM, Baas F, Eikelenboom P and Scheper W (2005). The unfolded protein response is activated in Alzheimer's disease. *Acta Neuropathol.* **110:** 165–172.

Hsiang YH, Hertzberg R, Hecht S and Liu LF (1985). Camptothecin induces protein-linked DNA breaks via mammalian DNA topoisomerase I. *J. Biol. Chem. 1985 260: 14873-14878.* **1985:** 14873-14878.

Huang AJ, Manning JE, Bandak TM, Ratau MC, Hanser KR and Silverstein SC (1993). Endothelial Cell Cytosolic Free Calcium Regulates Neutrophil Migration across Monolayers of Endothelial Cells. *The Journal of Cell Biology.* **120:** 1371–1380.

Hughes S and Chan-Ling T (2000). Roles of Endothelial Cell Migration and Apoptosis in Vascular Remodeling during Development of the Central Nervous System. *Microcirculation.* **7:** 317–333.

Jaffe EA, Nachman RL, Becker CG and Minick CR (1973). Culture of Human Endothelial Cells Derived from Umbilical Veins. *The Journal of Clinical Investigation.* **52:** 2745–2756.

Jakobsson L, Franco CA, Bentley K, Collins RT, Ponsioen B, Aspalter IM, Rosewell I, Busse M, Thurston G, Medvinsky A, Schulte-Merker S and Gerhardt H (2010). Endothelial cells dynamically compete for the tip cell position during angiogenic sprouting. *Nat Cell Biol.* **12:** 943–953.

Jamora C, Dennert G and Lee AS (1996). Inhibition of tumor growth progression by suppresion of stress protein GRP78/BiP induction in fibrosarcoma B/C10ME. *Proc Natl Acad Sci.* **93:** 7690–7694.

Kalejta RF, Shenk T, Beavis AJ (1997). Use of a membrane-localized green fluorescent protein allows simultaneous identification of transfected cells and cell cycle analysis by flow cytometry. *Cytometry.; 29(4):286-291.* **29:** 286–291.

Kamei M, Brian Saunders W, Bayless KJ, Dye L, Davis GE and Weinstein BM (2006). Endothelial tubes assemble from intracellular vacuoles in vivo. *Nature.* **442:** 453–456.

Karali E, Bellou S, Stellas D, Klinakis A, Murphy C and Fotsis T (2014). VEGF Signals through ATF6 and PERK to Promote Endothelial Cell Survival and Angiogenesis in the Absence of ER Stress. *Molecular Cell.* **54:** 559–572.

Katanasaka Y, Ishii T, Asai T, Naitou H, Maeda N, Koizumi F, Miyagawa S, Ohashi N and Oku N (2010). Cancer antineovascular therapy with liposome drug delivery systems targeted to BiP/GRP78. *Int. J. Cancer.* **127:** 2685–2698.

Kearney JB, Kappas NC, Ellerstrom C, DiPaola W and Bautch VL (2004). The VEGF receptor flt-1 (VEGFR-1) is a positive modulator of vascular sprout formation and branching morphogenesis. *Blood.* **103:** 4527–4535.

Khakoo AY and Finkel T (2005). Endothelial Progenitor Cells*. *Annu. Rev. Med.* **56:** 79–101.

Kozutsumi Y, Segal M, Normington K, Gething M and Sambrook J (1988). The presence of malfolded proteins in the endoplasmatic reticulum signals the induction of glucose-related proteins. *Nature.* **332:** 462–464.

Kranz A, Rau C, Kochs M and Waltenberger J (2000). Elevation of Vascular Endothelial Growth Factor-A Serum Levels Following Acute Myocardial Infarction. Evidence for its Origin and Functional Significance. *J Mol Cell Cardiol.* **32:** 65–72.

Krol J, Loedige I and Filipowicz W (2010). The widespread regulation of microRNA biogenesis, function and decay. *Nat Rev Genet.* **11:** 597–610.

Kroll J and Waltenberger J (2000). Regulation der Endothelfunktion und der Angiogenese durch den Vaskulären Endothelialen Wachstumsfaktor-A (VEGF-A). *Z Kardiol.* **89:** 206–218.

Krump-Konvalinkova V, Bittinger F, Unger RE, Peters K, Lehr H and Kirkpatrick C (2001). Generation of Human Pulmonary Microvascular Endothelial Cell Lines. *Laboratory investigation.* **81:** 1717–1727.

Kuehbacher A, Urbich C, Zeiher AM and Dimmeler S (2007). Role of Dicer and Drosha for Endothelial MicroRNA Expression and Angiogenesis. *Circulation Research.* **101:** 59–68.

Kuo L, Hung C, Chen W, Chang Y and Wei P (2013). Glucose-regulated protein 78 silencing down-regulates vascular endothelial growth factor/vascular endothelial growth factor receptor 2 pathway to suppress human colon cancer tumor growth. *Journal of Surgical Research.* **185:** 264–272.

Lacour P, Heimrich B and Pröls F (2007). Induction of cellular stress and chaperone activation in organotypic slice cultures of hippocampus. *Journal of Neuroscience Methods.* **166:** 24–31.

Laemmli UK (1970). Cleavage of Structural Proteins during the Assembly of the Head of Bacteriophage T4. *Nature.* **227:** 680–685.

Lamalice L, Houle F, Jourdan G and Huot J (2004). Phosphorylation of tyrosine 1214 on VEGFR2 is required for VEGF-induced activation of Cdc42 upstream of SAPK2/p38. *Oncogene.* **23:** 434–445.

Lamalice L, Le Boeuf F and Huot J (2007). Endothelial Cell Migration During Angiogenesis. *Circulation Research.* **100:** 782–794.

Lee K, Tirasophon W, Shen X, Michalak M, Prywes R, Okada T, Yoshida H, Mori K and Kaufman RJ (2002). IRE1-mediated unconventional mRNA splicing and S2P-mediated

ATF6 cleavage merge to regulate XBP1 in signaling the unfolded protein response. *Genes & Development.* **16:** 452–466.

Lehmann U, Hasemeier B, Christgen M, Müller M, Römermann D, Länger F and Kreipe H (2008). Epigenetic inactivation of microRNA gene hsa-mir-9-1 in human breast cancer. *J. Pathol.* **214:** 17–24.

Leslie JD, Ariza-McNaughton L, Bermange AL, McAdow R, Johnson SL and Lewis J (2007). Endothelial signalling by the Notch ligand Delta-like 4 restricts angiogenesis. *Development.* **134:** 839–844.

Levy AP, Levy NS and Goldberg MA (1996). Hypoxia-inducible Protein Binding to Vascular Endothelial Growth Factor mRNA and Its Modulation by the von Hippel-Lindau Protein. *Journal of Biological Chemistry.* **271:** 25492–25497.

Ley K (1996). Molecular mechanisms of leukocyte recruitment in the inflammatory process. *Cardiovascular Research.* **32:** 733–742.

Ley K, Laudanna C, Cybulsky MI and Nourshargh S (2007). Getting to the site of inflammation: the leukocyte adhesion cascade updated. *Nat Rev Immunol.* **7:** 678–689.

Li X, Zhang K and Li Z (2011). Unfolded protein response in cancer: the Physician's perspective. *J Hematol Oncol.* **4:** 8.

Limaye V and Vadas M (2007). The vascular endothelium: structure and function. *Mechanisms of Vascular Disease:* 1–10.

Lin JH, Li H, Yasumura D, Cohen HR, Zhang C, Panning B, Shokat KM, LaVail MM and Walter P (2007). IRE1 Signaling Affects Cell Fate During the Unfolded Protein Response. *Science.* **318:** 944–949.

Lin JH, Walter P and Yen TB (2008). Endoplasmic Reticulum Stress in Disease Pathogenesis. *Annu. Rev. Pathol. Mech. Dis.* **3:** 399–425.

Liu L, Qi X, Chen Z, Shaw L, Cai J, Smith LH, Grant MB and Boulton ME (2013). Targeting the IRE1α/XBP1 and ATF6 Arms of the Unfolded Protein Response Enhances VEGF Blockade to Prevent Retinal and Choroidal Neovascularization. *The American Journal of Pathology.* **182:** 1412–1424.

Liu X, Garriga P and Khorana HG (1996). Structure and function in rhodopsin: Correct folding and misfolding in two point mutants in the intradiscal domain of rhodopsin indentified in retinitis pigmentosa. *Proc Natl Acad Sci.* **93:** 4554–4559.

Lobov IB, Renard RA, Papadopulos N, Gale NW, Thurston G, Yancopoulos GD and Wiegand SJ (2007). Delta-like ligand 4 (Dll49 is induced by VEGF as a negative regulator of angiogenic sprouting. *PNAS.* **107:** 3219–3224.

Lowe JB (2003). Glycan-dependent leukocyte adhesion and recruitment in inflammation. *Current Opinion in Cell Biology.* **15:** 531–538.

Luo S, Mao C, Lee B and Lee AS (2006). GRP78/BiP Is Required for Cell Proliferation and Protecting the Inner Cell Mass from Apoptosis during Early Mouse Embryonic Development. *Molecular and Cellular Biology.* **26:** 5688–5697.

Maguire JA, Mulugeta S and Beers MF (2011). Endoplasmic Reticulum Stress Induced by Surfactant Protein C BRICHOS Mutants Promotes Proinflammatory Signaling by Epithelial Cells. *Am J Respir Cell Mol Biol.* **44:** 404–414.

Mao XR and Crowder CM (2010). Protein Misfolding Induces Hypoxic Preconditioning via a Subset of the Unfolded Protein Response Machinery. *Molecular and Cellular Biology.* **30:** 5033–5042.

Marjon PL, Bobrovnikova-Marjon EV and Abcouwer SF (2004). Expression of the pro-angiogenic factors vascular endothelial growth factor and interleukin-8/CXCL8 by human breast carcinomas is responsive to nutrient deprivation and endoplasmic reticulum stress. *Molecular Cancer.* **3:** 1–12.

Martin P (1997). Wound Healing--Aiming for Perfect Skin Regeneration. *Science.* **276:** 75–81.

Masuzawa M, Fujimura T, Hamasa Y, Fujita, Y., Hara, H., Nishiyama S, Katsuoka K, Tamauchi H and Sakurai Y (1999). Establishment of a Human Hemangiosarcoma Cell Line (ISO-HAS). *Int. J. Cancer.* **81:** 305–308.

Maurel M, Chevet E, Tavernier J and Gerlo S (2014). Getting RIDD of RNA: IRE1 in cell fate regulation. *Trends in Biochemical Sciences.* **39:** 245–254.

Mayer M, Kies U, Kammermeier R and Buchner J (2000). BiP and PDI Cooperate in the Oxidative Folding of Antibodiesin Vitro. *Journal of Biological Chemistry.* **275:** 29421–29425.

Midwood KS, Williams LV and Schwarzbauer JE (2004). Tissue repair and the dynamics of the extracellular matrix. *The International Journal of Biochemistry & Cell Biology.* **36:** 1031–1037.

Misra UK and Pizzo SV (2010). Modulation of the unfolded protein response in prostate cancer cells by antibody-directed against the carboxyl-terminal domain of GRP78. *Apoptosis.* **15:** 173–182.

Mitchell PS, Parkin RK, Kroh EM, Fritz BR, Wyman SK, Pogosova-Agadjanyan EL, Peterson A, Noteboom J, O´Briant KC, Allen A, Lin DW, Urban N, Drescher CW, Knudsen BS, Stirewalt DL, Gentleman R, Vessella RL, Nelson PS, Martin DB and

Tewari M (2008). Circulating microRNAs as stable blood-based markers for cancer detection. *PNAS.* **105:** 10513–10518.

Montesano R and Orci L (1988). Transforming growth factor b stimulates collagen-matrix contraction by fibroblasts: Implications for wound healing. *Proc Natl Acad Sci.* **85:** 4891–4897.

Montesano R, Orci L and Vassalli P. (1983). In Vitro Rapid Organization of Endothelial Cells into Capillary-like Networks Is Promoted by Collagen Matrices. *J Cell Biol.* **97:** 1648–1652.

Mountzios G, Pentheroudakis G and Carmeliet P (2014). Bevacizumab and micrometastases: Revisiting the preclinical and clinical rollercoaster. *Pharmacology & Therapeutics.* **141:** 117–124.

Mujcic H, Rzymski T, Rouschop KM, Koritzinsky M, Milani M, Harris AL and Wouters BG (2009). Hypoxic activation of the unfolded protein response (UPR) induces expression of the metastasis-associated gene LAMP3. *Radiotherapy and Oncology.* **92:** 450–459.

Mulvey M, Arias C and Mohr I (2007). Maintenance of Endoplasmic Reticulum (ER) Homeostasis in Herpes Simplex Virus Type 1-Infected Cells through the Association of a Viral Glycoprotein with PERK, a Cellular ER Stress Sensor. *Journal of Virology.* **81:** 3377–3390.

Mumm JS and Kopan R (2000). Notch Signaling: From the Outside In. *Developmental Biology.* **228:** 151–165.

Murota S, Onodera M and Morita I (2000). Regulation of Angiogenesis by Controlling VEGF Receptor. *Ann N Y Acad Sci.* **902:** 208–212.

Nakamura S, Takizawa H, Shimazawa M, Hashimoto Y, Sugitani S, Tsuruma K, Hara H and Chen J (2013). Mild Endoplasmic Reticulum Stress Promotes Retinal Neovascularization via Induction of BiP/GRP78. *PLoS ONE.* **8:** e60517.

Nissen NN, Polverini PJ, Koch AE, Volin MV, Gamelli RL and DiPietro LA (1998). Vascular Endothelial Growth Factor Mediates Angiogenic Activity during the Proliferative Phase of Wound Healing. *American Journal of Pathology.* **152:** 1445–1452.

Norton K, Pandey N, Han Z and Popel A (2014). Antiangiogenic cancer drug sunitinib exhibits unexpected proangiogenic effects on endothelial cells. *OTT.* **7:** 1571–1582.

Numnum TM, Rocconi RP, Whitworth J and Barnes MN (2006). The use of bevacizumab to palliate symptomatic ascites in patients with refractory ovarian carcinoma. *Gynecologic Oncology.* **102:** 425–428.

Obeng EA, Calson LM, Gutman DM, Harrington Jr., W. J., Lee KP and Boise L (2006). proteasome inhibitors induce a terminal UPR in multiple myeloma cells. *Blood.* **107:** 4907–4916.

Oliver KE and McGuire WP (2014). Ovarian Cancer and Antiangiogenic Therapy: Caveat Emptor. *Journal of Clinical Oncology.* **32:** 1–5.

Olsson A, Dimberg A, Kreuger J and Claesson-Welsh L (2006). VEGF receptor signalling — in control of vascular function. *Nat Rev Mol Cell Biol.* **7:** 359–371.

Osdoit S and Rosa J (2001). Fibrin Clot Retraction by Human Platelets Correlates with alpha IIbbeta 3 Integrin-dependent Protein Tyrosine Dephosphorylation. *Journal of Biological Chemistry.* **276:** 6703–6710.

Patel KD, Cuvelier SL and Wiehler S (2002). Selectins: critical mediators of leukocyte recruitment. *Seminars in Immunology.* **14:** 73–81.

Paton AW, Beddoe T, Thorpe CM, Whisstock JC, Wilce MCJ, Rossjohn J, Talbot UM and Paton JC (2006). AB5 subtilase cytotoxin inactivates the endoplasmic reticulum chaperone BiP. *Nature.* **443:** 548–552.

Pavio N, Romano PR, Graczyk TM, Feinstone SM and Taylor DR (2003). Protein Synthesis and Endoplasmic Reticulum Stress Can Be Modulated by the Hepatitis C Virus Envelope Protein E2 through the Eukaryotic Initiation Factor 2 Kinase PERK. *Journal of Virology.* **77:** 3578–3585.

Pereira ER, Liao N, Neale GA, Hendershot LM and Jin D (2010). Transcriptional and Post-Transcriptional Regulation of Proangiogenic Factors by the Unfolded Protein Response. *PLoS ONE.* **5:** e12521.

Peters K, Schmidt H, Unger RE, Otto M, Kamp G and Kirkpatrick C (2002). Software-supported image quantification of angiogenesis in an in vitro culture system: application to studies of biocompatibility. *Biomaterials.* **23:** 3413–3419.

Peters K, Unger RE, Brunner J and Kirkpatrick C (2003). Molecular basis of endothelial dysfunction in sepsis. *Cardiovascular Research.* **60:** 49–57.

Pichiorri F, Suh S, Rocci A, Luca L de, Taccioli C, Santhanam R, Zhou W, Benson DM, Hofmainster C, Alder H, Garofalo M, Di Leva G, Volinia S, Lin H, Perrotti D, Kuehl M, Aqeilan RI, Palumbo A and Croce CM (2010). Downregulation of p53-inducible

microRNAs 192, 194, and 215 Impairs the p53/MDM2 Autoregulatory Loop in Multiple Myeloma Development. *Cancer Cell.* **18:** 367–381.

Pluquet O, Qu L, Baltzis D and Koromilas AE (2005). Endoplasmic Reticulum Stress Accelerates p53 Degradation by the Cooperative Actions of Hdm2 and Glycogen Synthase Kinase 3. *Molecular and Cellular Biology.* **25:** 9392–9405.

Poliseno L, Tuccoli A, Mariani L, Evangelista M, Citti L, Woods K, Mercatanti A, Hammond S and Rainaldi G (2006). MicroRNAs modulate the angiogenic properties of HUVECs. *Blood.* **108:** 3068–3071.

Pootrakul L, Datar RH, Shi S, Cai J, Hawes D, Groshen SG, Lee AS and Cote RJ (2006). Expression of Stress Response Protein Grp78 Is Associated with the Development of Castration-Resistant Prostate Cancer. *Clinical Cancer Research.* **12:** 5987–5993.

Pouysségur J, Shiu RP and Pastan I (1977). Induction of two transformation-sensitive membrane polypeptides in normal fibroblasts by a block in glycoprotein synthesis or glucose deprivation. *Cell.* **11:** 941–947.

Price N and Tsvetanova B (2007). Biosynthesis of the Tunicamycins: A review. *J. Antibiot. 60(8): 485–491, 2007.* **60:** 485–491.

Prior BM, Yang HT and Terjung RL (2004). What makes vessels grow with exercise training? *Journal of Applied Physiology.* **97:** 1119–1128.

Reinhart-King CA. Endothelial Cell Adhesion and Migration. *Methods in Enzymology.* **443:** 45–64.

Reitsma S, Slaaf DW, Vink H, van Zandvoort, Marc A. M. J. and oude Egbrink, Mirjam G. A. (2007). The endothelial glycocalyx: composition, functions, and visualization. *Pflugers Arch - Eur J Physiol.* **454:** 345–359.

Risau W (1995). Differentiation of endothelium. *FASEB J.* **9:** 926–933.

Risau W (1997). Mechanisms of angiogenesis. *Nature.* **386:** 671–674.

Romero-Ramirez L, Cao H, Nelson D, Hammond E, Lee A, Yoshida H, Mori K, Glimcher LH, Denko NC, Giaccia AJ, Le Q and Koong AC (2004). XBP1 Is Essential for Survival under Hypoxic Conditions and Is Require for Tumor Growth. *Cancer Research.* **64:** 5943–5947.

Romero-Ramirez L, Cao H, Regalado MP, Kambham N, Siemann D, Kim JJ, Le QT and Koong AC (2009). X Box-Binding Protein 1 Regulates Angiogenesis in Human Pancreatic Adenocarcinomas. *Translational Oncology.* **2:** 31–38.

Ron D (2002). Translational control in the endoplasmic reticulum stress response. *J. Clin. Invest.* **110:** 1383–1388.

Ron D and Walter P (2007). Signal integration in the endoplasmic reticulum unfolded protein response. *Nat Rev Mol Cell Biol.* **8:** 519–529.

Ruf W and Ruggeri ZM (2010). Neutrophils release brakes of coagulation. *Blood.* **116:** 1344–1351.

Ruhrberg C, Gerhardt H, Golding M, Watson R, Ioannidou S, Fujisawa H, Betsholtz C and Shima DT (2002). Spatially restricted patterning cues provided by heparin-binding VEGF-A control blood vessel branching morphogenesis. *Genes & Development.* **16:** 2684–2698.

Ryoo HD, Domingos PM, Kang M and Steller H (2007). UPR in a Drosophila model for retinal degeneration. *The EMBO Journal.* **26:** 242–252.

Rzymski T and Harris AL (2007). The Unfolded Protein Response and Integrated Stress Response to Anoxia. *Clinical Cancer Research.* **13:** 2537–2540.

Salminen A and Kauppinen A (2010). Endoplasmatic Reticulum Stress in Age-Related Macular Degeneration: Trigger for Neovascularization. *Mol. Med.* **16:** 1.

Schadewijk A, Wout EFA, Stolk J and Hiemstra PS (2012). A quantitative method for detection of spliced X-box binding protein-1 (XBP1) mRNA as a measure of endoplasmic reticulum (ER) stress. *Cell Stress and Chaperones.* **17:** 275–279.

Schafer AI (1995). Effects of Nonsteroidal Antiinflammatory Drugs on Platelet Function and Systemic Hemostasis. *J Clin Pharmacol.* **35:** 209–219.

Schindler AJ and Schekman R (2009). In vitro reconstitution of ER-stress induced ATF6 transport in COPII vesicles. *PNAS.* **106:** 17775–17780.

Schmidt T and Carmeliet P (2010). Bridges that guide and unite. *Nature.* **465:** 697–699.

Schröder M and Kaufman RJ (2005). THE MAMMALIAN UNFOLDED PROTEIN RESPONSE. *Annu. Rev. Biochem.* **74:** 739–789.

Senger DR and Davis GE (2011). Angiogenesis. *Cold Spring Harbor Perspectives in Biology.* **3:** a005090.

Shalaby F, Rossant J, Yamaguchi TP, Gertsenstein M, Wu X, Breitman ML and Schuh AC (1995). Failure of blood-island formation and vasculogenesis in Flk-1-deficient mice. *Nature.* **376:** 62–66.

Shang J (2005). Quantitative measurement of events in the mammalian unfolded protein response. *Methods.* **35:** 390–394.

Shao Q, Ren P, Li, Y., Peng, B., Dai L, Lei N, Yao W, Zaho G, Li L and Zhang J (2012). Autoantibodies against glucose-regulated protein 78 as serological diagnostic biomarkers in hepatocellular carcinoma. *Int J Oncol.* **41:** 1061–1067.

Shen B, Lee DY, Gerber H, Keyt BA, Ferrara N and Zioncheck TF (1998). Homologous Up-regulation of KDR/Flk-1 Receptor Expression by Vascular Endothelial Growth Factor in Vitro. *The Journal of Biological Chemistry.* **273:** 29979–29985.

Shen J, Chen X, Hendershot LM and Prywes R (2002). ER Stress Regulation of ATF6 Localization by Dissociation of BIP/GRP78 Binding and Unmasking of Golgi Localization Signals. *Developmental Cell.* **3:** 99–111.

Shiraishi H, Okamoto H, Yoshimura A and Yoshida H (2006). ER stress-induced apoptosis and caspase-12 activation occurs downstream of mitochondrial apoptosis involving Apaf-1. *Journal of Cell Science.* **119:** 3958–3966.

Shuda M, Kondoh N, Imazeki N, Tanaka K, Okada T, Mori K, Hada A, Arai M, Wakatsuki T, Matsubara O, Yamamoto N and Yamamoto M (2003). Activation of the ATF6, XBP1 and grp78 genes in human hepatocellular carcinoma: a possible involvement of the ER stress pathway in hepatocarcinogenesis. *Journal of Hepatology.* **38:** 605–614.

Siemerink MJ, Klaassen I, Vogels IMC, Griffioen AW, Noorden CJF and Schlingemann RO (2012). CD34 marks angiogenic tip cells in human vascular endothelial cell cultures. *Angiogenesis.* **15:** 151–163.

Sonkoly E and Pivarcsi A (2009). Advances in microRNAs: implications for immunity and inflammatory diseases. *Journal of Cellular and Molecular Medicine.* **13:** 24–38.

Sonkoly E, Wei T, Janson PC, Sääf A, Lundeberg L, Tengvall-Linder M, Norstedt G, Alenius H, Homey B, Scheynius A, Ståhle M, Pivarcsi A and Zimmer J (2007). MicroRNAs: Novel Regulators Involved in the Pathogenesis of Psoriasis? *PLoS ONE.* **2:** e610.

Stanczyk J, Pedrioli, Deena M. Leslie, Brentano F, Sanchez-Pernaute O, Kolling C, Gay RE, Detmar M, Gay S and Kyburz D (2008). Altered expression of MicroRNA in synovial fibroblasts and synovial tissue in rheumatoid arthritis. *Arthritis & Rheumatism.* **58:** 1001–1009.

Stehouwer C, Lambert J, Donker, A. J. M. and van Hinsbergh, V. W. M. (1997). Endothelial dysfunction and pathogenesis of diabetic angiopathy. *Cardiovascular Research.* **34:** 55–68.

Strilić B, Kučera T, Eglinger J, Hughes MR, McNagny KM, Tsukita S, Dejana E, Ferrara N and Lammert E (2009). The Molecular Basis of Vascular Lumen Formation in the Developing Mouse Aorta. *Developmental Cell.* **17:** 505–515.

Suarez Y, Fernandez-Hernando C, Pober JS and Sessa WC (2007). Dicer Dependent MicroRNAs Regulate Gene Expression and Functions in Human Endothelial Cells. *Circulation Research.* **100:** 1164–1173.

Suarez Y and Sessa WC (2009). MicroRNAs As Novel Regulators of Angiogenesis. *Circulation Research.* **104:** 442–454.

Sumpio BE, Timothy Riley J and Dardik A (2002). Cells in focus: endothelial cell. *The International Journal of Biochemistry & Cell Biology.* **34:** 1508–1512.

Sweeney SM, Guy CA, Fields GB and San Antonio, J. D. (1998). Defining the domains of type I collagen involved in heparin-binding and endothelial tube formation. *Proc Natl Acad Sci.* **95:** 7275–7280.

Szegezdi E, Reed Herbert K, Kavanagh ET, Samali A and Gorman AM (2008). Nerve growth factor blocks thapsigargin-induced apoptosis at the level of the mitochondrion via regulation of Bim. *Journal of Cellular and Molecular Medicine.* **12:** 2482–2496.

Tabas I and Ron D (2011). Integrating the mechanisms of apoptosis induced by endoplasmic reticulum stress. *Nat Cell Biol.* **13:** 184–190.

Tan Z, Randall G, Fan J, Camoretti-Mercado B, Brockman-Schneider R, Pan L, Solway J, Gern JE, Lemanske RF, Nicolae D and Ober C (2007). Allele-Specific Targeting of microRNAs to HLA-G and Risk of Asthma. *The American Journal of Human Genetics.* **81:** 829–834.

Thurston G and Kitajewski J (2008). VEGF and Delta-Notch: interacting signalling pathways in tumour angiogenesis. *Br J Cancer.* **99:** 1204–1209.

Tischer E, Mitchell R, Hartman, T., Silva, M., Gospodarowicz D, Fiddes JC and Abraham JA (1991). The Human Gene for Vascular Endothelial Growth Factor. Multiple Protein Forms are Encoded through Alternative Exon Splicing. *The Journal of Biological Chemistry.* **266:** 11947–11954.

Unger RE, Krump-Konvalinkova V, Peters K and Kirkpatrick C (2002). In Vitro Expression of the Endothelial Phenotype: Comparative Study of Primary Isolated Cells

and Cell Lines, Including the Novel Cell Line HPMEC-ST1.6R. *Microvascular Research.* **64:** 384–397.

Uramoto H, Sugio K, Oyama T, Nakata S, Ono K, Yoshimastu T, Morita M and Yasumoto K (2005). Expression of endoplasmic reticulum molecular chaperone Grp78 in human lung cancer and its clinical significance. *Lung Cancer.* **49:** 55–62.

Urano F, Wang X, Bertolotti A, Zhang Y, Chung P, Harding HP and Ron D (2000). Coupling of Stress in the ER to Activation of JNK Protein Kinases by Transmembrane Protein Kinase IRE1. *Science.* **287:** 664–666.

Urra H and Hetz C (2014). A Novel ER Stress-Independent Function of the UPR in Angiogenesis. *Molecular Cell.* **54:** 542–544.

van Zee, K. J., DeForge LE, Fischer E, Marano MA, Kenney JS, Remick DG, Lowry SF and Moldawer LL (1991). IL-8 In Septic Shock, Endotoxemia, And After IL-1 Administration. *J Immunol.* **146:** 3478–3482.

Veikkola T and Alitalo K (1999). VEGFs, receptors and angiogenesis. *Cancer Biology.* **9:** 211–220.

Velnar T, Bailey T and Smrkolj V (2009). The Wound Healing Process: An Overview of the Cellular and Molecular Mechanisms. *Journal of International Medical Research.* **37:** 1528–1542.

Vermes I, Haanen C, Steffens-Nakken H and Reutellingsperger C (1995). A novel assay for apoptosis Flow cytometric detection of phosphatidylserine expression on early apoptotic cells using fluorescein labelled Annexin V. *Journal of Immunological Methods.* **184:** 39–51.

Virrey JJ, Dong D, Stiles C, Patterson JB, Pen L, Ni M, Schonthal AH, Chen TC, Hofman FM and Lee AS (2008). Stress Chaperone GRP78/BiP Confers Chemoresistance to Tumor-Associated Endothelial Cells. *Molecular Cancer Research.* **6:** 1268–1275.

Visse R and Nagase H (2003). Matrix Metalloproteinases and Tissue Inhibitors of Metalloproteinases: Structure, Function, and Biochemistry. *Circulation Research.* **92:** 827–839.

Waltenberger J, Claesson-Welsh L, Siegbahn A, Shibuya M and Heldin CH (1994). Different signal transduction properties of KDR and Flt1, two receptors for vascular endothelial growth factor. *Journal of Biological Chemistry.* **269:** 26988–26995.

Walter P and Ron D (2011). The Unfolded Protein Response: From Stress Pathway to Homeostatic Regulation. *Science.* **334:** 1081–1086.

Wang M, Wey S, Zhang Y, Ye R and Lee AS (2009). Role of the Unfolded Protein Response Regulator GRP78/BiP in Development, Cancer, and Neurological Disorders. *Antioxidants & Redox Signaling.* **11:** 2307–2316.

Wang S, Voisin M., Larbi K., Dangerfield J., Scheiermann C., Tran M., Maxwell P.H., Sorokin L. and Noushargh S. (2006). Venular basement membranes contain specific matrix protein low expression regions that act as exit points for emigrating neutrophils. *Journal of Experimental Medicine.* **203:** 1519–1532.

Weber K, Klickstein LB, Weber PC and Weber C (1998). Chemokine-induced monocyte transmigration requires cdc42-mediated cytoskeletal changes. *Eur. J. Immunol.* **28:** 2245–2251.

Wek RC, Jiang HY and Anthony TG (2006). Coping with stress: eIF2 kinases and translational control. *Biochemical Society Transactions.* **34:** 7–11.

Wen P, Song D, Ye H, Wu X, Jiang L, Tang B, Zhou Y, Fang L, Cao H, He W, Yang Y, Dai C, Yang J and Sadayappan S (2014). Circulating MiR-133a as a Biomarker Predicts Cardiac Hypertrophy in Chronic Hemodialysis Patients. *PLoS ONE.* **9:** e103079.

Werner S and Grose R (2003). Regulation of Wound Healing by Growth Factors and Cytokines. *Physiol Rev.* **83:** 835–870.

Williams CK, Li J, Murga M, Harris AL and Tosato G (2005). Up-regulation of the Notch ligand Delta-like 4 inhibits VEGF-induced endothelial cell function. *Blood.* **107:** 931–939.

Wolff B, burns AR, Middleton J and Rot A (1998). Endothelial Cell "Memory" of Inflammatory Stimulation: Human Venular Endothelial Cells Store Interleukin 8 in Weibel-Palade Bodies. *J. Exp. Med.* **188:** 1757–1762.

Wong VW and Crawford JD (2013). Vasculogenic Cytokines in Wound Healing. *BioMed Research International.* **2013:** 1–11.

Würdinger T, Tannous BA, Saydam O, Skog J, Grau S, Soutschek J, Weissleder R, Breakefield XO and Krichevsky AM (2008). miR-296 Regulates Growth Factor Receptor Overexpression in Angiogenic Endothelial Cells. *Cancer Cell.* **14:** 382–393.

Xu D, Perez RE, Rezaiekhaligh MH, Bourdi M and Truog WE (2009). Knockdown of ERp57 increases BiP/GRP78 induction and protects against hyperoxia and tunicamycin-induced apoptosis. *AJP: Lung Cellular and Molecular Physiology.* **297:** L44.

Xue X, Piao J, Nakajima A, Sakon-Komazawa S, Kojima Y, Mori K, Yagita H, Okumura K, Harding H and Nakano H (2005). Tumor Necrosis Factor (TNF) Induces the Unfolded Protein Response (UPR) in a Reactive Oxygen Species (ROS)-dependent Fashion, and the UPR Counteracts ROS Accumulation by TNF. *Journal of Biological Chemistry.* **280:** 33917–33925.

Yang W, Lee D and Ben-David Y (2011). The roles of microRNAs in tumorigenesis and angiogenesis. *Int J Physiol Pathophysiol Pharmacol.* **3:** 140–155.

Yang X, Du WW, Li H, Liu F, Khorshidi A, Rutnam ZJ and Yang BB (2013). Both mature miR-17-5p and passenger strand miR-17-3p target TIMP3 and induce prostate tumor growth and invasion. *Nucleic Acids Research.* **41:** 9688–9704.

Zachary I (2003). VEGF signalling: integration and multi-tasking in endothelial cell biology. *Biochemical Society Transactions.* **31:** 1171–1177.

Zadeh G and Guha A (2003). Angiogenesis in Nervous System Disorders. *Neurosurgery.* **53:** 1362–1376.

Zeng L, Xiao Q, Chen M, Margariti A, Martin D, Ivetic A, Xu H, Mason J, Wang W, Cockerill G, Mori K, Li JY, Chien S, Hu Y and Xu Q (2013). Vascular Endothelial Cell Growth-Activated XBP1 Splicing in Endothelial Cells Is Crucial for Angiogenesis. *Circulation.* **127:** 1712–1722.

Zhang Y, Liu R, Ni M, Gill P and Lee AS (2010). Cell Surface Relocalization of the Endoplasmic Reticulum Chaperone and Unfolded Protein Response Regulator GRP78/BiP. *Journal of Biological Chemistry.* **285:** 15065–15075.

Zheng H, Takahashi H, Li X, Hara T, Masuda S, Guan Y and Takano Y (2008). Overexpression of GRP78 and GRP94 are markers for aggressive behavior and poor prognosis in gastric carcinomas. *Human Pathology.* **39:** 1042–1049.

8 List of figures

9 List of tables

10 Curriculum vitae

Name:

Date/Place of Birth:

Nationality:

Address:

Education:

2011 - until today

2010 - 2011

2005 - 2010

1996 - 2005

Scientific publications:

Freese C., Schreiner D., Anspach L., Bantz C., Maskos M., Unger R. E., Kirkpatrick C. J. (2014) *In vitro investigation of silica nanoparticle uptake into human endothelial cells under physiological cyclic stretch*. Particle and Fibre Toxicology, 11:68.

Tsaryk R., Bartholomä N., Simiantonaki N., Anspach L., Peters K., Heilmann C., Kirkpatrick C. J., Pröls F. (2015; submitted in British J Dermatology) *Upregulated levels of ER resident chaperones in chronic wounds promote inflammation*.

Tsaryk R., Gloria, A.; Russo, T.; Anspach, L.; De Santis, R.; Ghanaati, S.; Ronald E Unger, R. E.; Ambrosio, L.; Kirkpatrick, C. J. (2015, submitted in Acta Biomaterialia) *Collagen-low molecular weight hyaluronic acid semi-interpenetrating network loaded with gelatin microspheres for cell and growth factor delivery for nucleus pulposus regeneration.*

Conference contribution:

Oral presentations:

Anspach L., Tsaryk R., Pröls F., Kirkpatrick C.J. *The role of chaperone BiP in angiogenesis and inflammation*. VI International Congress on Stress Proteins in Biology and Medicine. Sheffield, United Kingdom, August 18-22, 2013

Anspach L., Tsaryk R., Pröls F., Kirkpatrick C.J. *Regulation of BiP-mediated response in endothelial cells.* Human Disease Mapping Conference 2014, Dublin, Ireland, January 29-30, 2014

Poster presentations:

Anspach L., Tsaryk R., Pröls F., Kirkpatrick C.J. *Unfolded Protein Response (UPR) as a possible target for angiogenesis regulation in tissue engineering*. 3rd TERMIS World Congress 2012, Vienna, Austria, September 5-8, 2012

Anspach L., Tsaryk R., Salamon A., Unger R. E., Peters K., Kirkpatrick C.J. *Assessment of the effects of Co^{2+} and anoxia on gene expression in endothelial cells in vitro.* Annual Meeting of the DGBM. Dresden, Germany, November 6-8, 2014

11 Danksagung